

EIDESSTATTLICHE ERKLÄRUNG

Ich erkläre an Eides statt, dass ich die vorliegende Arbeit selbstständig verfasst, andere als die angegebenen Quellen/Hilfsmittel nicht benutzt, und die den benutzten Quellen wörtlich und inhaltlich entnommenen Stellen als solche kenntlich gemacht habe. Das in TUGRAZonline hochgeladene Textdokument ist mit der vorliegenden Dissertation identisch.

Datum

Unterschrift

Abstract

Crystallization from solution as well as liquid phase adsorption on porous adsorbents are suitable unit operations to separate linear and branched isomers. Because branched isomers are barely available in high purity for experiments, the underlying phase equilibria are often not accessible.

To overcome this limitation, a methodology for predicting phase equilibria of systems containing branched molecules was developed in this work. In order to consider the molecular architecture of linear and branched molecules, the Lattice Cluster Theory (LCT) in combination with a chemical association model was applied. Basic idea of the developed methodology is to combine model parameters that were adjusted to experimental data of linear molecules with information about the molecular architecture of the branched isomers. The methodology was first tested for predicting liquid-liquid equilibria (LLE) of binary and ternary systems showing only self-association of the solvent. For all systems investigated, the predicted phase equilibria showed a very good agreement with the experimental data. However, for systems showing self-association as well as cross-association it was seen that the predictions were not that accurate.

In case of crystallization from solution, oiling out, a superposition of LLE and solid-liquid equilibrium (SLE), has to be considered. Thus, the model framework must be able to calculate LLE and SLE simultaneously meaning that the same set of model parameters is applied. For systems showing only self-association as well as for one system showing self-association and cross-association, it could be shown that the LCT in combination with a chemical association model is well-suited to calculate LLE and SLE simultaneously.

Regarding adsorption, a new model for the liquid phase adsorption of isomers was developed based on the LCT. Besides calculating the adsorption isotherm, it also considers the adsorbent's swelling behavior based on the affine network theory. It was applied to two binary systems containing a linear and a branched isomer as well as to three porous adsorbents having different pore size distributions. In all cases, the adsorption isotherms could be described in very good agreement with experimental data.

Table of contents

Abstract	I
Table of contents	II
List of symbols	IV
Abbreviations	VIII
1 Introduction	1
2 State of the art	5
2.1 Industrial applications for isomers separation processes	6
2.1.1 Separation of xylene isomers	6
2.1.2 Separation of hexane isomers.....	8
2.1.3 Separation of enantiomers.....	10
2.1.4 Challenges	11
2.2 Thermodynamic models in literature.....	13
2.2.1 UNIFAC.....	13
2.2.2 COSMO	16
2.2.3 Lattice Cluster Theory.....	19
3 Theoretical Framework	23
3.1 Thermodynamic background	24
3.1.1 Flory-Huggins Theory.....	24
3.1.2 Lattice Cluster Theory.....	26
3.1.3 Chemical Association Lattice Model	27
3.1.4 Extended Chemical Association Lattice Model	28
3.1.5 Density Gradient Theory.....	30
3.2 Model development	32
3.2.1 Crystallization	32
3.2.2 Adsorption.....	36
4 Materials and Methods	39
4.1 Materials	40
4.1.1 LLE and SLE experiments	40
4.1.2 Interfacial tension.....	41
4.1.3 Adsorption isotherms	41
4.2 Experimental procedures	42
4.2.1 Liquid-liquid equilibrium.....	42
4.2.2 Solid-liquid equilibrium	44
4.2.3 Interfacial tension	46

4.2.4	Pore Size Distribution	47
4.2.5	Adsorption isotherms	47
4.3	Analytics.....	49
4.3.1	Gas chromatography	49
4.3.2	Total amount adsorbed.....	51
5	Results	53
5.1	Crystallization.....	54
5.1.1	Predicting binary LLE of systems containing branched molecules.....	54
5.1.2	Simultaneous modelling of binary LLE and SLE	67
5.1.3	Prediction of ternary phase behavior including linear and branched molecules.....	69
5.1.4	Extension to systems showing cross association	73
5.2	Adsorption	83
5.2.1	Pore size distribution.....	83
5.2.2	Binary system n-octane + 2,2,4-trimethylpentane.....	84
5.2.3	Binary system n-hexane + 2,3-dimethylbutane	90
5.3	Application in process design	97
6	Conclusion and outlook	101
	References	105
	List of figures	115
	List of tables	122
	Appendix A: Further results	128
	Appendix B: Experimental data	131

List of symbols

Latin letters	Unit	Description
a	K	Functional group interaction parameter
b	-	Functional group interaction parameter
c	K^{-1}	Functional group interaction parameter
$c_{Network}$	-	Network parameter
C_A, C_B	-	Quantities within ECALM
d	m	Diameter
E_1, E_2	$J mol^{-1}$	Enthalpic corrections of first and second order
E	$N C^{-1}$	Electric field
f	-	Correction factor
$g_0(X)$	$J mol^{-1}$	Gibbs free energy of a homogeneous solution
G	$J mol^{-1}$	Gibbs free energy
h	$J mol^{-1}$	Specific enthalpy
H	J	Enthalpy
I_0	m^2	Interfacial area
k_B	$J K^{-1}$	Boltzmann constant
K	-	Equilibrium association constant
K_0	-	Pre-factor defined in Eq. (3-9)
m	kg	Mass
n	mol	Number of molecules
N	-	Number of segments
$N_{1,i}$	-	Number of bonds
$N_{2,i}$	-	Number of two consecutive bonds
$N_{3,i}$	-	Number of three consecutive bonds
$N_{\perp,i}$	-	Number of points at which three bonds meet a lattice site

Latin letters	Unit	Description
$N_{1,1,i}$	-	Number of ways of selecting two non-sequential bonds on the same chain
$N_{1,2,i}$	-	Number of ways of selecting two consecutive bonds and one non-sequential on the same chain
$n(r)$	-	Surface normal vector
p	-	Probability
PR	-	Phase ratio
q	m^2	Molecular surface area
Q	m^2	Functional group surface area
R	$J mol^{-1} K^{-1}$	Universal gas constant
R	m	Segment radius
R	m^3	Functional group volume
S	$J K^{-1}$	Entropy
T	K	Temperature
V	m^3	Volume
w	-	Mass fraction
x	-	Mole fraction
\bar{y}	-	Mole fraction within cross-associate
z	-	Lattice coordination number
Z_{OH}	-	Number of hydroxyl groups

Greek letters	Unit	Description
χ	$J mol^{-1}$	FH interaction parameter
ε	J	Interaction energy
ε	$F m^{-1}$	Permittivity
ϕ	-	Segment fraction
Γ	-	Residual activity coefficient
γ	-	Activity coefficient
η	-	Cross-association parameter
κ	$J mol m^{-4}$	Influence parameter of DGT
μ	$J mol^{-1}$	Chemical potential
θ	-	Area fraction
ρ	$kg m^{-3}$	Density
σ	$N m^{-1}$	Interfacial tension
σ	$C m^{-2}$	Surface charge
ω	s^{-1}	Rotating frequency
Ω	$J mol^{-1}$	Grand thermodynamic potential

Subscripts	Description
0	Origin
<i>calc</i>	Calculated
<i>eff</i>	Effective
<i>exp</i>	Experimental
<i>i</i>	Component i
<i>ij</i>	Interaction between component i and j
<i>k</i>	Functional group k
<i>mn</i>	Interaction between functional groups m and n
<i>pol</i>	Polarization
<i>r, r'</i>	Degree of associating chain
<i>s</i>	Segment-molar

Superscripts	Description
<i>as</i>	Association
<i>C</i>	Combinatorial
<i>(ca)</i>	Cross-association
<i>CALM</i>	Chemical Association Lattice Model
<i>ECALM</i>	Extended Chemical Association Lattice Model
<i>Eq</i>	Equilibrium
<i>LCT</i>	Lattice Cluster Theory
<i>R</i>	Residual
<i>SL</i>	Solid-liquid phase transition

Abbreviations

Abbreviation	Description
ARD	Average relative deviation
CALM	Chemical Association Lattice Model
COSMO	Conductor-like Screening Model
COSMO-SAC	Conductor-like Screening Model – Segment Activity Coefficient
DFT	Density Functional Theory
DGT	Density Gradient Theory
DMT	Dimethyl terephthalate
DSC	Differential scanning calorimetry
ECALM	Extended Chemical Association Lattice Model
EOS	Equation of State
FH	Flory-Huggins Theory
GC	Gas chromatography
LCT	Lattice Cluster Theory
LLE	Liquid-liquid equilibrium
PET	Polyethylene terephthalate
RAST	Real Adsorbed Solution Theory
RON	Research octane number
SLE	Solid-liquid equilibrium
TMS	Thermomorphic multicomponent solvent system
UCST	Upper critical solution temperature
UNIFAC	Universal Quasichemical Functional Group Activity Coefficients
UNIQUAC	Universal Quasichemical

1 Introduction

In chemical industry there are several reactions, where a linear product and a number of its branched isomers are produced simultaneously. This is mainly the case when unsaturated components get converted like in hydroformylation or hydroesterification reactions. Depending on the later application, usually only one of the molecules is of interest. While normally the linear isomer is of greater importance, there are also applications for the branched isomer as flavor or fragrance. There are several efforts in designing catalyst systems in order to shift the production to the desired product; however, an exclusive production of the desired isomer can up to now not be achieved. Therefore, a separation of linear and branched isomer is necessary. This is a challenging task because of close physical properties. Nevertheless, significant differences in melting temperature and molecular architecture can be found between linear and branched molecules. Thus, crystallization and adsorption on porous solids are suitable unit operations for separating isomers. When crystallization is performed from solution, an oiling out can occur. This superposition of liquid-liquid equilibrium (LLE) and solid-liquid equilibrium (SLE) has got a significant influence on the final product properties. Hence, the knowledge of the phase equilibria and in particular of a possible oiling out is essential in order to design and control crystallization processes.

Main objective of this work is to gain the necessary physical knowledge in order to set up process models for the separation of isomers. Therefore, LLE and SLE in case of crystallization from solution and adsorption isotherms in case of adsorption have to be known. Commonly, thermodynamic modeling is applied to calculate these phase equilibria. Thereby, experiments with highly pure components are performed in order to adjust the necessary model parameters. Regarding branched isomers, this procedure is often not possible because branched isomers are barely available in high purity. To overcome this limitation, the development of a methodology for predicting phase equilibria of systems including branched molecules is one objective of this work. In order to consider the molecular architecture of linear and branched molecules, a thermodynamic model which is able to consider the molecular architecture has to be applied. The lattice cluster theory (LCT), which represents a further development of the well-known Flory-Huggins theory (FH), seems to be appropriate for this task. While FH is only able to consider linear molecules, the LCT offers the possibility of introducing branching to molecules by definition of architecture parameters that

can be a-priori derived from the chemical formula. In presence of polar components, the LCT has to be combined with an association model in order to consider associative interactions.

Basic idea of predicting phase equilibria of systems containing branched molecules is to combine model parameters that were adjusted to experimental data of linear molecules with architecture parameters of branched molecules. When applying the LCT in an incompressible version, which is totally sufficient for LLE, SLE and liquid phase adsorption isotherms, this means that for a binary system one interaction energy has to be adjusted to experimental data. Since no experimental data of branched molecules are available, the question is how this parameter can be defined for a binary system including a branched molecule. One possibility is to adjust the interaction energy for the corresponding linear isomer and use the same interaction energy for linear and branched isomer. Another possibility would be to extrapolate within a homologue series. Therefore, it has to be checked first whether there is a dependence of interaction energy and chain length. The methodology should be able to differentiate between isomers, including those where the only difference is in the position of one side group. If a prediction of binary systems including a branched isomer is possible, the subsequent challenge is to predict phase equilibria of ternary systems including a linear and a branched isomer. The model should be able to predict the ternary phase equilibria based on the binary subsystems, meaning that no further adjustment of model parameters to ternary data is performed. Furthermore, the temperature dependence of the investigated phase equilibria has to be covered quantitatively. First, systems only showing self-association of the solvent are investigated in order to prove the named challenges. Therefore, the LCT is combined with the chemical association lattice model (CALM). Subsequently, the complexity of the system is raised by introducing cross-association, wherefore the LCT is combined with the extended chemical association lattice model (ECALM). The accuracy of the predictions is evaluated by comparison with experiments.

In order to be suitable for the design of crystallization processes from solution, the LCT must be also able to simultaneously calculate LLE and SLE. In literature it can be seen, that other models are not able to describe LLE and SLE quantitatively with the same set of model parameters. Regarding the LCT, a quantitatively calculation of LLE and SLE was successfully shown for binary solutions of hyperbranched polymers. Objective of this work is to check whether the LCT in combination with an association model is also able to calculate the superposition of LLE and SLE for smaller molecules. The model parameters, which were already used to calculate LLE, should also be used for the calculation of SLE. While for the

calculation of binary systems LLE data are available, the calculation of ternary systems including a linear isomer, a branched isomer and a solvent is a special challenge. Here, only experimental data of the binary subsystem containing linear isomer and solvent are available. To investigate the influence of different association schemes on the accuracy of the calculation, systems showing only self-association and systems showing self-association and cross association are investigated. All calculations are compared with experimental data.

Last objective of this work is the development of a new model to describe liquid phase adsorption of isomers, where the pore size distribution of the adsorbent is crucial for the separation efficiency. Up to now, a prediction of adsorption isotherms considering the pore size distribution of the adsorbent is only possible by a density functional theory (DFT) approach. However, such an approach requires a high numerical effort, wherefore it is not suitable in process simulation. In this work, a simpler model based on an incompressible version of the LCT is developed, which assumes equilibrium between bulk phase and adsorbed phase. Depending on the pore size distribution of the adsorbent, various kinds of separation efficiencies can be achieved ranging from an almost perfect separation to no separation. Challenge of the new model is to describe all kinds of separation efficiencies. Therefore, the information of different adsorption strengths of linear and branched isomers caused by the pore size distribution has to be definable in the model. Idea is to treat the adsorbent as individual component offering the possibility to define different interaction energies of linear and branched isomer with the adsorbent. Additionally, swelling of the adsorbent, which can be caused by solid-fluid interactions, should be considered based on the affine network theory. This is an interesting feature of the model in order to describe the phase ratio of bulk phase and adsorbed phase, which is important in process design. Experimental liquid phase adsorption isotherms as well as swelling data are used to evaluate the accuracy of the developed model.

2 State of the art

In the first part of this chapter, a short overview of important industrial applications for the separation of isomers by means of crystallization and adsorption is given. In the second part of this chapter, existing thermodynamic models that can be used for the investigation of systems containing linear and branched molecules are introduced and their applicability in predicting phase equilibria of systems containing branched molecules is discussed.

The scientific work published in this chapter was performed by T. Goetsch. Scientific advice was given by T. Zeiner.

2.1 Industrial applications for isomer separation processes

Hydroformylation¹ and hydroesterification² are only two examples of reactions where linear and branched molecules are produced simultaneously. Depending on the later application, only one of the molecules is of interest. While normally the linear isomer is of greater importance, there are also applications for the branched isomer³. Numerous efforts for designing catalyst systems that shift the production to the desired product can be found in literature. Nevertheless, linear and branched isomers cannot be produced alone⁴, wherefore a subsequent separation of linear and branched isomers is usually necessary. In this chapter, three important isomer separation processes will be introduced, i.e. separation of xylene isomers, hexane isomers and enantiomers, and the challenges accompanying these separations by means of crystallization and adsorption will be emphasized.

2.1.1 Separation of xylene isomers

The separation of xylene isomers is one of the most important industrial applications of isomer separations. In the production of xylene always the three isomers ortho-xylene, meta-xylene and para-xylene are produced simultaneously⁵. For industrial application para-xylene is the most important one. It is first converted to terephthalic acid and afterwards to dimethyl terephthalate (DMT). Together with ethylene glycol DMT is then converted to polyethylene terephthalate (PET)⁶. The other xylene isomers can be used in fuels for airplanes, in rubber industry or as cleaning agents⁵. Regarding the physical properties of the three xylene isomers, distillation is not suitable to separate them, because of too close boiling points. Instead, crystallization can be applied to gain para-xylene since it has the highest melting temperature of all three isomers (Table 1).

Table 1: Melting temperatures of ortho-xylene, meta-xylene and para-xylene⁵.

Molecule	Melting temperature /K
ortho-xylene	248.0
meta-xylene	225.3
para-xylene	286.5

These large differences in melting temperatures can always be found between linear and branched isomers. In fact, the degree of branching has got an effect on the symmetry of a molecule. The more unsymmetrical a molecule is, the lower the melting temperature will be⁷. This effect is shown in Figure 1 for different mono-branched alkanes.

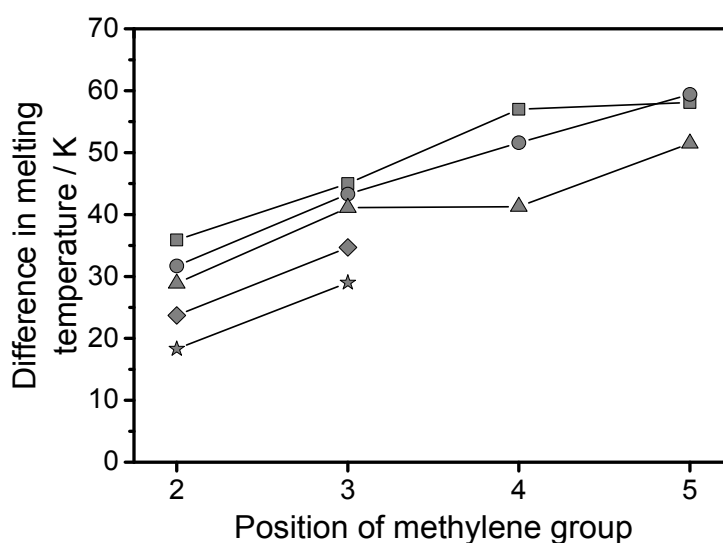


Figure 1: Difference in melting temperature between linear alkanes and their mono-branched isomers depending on the position of the methylene group (squares: C12; circles: C14; triangles: C16; diamonds: C18; stars: C20). Data were taken from literature⁸⁻¹¹.

The difference in melting temperature between linear alkanes having chain lengths between 12 and 20 and their mono-branched isomers is shown as a function of the position of the methylene group, where the degree of branching is increasing from position 2 to 5. It can be seen that the difference in melting temperatures between the isomers is increasing as the degree of branching gets larger. Even larger differences in melting temperature can be observed for isomers having more than one branch.

Crystallization is characterized by a lower energy consumption and lower process temperature compared to other thermal separations, wherefore a moderate treatment of the compounds is achieved¹². However, concerning the separation of isomers by means of crystallization, several aspects have to be considered in order to achieve the desired product properties. First of all, the mixture of isomers has to be in a supersaturated state, wherefore the underlying SLE has to be known. For primary nucleation, a relatively high supersaturation is necessary. By adding seed crystals, secondary nucleation can be forced already at low supersaturations. The crystal growth is then dependent on several process conditions like temperature or shear forces of a stirrer. At the end, crystals can form agglomerates or aggregates, which again can have an influence on the final product properties.¹³

Regarding the separation of xylene isomers, the final crystal size distribution is decisive for the quality of the product. It can be realized by a well-defined cooling profile. In order to gain

large crystals, the solution should be cooled down slowly in the beginning and more rapidly in the end of the crystallization process¹⁴. Despite the general applicability of crystallization to separate xylene isomers, its capacity is much lower compared to distillation processes. Moreover, the separation can be restricted to an eutectic¹⁵. Therefore, a combination of distillation and crystallization can be beneficial by exploiting the benefits of both unit operations¹⁶. Besides separating xylene isomers the combination of distillation and crystallization was already applied for example for the separation of carbon acids¹⁷.

2.1.2 Separation of hexane isomers

The separation of hexane isomers is another example of isomer separation in industrial scale. Hexane isomers are mainly used in gasoline, where the quality of the gasoline is characterized by the research octane number (RON). The higher the RON of a molecule is the more efficiently does it burn. Comparing RON of linear and branched hexane isomers results in great differences (Table 2)

Table 2: Research octane number of five different hexane isomers⁷.

Molecule	Research octane number
n-hexane	30.0
2-methylpentane	74.5
3-methylpentane	75.5
2,2-dimethylbutane	94.0
2,3-dimethylbutane	105.0

Regarding Table 2, it is evident that branched hexane isomers are more desired in gasoline than the linear one. The branched isomers are produced via catalytic isomerization leading to a mixture of linear and branched hexane isomers with an amount of 10 to 30% of each isomer¹⁸. Since the separation of isomers is a challenging task, RON of gasoline was often raised by the addition of olefins and aromatics¹⁸. Recently, new regulations were adopted to reduce the amount of gasoline additives in order to reduce the negative impact of gasoline on the environment¹⁹. Hence, an efficient separation of hexane isomers is required. In contrast to the separation of xylene isomers, crystallization is not appropriate for this separation, even though the isomers show significantly different melting temperatures. Since the mixture has to be cooled down to temperatures between 120 and 180 K, crystallization would not be energy efficient⁷. Instead adsorption on porous adsorbents can be applied to efficiently separate the

hexane isomers, where their different molecular architectures, leading to different kinetic diameters, can be utilized to apply size exclusion adsorption²⁰. Another effect leading to a separation between linear and branched molecules is a denser packing of the linear molecules on the surface⁷. However, the size exclusion effect is supposed to dominate, wherefore the choice of an adsorbent having the right pore size distribution is essential for the performance of the adsorption process.

Table 3: Kinetic diameters of n-hexane, 2-methylpentane, 3-methylpentane, 2,2-dimethylbutane and 2,3-dimethylbutane²¹.

Molecule	Kinetic diameter / Å
n-hexane	4.3
2-methylpentane	5.0
3-methylpentane	5.0
2,2-dimethylbutane	6.2
2,3-dimethylbutane	6.2

Ideally, the porous adsorbent offers pore sizes allowing the linear molecule to enter and rejecting the branched molecules resulting in a perfect separation of the linear isomer. Adsorbents having broad pore size distributions usually do not achieve sharp separations. In these cases, linear as well as branched isomers can enter the pores and adsorb onto the surface of the pores. Even though linear and branched isomers are of the same class of molecules their ability to adsorb onto the surface is not equal. According to Herm et al.¹⁸ the branched isomers have got a smaller number of atoms, which can interact with the surface leading to weaker van der Waals interactions compared to the linear isomers. This leads to a preferential adsorption of linear molecules. Additionally, the ability of the linear isomers of building denser packings can lead to a replacing of already adsorbed branched isomers⁷.

Currently, the separation of hexane isomers is performed applying zeolites having a pore size of 5 Å⁷. Referring to Table 3, n-hexane can be removed by zeolite 5A resulting in a gasoline with a RON of 83¹⁸. The separated n-hexane is recycled to the isomerization reaction in order to increase the overall yield of the process.

2.1.3 Separation of enantiomers

The separation of enantiomers, stereo-isomers acting like image and mirror image, is of great importance in the production of chiral pharmaceutical compounds or food additives²². Even though the only difference between enantiomers is the optical rotation, often only one enantiomer shows the desired effect, e.g. a pharmaceutical activity. The other enantiomer can show no pharmaceutical activity or in some cases even a harmful activity²³. Therefore, the suppliers are urged to produce the pure active enantiomer²⁴. An asymmetric catalysis can be applied to produce the pure enantiomer directly; however this procedure is very elaborative and can lead to uneconomical processes²⁵. Instead, it seems to be more promising to produce a racemic mixture containing both enantiomers in equal amounts and separate the desired one afterwards. The undesired enantiomer can be recycled to a racemization step in order to raise the yield up to 100%²⁵. In general, crystallization as well as adsorption (chromatography) are capable to perform a racemic separation. Regarding chromatography there is a number of chiral stationary phases for a racemic separation²⁶. Furthermore, there are possibilities of tuning the mobile phase in order to enhance the separation efficiency²⁷. To enhance the productivity of chromatography a simulated moving bed can be applied²⁸. However, with increasing product purity the productivity decreases²⁸. Another disadvantage is that chromatographic processes are quite expensive in general²⁴. On the other hand, crystallization is usually cheaper than chromatography²⁹. If the desired enantiomer is already available in a small amount it can be used as seed crystals for preferential crystallization²⁴. The seed crystals are supposed to grow while the other enantiomer does not nucleate. While the seed crystals grow, the supersaturation is reduced leading to a lower optical purity of the final crystals. In order to design a better overall process it could be beneficial to combine chromatography and crystallization³⁰. Chromatography would be the first step in this hybrid process to increase the concentration of the desired enantiomer to a certain point assuring a sufficient productivity. The pure enantiomer can afterwards be obtained in the crystallization step. This concept can eliminate the bottleneck of the stand-alone chromatography while increasing the overall efficiency of the process²⁵. The combination of chromatography and crystallization for an enantiomeric separation was already applied for the separation of praziquantel²³, mandelic acid³¹ or threonine³².

2.1.4 Challenges

For the design of crystallization as well as adsorption processes, the underlying phase equilibria have to be known, i.e. the SLE for crystallization and the adsorption isotherm for adsorption. When crystallization is not performed from melt but from solution, a possible oiling out has to be considered, which is shown graphically in Figure 2 for binary systems.

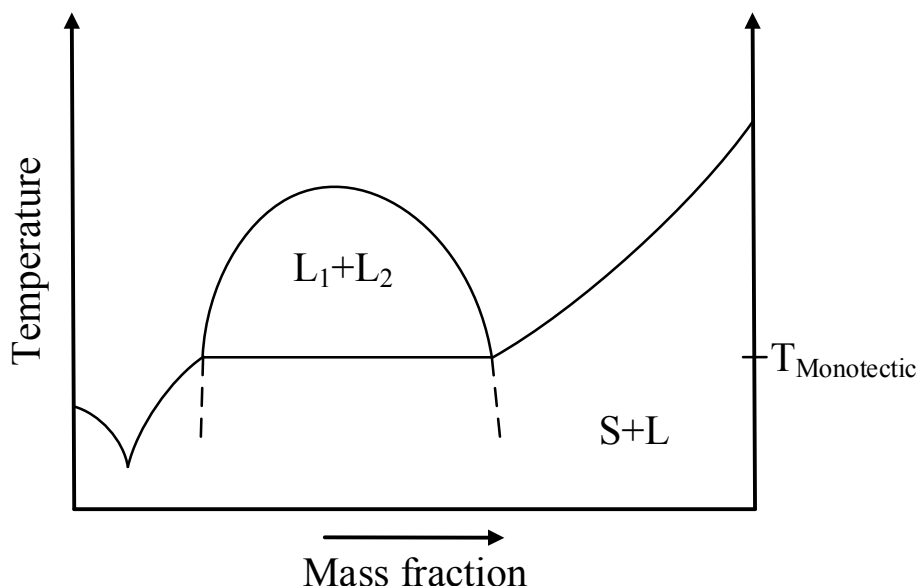


Figure 2: Oiling out in binary systems.

It can be seen that LLE and SLE intersect each other. Below the SLE curve, the LLE is shown as a dashed line, which shows that the LLE is only metastable in this region. According to the phase rule of Gibbs, there is only one temperature, where two liquid phases and one solid phase can exist in equilibrium. This temperature is called monotectic temperature. The superposition of LLE and SLE has got a significant influence on the final product properties. According to Kiesow et al.^{33,34} the crystal size and crystal shape is affected by the oiling out. Moreover, Yang and Rasmuson^{35,36} reported about much smaller crystals and more agglomeration due to the formation of a LLE. Furthermore, a broader crystal size distribution in comparison to crystallization without oiling out was observed. According to Cahn³⁷, in regions where LLE and SLE superposes, a formation of solid phase is always accompanied with a previous or simultaneous formation of a second liquid phase. In special cases, oiling out only occur in supersaturated solutions. Here, oiling out can be prevented by suitable process conditions. Lu et al.³⁸ reported that oiling out can be suppressed by small cooling rates or initial seeding, so that crystals can be formed prior to the formation of a second liquid. Thus, for the design of suitable crystallization processes, a liquid-liquid phase separation prior

to the formation of crystals has to be avoided. Hence, crystallization has to be performed in concentration ranges outside the LLE.

As already mentioned in the introduction, an experimental determination of LLE and SLE containing branched molecules is often not possible. Thus, it would be desirable to predict these phase equilibria by thermodynamic modeling. In literature, there are only a few investigations dealing with the molecular architecture's effect of isomers on phase equilibria. Hofman et al.³⁹ as well as Reda et al.⁴⁰ investigated binary LLE of isomeric C8 aliphatic solutions of monoethers in nitromethane and acetonitrile, respectively. They tried to predict the phase equilibria applying the modified UNIFAC⁴¹ model as well as the COSMO-SAC⁴² model. Both predictive models were not able to give quantitative predictions. Applying other, non-predictive thermodynamic models is not applicable, because the required pure component parameters cannot be specified due to missing experimental data.

Regarding the separation of isomers by means of adsorption, the mixture adsorption isotherms have to be known in order to design a suitable process. For the same reasons as for crystallization, an experimental determination is often not possible. Thus, a prediction of mixture adsorption isotherms by thermodynamic modeling is necessary. This is even more difficult than predicting LLE, because of the presence of a solid adsorbent. Since isomers are separated by means of size exclusion, the pore size distribution of the adsorbent is decisive for the separation efficiency and has therefore to be considered by the thermodynamic model. This is possible by a DFT approach as described by Zimmermann et al.⁴³. They described how pure component adsorption isotherms of branched isomers as well as mixture adsorption isotherms of linear and branched isomers can be predicted based on pure component adsorption isotherms of linear isomers. Moreover, operating conditions were varied in order to define optimal operating conditions. In general, adsorption of isomers can be performed from gaseous or liquid phase. However, as described by Zimmermann et al.⁴³ adsorption from liquid phase leads to a better separation efficiency as shown in Figure 3, wherefore the adsorption of isomers is investigated from the liquid phase in this work.

The combination of DFT and LCT is a powerful tool for predicting pure component adsorption isotherms of branched molecules as well as for predicting mixture adsorption isotherms of linear and branched molecules. However, the numerical effort is too high in order to use this combination in process simulation or process optimization, wherefore there is a need for a simpler model.

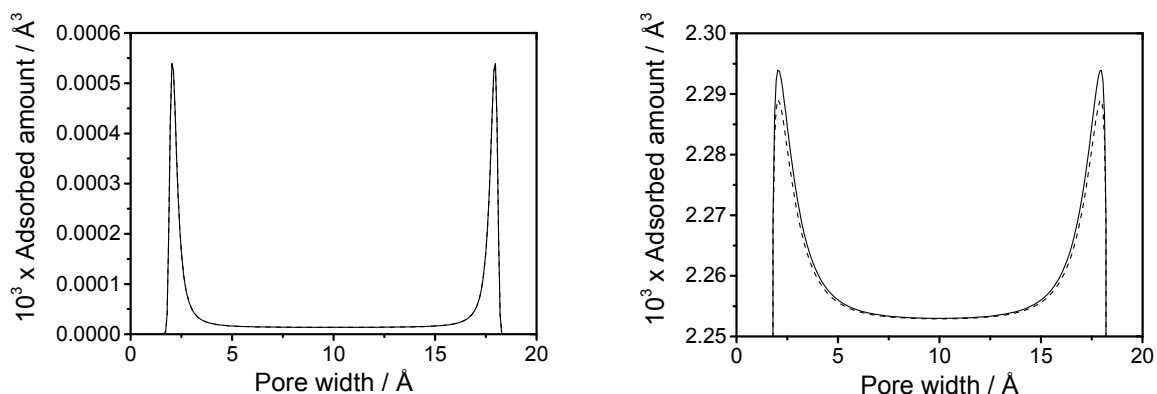


Figure 3: Adsorption isotherms of the binary system n-hexane (solid lines) + 2,3-dimethylbutane (dashed lines) at temperature of 273K and pressure of 100 Pa (left side) and 1 bar (right side). Data were taken from⁴³.

2.2 Thermodynamic models in literature

In this chapter, two predictive thermodynamic models, i.e. modified UNIFAC⁴¹ and COSMO-SAC⁴² will be shortly introduced. Both of them were already applied to isomer systems in literature. They will be applied for the prediction of binary LLE of hexane isomers dissolved in methanol in order to show their shortcomings for predicting phase equilibria of systems including branched molecules. Afterwards, the LCT will be introduced as a possible alternative to the former two models for predicting phase equilibria of systems containing linear and branched molecules.

2.2.1 UNIFAC

Group contribution methods are often applied in process design. When thermodynamic data are rare, they offer a convenient way of predicting the missing data. Probably the most often used group contribution method is UNIFAC (**U**niversal **Q**uasichemical **F**unctional **G**roup **A**ctivity **C**oefficients). UNIFAC was developed by Fredenslund et al.⁴⁴. Within UNIFAC, molecules are divided into functional groups, e.g. hydrocarbon groups, alcohol groups or ester group. Thereby a broad variety of molecules can be built of only a few functional groups, and the thermodynamic properties of the molecules can be calculated as the sum of individual contributions of each functional group present within the molecules. Basic assumption for this procedure is that contributions attributed to a functional group are independent of other

functional groups⁴⁴. A system is then regarded as a solution of functional groups, similar to earlier group contribution methods^{45,46}, rather than a solution of molecules.

UNIFAC is an extension of the UNIQUAC (Universal Quasichemical) equation⁴⁷, where the activity coefficient γ_i is divided into two contributions; one combinatorial contribution γ_i^C considering differences of the molecules in size and shape and one residual contribution γ_i^R considering the molecular interactions:

$$\ln(\gamma_i) = \ln(\gamma_i^C) + \ln(\gamma_i^R) \quad (2-1)$$

According to the results of Fredenslund et al.⁴⁴ vapor-liquid equilibria can be predicted quite accurately with UNIFAC. However, liquid-liquid equilibria can only be predicted approximately. Therefore, Magnussen et al.⁴⁸ introduced UNIFAC-LLE, a special version of UNIFAC suitable for the prediction of liquid-liquid equilibria, where the same equations but different functional group parameters are used. Significant improvements in comparison to the original UNIFAC version could be observed for the prediction of ternary LLE⁴⁸. Nonetheless, the prediction of binary LLE is not that accurate. According to Gupte and Danner⁴⁹, the reason for this finding is that only isothermal LLE data were used for the adjustment of functional group parameters. In order to overcome this shortcoming, Weidlich and Gmehling⁴¹ developed a modified version of UNIFAC (mod. UNIFAC), where combinatorial as well as residual contribution were modified. This mod. UNIFAC version was applied in this work for the prediction of binary LLE. The definitions of combinatorial and residual contribution read as:

$$\ln(\gamma_i^C) = 1 - \phi_i' + \ln(\phi_i') - 5q_i \left[1 - \frac{\phi_i}{\theta_i} + \ln\left(\frac{\phi_i}{\theta_i}\right) \right] \quad (2-2)$$

$$\ln(\gamma_i^R) = \sum_k v_k^{(i)} \left[\ln(\Gamma_k) - \ln(\Gamma_k^{(i)}) \right] \quad (2-3)$$

Within Eq. (2-2), ϕ_i represents the segment fraction of component i, θ_i represents the area fraction of component i, q_i is the molecular surface area and ϕ_i' is a segment fraction modified by an empirical exponent of 3/4. Eq. (2-3) contains the group residual activity coefficient Γ_k and the group residual activity coefficient in a reference solution $\Gamma_k^{(i)}$. Moreover, Eqs. (2-2) and (2-3) contain volumes R_k and surface areas Q_k of the individual

functional groups as well as the functional group interaction parameters a_{mn} , b_{mn} and c_{mn} , which are simultaneously adjusted to an experimental data base. For a detailed description of the different UNIFAC versions, please refer to the literature^{41,44,48}.

In order to prove whether group contribution methods are suitable for predicting phase equilibria of systems containing linear and branched isomers, mod. UNIFAC was applied for the prediction of binary LLE of four hexane isomers, namely n-hexane, 2-methylpentane, 3-methylpentane and 2,3-dimethylbutane, dissolved in methanol. The predicted binary LLE are illustrated in Figure 4 (Calculations were performed with Aspen Plus[®] 8.8).

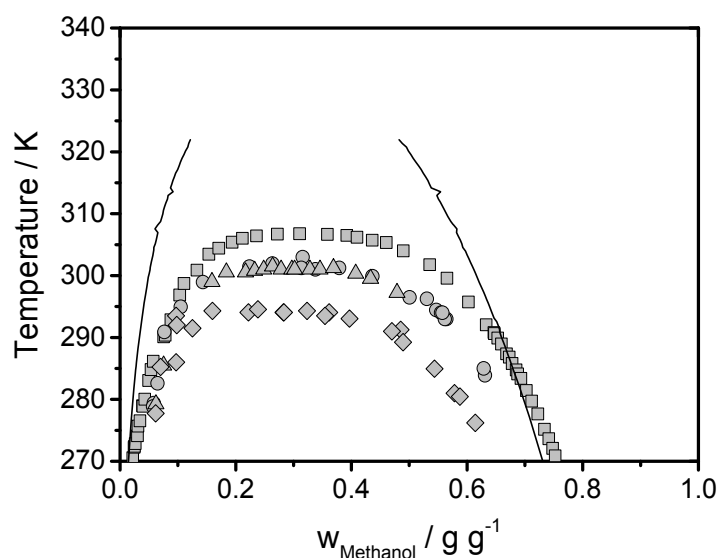


Figure 4: Binary LLE of n-hexane (squares), 2-methylpentane (circles), 3-methylpentane (triangles) and 2,3-dimethylbutane (diamonds) dissolved in methanol. The solid line denotes the prediction of mod. UNIFAC for all systems.

The experimental data show a great influence of the degree of branching on the upper critical solution temperature (UCST). For the highest degree of branching, i.e. 2,3-dimethylbutane dissolved in methanol, the lowest UCST is achieved. Regarding the predicted binary LLE, it can be seen that this influence of the degree of branching on the UCST is not covered. The mod. UNIFAC version, as group contribution methods in general, is not capable of differentiating between the four hexane isomers leading to the same predictions for all binary systems. Quantitative agreement between experiment and predictions are only visible for the system n-hexane / methanol for relatively low temperatures. Additionally, it can be seen, that the model predicts a hetero-azeotrope, indicated by an open binodal curve. Regarding the experimental data, it is obvious that none of the four binary systems will form a hetero-

azeotrope. In conclusion it can be stated, that group contribution methods in general are not capable of predicting quantitatively phase equilibria of systems containing linear and branched isomers

2.2.2 COSMO

Besides group contribution methods, COSMO (Conductor-like Screening Model) is another thermodynamic model having a predictive character developed by Klamt and Schüürmann⁵⁰. COSMO is a dielectric continuum model, where a dielectric continuum is surrounding a solute. This leads to a cavity within the dielectric continuum, which is formed by the solute. Because of the solute's charge distribution, a surface charge distribution on the interface between solute and dielectric continuum will be established. The calculation of the resulting screening charge density $\sigma(r)$, which is defined by the implicit Eq. (2-4), is the major challenge in order to calculate thermodynamic properties with COSMO⁵⁰.

$$4\pi\epsilon\sigma(r) = (\epsilon - 1)n(r)E^-(r) \quad (2-4)$$

Here, ϵ represents the permittivity, $n(r)$ denotes the surface normal vector at position r and $E^-(r)$ represents the total electric field at the surface's inner side at the same position, which is a function of the solute's charge distribution and the screening charge⁵⁰. It depends on the geometry of the interface whether Eq. (2-4) can be solved analytically or not. As was shown by Onsager⁵¹, this is only possible for spherical or ellipsoidal geometries. For arbitrary geometries Eq. (2-4) has to be solved numerically. According to Klamt and Schüürmann⁵⁰, a division of the interface into smaller segments having a constant charge density σ is therefore mandatory. They introduced a non-iterative methodology to solve Eq. (2-4) for arbitrarily shaped surfaces with the assumption of screening within a conductor. This assumption, regarding a solvent as a conductor, is only valid if the solvent possess the opposite surface charge density for all of the solute molecule's faces⁵². While water is a molecule, which offers these conductor-like properties for a lot of solutes, this assumption is not valid for most solvents. Because of their individual surface charge density, non-ideal combinations of surface segments of solvent and solute will arise leading to a non-perfect screening of the solutes within the solvent⁵².

In order to account for this non-ideal screening, Klamt⁵² introduced COSMO-RS (Conductor-like Screening Model for Real Solvents). The calculations within COSMO-RS are based on a

perfectly screened solute, where the ideal screening energy and the surface charge density are obtained by the original COSMO-model⁵⁰. Regarding real solvents, the surfaces of solute and solvent are divided into segments, resulting in pairs of contacting segments of solute and solvent, respectively. Every segment is assumed to possess a constant surface charge density. By averaging the surface charge densities of all segments of a molecule, a probability function $p(\sigma)$ can be derived⁵². This probability function, called σ -profile, is unique for every molecule. For mixtures of solvents, the σ -profile of the mixture can be determined out of the individual σ -profiles.

As already described above, non-ideal combinations of contacting segments will be present for real solvents. In contrast to ideally contacting segments the interaction energy of non-ideally contacting segments is not vanishing and has therefore to be quantified. This interaction energy, called misfit energy, is defined by Eq. (2-5), where σ_1 and σ_2 are the surface charges of the segments of molecule 1 and 2, respectively⁵².

$$E_{misfit} = \frac{1}{2} \alpha (\sigma_1 + \sigma_2)^2 \quad (2-5)$$

The framework of COSMO-RS was applied to investigate the solvation behavior of the real solvents water, acetone, benzene, n-octane and 1-octanol, where the results of COSMO-RS agreed well with the real solvation behavior⁵². Additionally, vapor pressure, octanol/water partition coefficient and surface tension were investigated as quantitative applications. Again, a good accordance of the calculations by COSMO-RS and the real physicochemical properties could be observed. Even though the results of Klamt⁵² agreed well with experimental data, potential for improvements to COSMO-RS was also mentioned. Therefore, Klamt et al.⁵³ introduced a refinement and a new parametrization of COSMO-RS including a new algorithm to close the cavity's surface, remove of outlying charges and generalization of hydrogen bonding. In total, eight general parameters and two parameters related to a chemical element were adjusted. Thereby, some of the former used values like segment radius ($R_{eff} = 1.5\text{\AA}$ instead of $R_{eff} = 1\text{\AA}$) or polarization correction factor ($f_{pol} = 0.48$ instead of $f_{pol} = 0.64$) were changed. For a complete summary of values for the adjustable parameters, the reader is referred to Klamt et. al⁵³.

According to Lin and Sandler⁴², COSMO-RS does not fulfill thermodynamic consistency requirements. Therefore, they re-derived a thermodynamically consistent version of COSMO,

called COSMO-SAC (COSMO segment activity coefficient model)⁴². Besides correcting the thermodynamic inconsistency, the number of adjustable parameters was reduced in comparison to COSMO-RS and a partial re-parametrization was performed. The new version was applied to calculate vapor-liquid equilibria (VLE), octanol/water partition coefficients and activity coefficients at infinite dilution. The accuracy of the calculations was comparable to the results of COSMO-RS. In order to compare the ability of COSMO to calculate phase equilibria of systems containing linear and branched isomers, the thermodynamically consistent version COSMO-SAC by Lin and Sandler⁴², implemented within Aspen Plus[®] 8.8, was applied for the prediction of the same four binary LLE, which are shown in Figure 4. The results are shown in Figure 5.

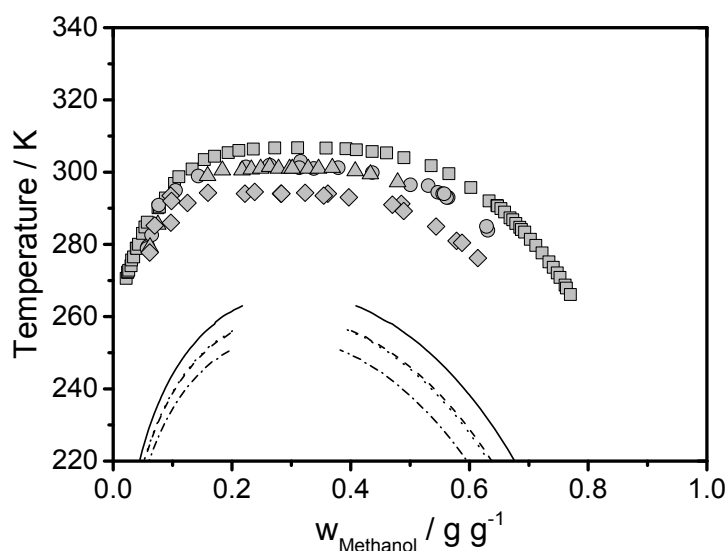


Figure 5: Binary LLE of n-hexane (squares), 2-methylpentane (circles), 3-methylpentane (triangles) and 2,3-dimethylbutane (diamonds) dissolved in methanol. The solid lines denote the prediction of COSMO-SAC (solid: n-hexane; dashed: 2-methylpentane; dotted: 3-methylpentane; dash-dotted: 2,3-dimethylbutane).

In contrast to UNIFAC, it can be seen that COSMO-SAC is able to differentiate between the hexane isomers. The influence of the degree of branching on the UCST as described in chapter 2.2.1 is covered qualitatively in the right way. However, deviations in temperature of approximately 40 – 50 K between experimental and predicted phase equilibria can be noticed. Thus, COSMO-based models, while able to differentiate between isomers, are not suitable for quantitative predictions of phase equilibria of systems containing linear and branched isomers.

2.2.3 Lattice Cluster Theory

Based on the works of Freed and coworkers⁵⁴⁻⁵⁸, who developed the LCT based on field theoretic considerations, Dudowicz et al.⁵⁹ re-derived the LCT algebraically. The LCT is a thermodynamic model that is able to take the molecular architecture, including branching, directly into account. It is written in terms of a double series of $1/z$ and $\Delta\varepsilon_{ij}/k_B T$ for calculating the Helmholtz free energy. Within this double series z represents the lattice coordination number of the lattice and $\Delta\varepsilon_{ij}/k_B T$ represents the dimensionless interaction energy of nearest neighbor segments. Referring to Dudowicz et al.⁵⁹, the series expansion is truncated at the second order because terms of higher order do not lead to significant better results. The framework of the LCT is described in more detail in chapter 3.1.2.

The LCT was already successfully applied for the calculation of binary LLE of hyperbranched polymer solutions⁶⁰⁻⁶², where the self-association of the hyperbranched polymer and the cross association between hyperbranched polymer and polar solvent was considered by CALM⁶³ and ECALM⁶⁴, respectively. Besides the chemical association models CALM and ECALM, the LCT was also combined with a modified Wertheim theory^{65,66} in order to calculate binary LLE of hyperbranched polymer solutions⁶⁷. While the aforementioned works considered the hyperbranched polymer as monodisperse, Enders and Browarzik⁶⁸ described how the polydispersity of the polymer can be considered within the calculations. By additionally combining the model with a density gradient theory (DGT) approach, the interfacial tension as well as the concentration profiles within the interface can be calculated^{62,67}. Based on a quantitative description of the binary LLE it was then shown in literature that ternary LLE of hyperbranched polymer solutions can be predicted based on the binary subsystems in good agreement to experimental data⁶⁹⁻⁷¹. Likewise hyperbranched polymer solutions, the LLE as well as the interfacial tension of aqueous two-phase systems can be calculated by the LCT in combination with an association model⁷²⁻⁷⁴.

Besides the calculation of LLE, the LCT was also applied for the calculation of SLE. Fischlschweiger et al.⁷⁵ applied the LCT in combination with ECALM for the calculation of binary SLE of linear and branched amino acids dissolved in water. Fischlschweiger and Enders⁷⁶ showed that the LCT is also able to calculate the SLE of binary alkane mixtures, where the alkanes have much shorter chain lengths, ranging from 6 to 24 carbon atoms, than hyperbranched polymers, which were mainly investigated with the LCT so far. As already mentioned in the introduction, there are systems where a superposition of LLE and SLE can

be observed. Langenbach et al.⁷⁷ calculated this superposition for the binary system containing polyethylene and diphenyl ether considering the semi-crystallinity of the polymer. Goetsch et al.⁷⁸ applied the LCT in combination with ECALM in order to calculate the superposition of LLE and SLE for binary solutions of a hyperbranched polymer and an alcohol. They showed a good agreement of calculation and experiments for both phase equilibria applying only one set of model parameters.

While for the description of LLE as well as SLE an incompressible version of the LCT is suitable since pressure has no significant influence on these phase equilibria, a compressible version of the LCT has to be applied for the calculation of vapor-liquid equilibria or processes that are conducted in gaseous phase. By introducing voids as additional component, Langenbach et al.⁷⁹ developed the LCT – equation of state (LCT-EOS) for pure components, which was afterwards extended to multi-component systems^{80,81}. The LCT-EOS was applied for the calculation of vapor pressures of linear and branched alkanes as well as for the calculation of binary VLE, where a good agreement between calculation and experiments was observed. Zimmermann et al.⁴³ applied the LCT-EOS in combination with the density functional theory (DFT) to calculate the adsorption of linear and branched alkanes on porous solids. This approach is a powerful tool since it offers the possibility of predicting pure component adsorption isotherms of branched molecules as well as adsorption isotherms of systems containing linear and branched molecules by only using model parameters that were fitted to linear component data.

The last sections prove that the LCT is a suitable model for the calculation of LLE and SLE as well as for the superposition of LLE and SLE of systems containing branched molecules. In chapter 2.2, it was shown that other models are not suitable for this task. Group contribution methods like UNIFAC are not able to differentiate between different isomers leading to the same predictions for different isomers neglecting the influence of branching on the phase equilibria. As shown in Figure 4, large deviations between experiments and predictions can be observed. COSMO-based models are superior to group contribution methods since they are able to differentiate between isomers. As illustrated in Figure 5 the effect of branching is considered qualitatively correct within these models. However, they are also not able to give quantitative correct predictions of phase equilibria containing branched molecules. In contrast to UNIFAC and COSMO, which predict phase equilibria without experimental data, the LCT does not go without experimental data. Experiments with linear molecules can be used for the

prediction of phase equilibria of systems containing branched molecules, which offers great potential.

Besides the work of Fischlschweiger and Enders⁷⁶, only LLE and SLE of large molecules like hyperbranched polymers were investigated in literature. In this work, the LCT will be applied to systems containing smaller molecules. Therefore, a methodology for predicting LLE and SLE of systems containing branched molecules will be developed where experiments with linear molecules will be used for the adjustment of model parameters (chapter 3.2). It is important that the methodology is able to consider small changes in molecular architecture in order to be universally applicable. The systems shown in Figure 4 and Figure 5 will be used to prove this requisite. Additionally, the model should be able to calculate LLE and SLE simultaneously meaning that only one set of model parameters is applied for the calculation of both phase equilibria. Both requisites have to be fulfilled for the development of crystallization processes.

Regarding the development of adsorption processes Zimmermann et al.⁴³ already introduced a powerful tool for predicting adsorption isotherms of systems containing branched molecules. However, the combination of LCT and DFT offers a high numerical effort, wherefore it is not applicable in process simulation. Therefore, a new model for the description of adsorption isotherms based on the LCT that is applicable in process simulation will be developed in this work. It will be applied to the liquid phase adsorption of binary alkane mixtures.

3 Theoretical Framework

In the first part of this chapter, the thermodynamic background of this work will be presented. The well-known Flory-Huggins theory will be described first. Then, the Lattice Cluster Theory, which was used for all calculations in this work, will be introduced. For systems showing association, an additional association model has to be used. Here, the Chemical Association Lattice Model for self-association and the Extended Chemical Association Lattice Model for cross-association will be presented. Last part of the thermodynamic background is the density gradient theory. It will be used in this work for the calculation of interfacial tensions.

In the second part of this chapter, the developed models for crystallization and adsorption processes will be introduced. Within the crystallization part, a methodology for predicting phase equilibria of systems containing branched molecules will be described. This methodology is based on the combination of Lattice Cluster Theory and an association model. Regarding the adsorption, a completely new model for calculating adsorption isotherms will be presented. Besides adsorption isotherms, the new model also considers the swelling of the adsorbent.

The scientific work published in this chapter was performed by T. Goetsch. Scientific advice was given by T. Zeiner. Parts of this chapter have been published in:

T. Goetsch, P. Zimmermann, R. van den Bongard, S. Enders, T. Zeiner: "Superposition of Liquid-Liquid and Solid-Liquid Equilibria of Linear and Branched Molecules: Binary Systems" *Ind. Eng. Chem. Res.* 55 (2016) 11167.

T. Goetsch, P. Zimmermann, R. van den Bongard, S. Enders, T. Zeiner: "Superposition of Liquid-Liquid and Solid-Liquid Equilibria of Linear and Branched Molecules: Ternary Systems" *Ind. Eng. Chem. Res.* 56 (2017) 417.

T. Goetsch, A. Danzer, P. Zimmermann, A. Köhler, K. Kissing, S. Enders, T. Zeiner: "Liquid-Liquid Equilibrium and Interfacial Tension of Hexane Isomers-Methanol Systems" *Ind. Eng. Chem. Res.* 56 (2017) 9743.

Reprinted with permission from the American Chemical Society.

3.1 Thermodynamic background

3.1.1 Flory-Huggins theory

The Flory-Huggins theory (FH), independently developed by Flory⁸² and Huggins⁸³, was one of the first thermodynamic models, which considered the difference in size of the present components. Therefore, a lattice was introduced on which the molecules, assumed as chains of joined segments, are distributed. This can exemplarily be seen in Figure 6 for a binary polymer solution.

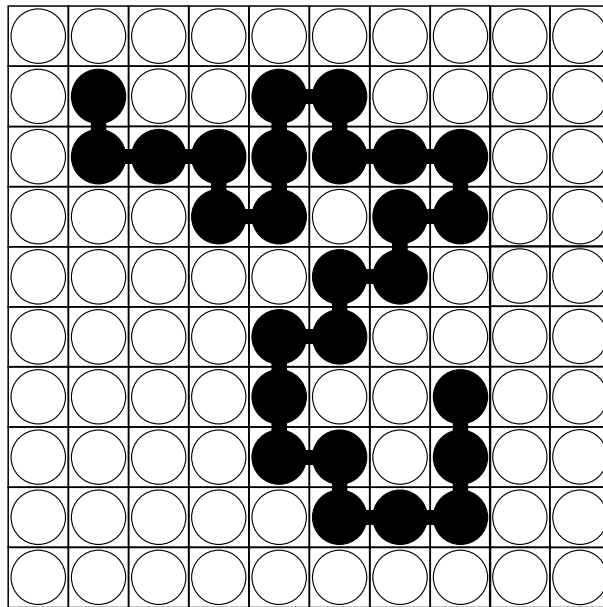


Figure 6: Two dimensional lattice containing a single polymer chain (black segments) and several solvent segments (white segments). Figure adapted from Flory⁸⁴.

The segments of the present components are assumed to have an equal size⁸⁴. Moreover, it was assumed that the components are monodisperse and every segment has got the same number of neighboring segments, which is described by the lattice coordination number z . When inserting another segment to the polymer chain, only the neighboring lattice sites at the front or at the end of the polymer chain are available. Therefore, FH is not able to describe branched molecules. For incompressible systems, an assumption that will be made throughout the entire thesis, thermodynamic properties of the system can be derived by the Gibbs free energy. The Gibbs free energy can be calculated by the enthalpy and entropy of mixing:

$$\Delta G = \Delta H - T\Delta S \quad (3-1)$$

For the entropic contribution, Flory derived the following segment-molar definition, where ϕ_i is the segment fraction of component i ⁸⁴:

$$\Delta S = -R \left(\frac{\phi_1}{N_1} \ln \phi_1 + \frac{\phi_2}{N_2} \ln \phi_2 \right) \quad (3-2)$$

$$\phi_i = \frac{N_i n_i}{\sum_j N_j n_j} \quad (3-3)$$

Regarding the enthalpic contribution to the Gibbs free energy, Eq. (3-4) was proposed by Flory so that the Gibbs free energy of a binary system can be calculated by Eq. (3-5)⁸⁴.

$$\Delta H = \chi \phi_1 \phi_2 \quad (3-4)$$

$$\Delta G = RT \left(\frac{\phi_1}{N_1} \ln \phi_1 + \frac{\phi_2}{N_2} \ln \phi_2 + \chi \phi_1 \phi_2 \right) \quad (3-5)$$

The FH interaction parameter χ can be expressed by $\chi = \frac{z \Delta \varepsilon_{12}}{2k_B T}$, where the interaction energy $\Delta \varepsilon_{12}$ is defined as $\Delta \varepsilon_{12} = \varepsilon_{11} + \varepsilon_{22} - 2\varepsilon_{12}$. Originally, χ was seen as a constant value for a pair of polymer and solvent, but later it could be shown that χ is dependent on temperature, concentration as well as on the molecular mass⁸⁵⁻⁸⁷. One example for an approach covering these dependencies was introduced by Koningsveld and Kleintjens⁸⁸.

However, even in the extended version, FH is only able to consider the direct neighbor of a segment. Therefore, FH cannot account for internal structures of the molecules, which is necessary to describe branching or describe molecules occupying several lattice sites⁵⁴. Moreover, chain correlations between different molecules are ignored⁸⁹. Thus, FH is not suitable for the calculation of systems containing linear and branched molecules. The Lattice Cluster Theory is able to solve these shortcomings and is therefore described in the upcoming section.

3.1.2 Lattice Cluster Theory

As introduced in chapter 2.2.3, the LCT is written as a double series of $1/z$ and $\Delta\varepsilon_{ij}/k_B T$, where z is the lattice coordination number and $\Delta\varepsilon_{ij}/k_B T$ the dimensionless interaction energy. The lattice coordination number was chosen to be 6 for all systems investigated in this work. The interaction energy $\Delta\varepsilon_{ij}$ is defined as:

$$\Delta\varepsilon_{ij} = \varepsilon_{ii} + \varepsilon_{jj} - 2\varepsilon_{ij} \quad (3-6)$$

ε_{ii} and ε_{jj} represent the interaction energy between two segments of type i and j , respectively, whereas ε_{ij} represents the interaction energy between one segment of type i and one segment of type j . Since the LCT is a lattice model like FH, the compositions of the mixture are expressed in terms of segment fractions (Eq. (3-3)).

As already mentioned before, the investigated systems of this work were assumed to be incompressible. Therefore, the Helmholtz free energy is equal to the Gibbs free energy. Written on a segment-molar base for a multicomponent system, the LCT is defined as follows^{89,90}:

$$\frac{\Delta G_s^{LCT}}{RT} = \sum_i \frac{\phi_i}{N_i} \ln \phi_i - \frac{\Delta S}{R} - \frac{\Delta E_1}{RT} - \frac{\Delta E_2}{RT} \quad (3-7)$$

From Eq. (3-7) it can be easily seen that the LCT is based on FH since the first term equals the entropic part of FH (Eq. (3-2)). The other three terms contain corrections to the FH mean field, where ΔS represents the entropic corrections and ΔE_1 and ΔE_2 represent the enthalpic corrections of first and second order, respectively. ΔS , ΔE_1 and ΔE_2 can be derived using the tables I, II and III reported by Dudowicz and Freed⁸⁹ and the corrections made by Dudowicz et al.⁹¹. The exact expressions can be found in literature⁷². To take the molecular architecture into consideration, the LCT offers architecture parameters. Originally, six architecture parameters were supposed to be necessary to define the molecular architecture properly⁹²: the number of bonds $N_{1,i}$, the number of two consecutive bonds $N_{2,i}$, the number of three consecutive bonds $N_{3,i}$, the number of points at which three bonds meet a lattice site $N_{\perp,i}$, the number of ways of selecting two non-sequential bonds on the same chain $N_{1,1,i}$ and the number of ways of selecting two consecutive bonds and one non-sequential bond on the

same chain $N_{1,2,i}$. Later, it could be shown by Langenbach et al.⁹³, that some of the architecture parameters are connected to each other so that a reformulation of the LCT with only the first three architecture parameters is possible. The architecture parameters of the molecules investigated in this work can be found in chapter 5.

The LCT is a further development of FH. Thus, the well-known FH mean field approximation can be recovered when z approaches infinity ($z \rightarrow \infty$). When z increases, the interaction energy $\Delta\varepsilon_{ij}$, which is related to one contact point, decreases but the term $z\Delta\varepsilon_{ij}$, which corresponds to a whole segment stays finite. For the limit of an infinite lattice coordination number $\Delta\varepsilon_{ij}$ vanishes and the only term that remains is the FH parameter $\chi = \frac{z\Delta\varepsilon_{12}}{2k_B T}$.

FH as well as LCT only consider van der Waals interactions. When investigating systems with strongly polar components, like alcohols or ethylene glycol in this work, associative interactions have also to be considered within the thermodynamic modeling. Therefore, the LCT has to be combined with an association model.

3.1.3 Chemical Association Lattice Model

In general, associative interactions can be described by chemical or physical theories. While the physical theory treats hydrogen bonding as strong interactions, chemical theory is based on the mass action law at association equilibrium⁶³. One famous association model based on a physical theory was introduced by Wertheim^{94,95}. Since Wertheim's theory requires a high numerical effort, including an additional iteration, and simpler association models are sufficient for the description of association in this work, CALM developed by Browarzik⁶³ was applied in this work to systems showing only self-association of the solvent.

CALM was developed to describe binary and ternary systems including one associating component. It allows for the calculation of the excess Gibbs energy without numerical iteration. Within CALM, the self-association of the solvent (A) is regarded as a chemical equilibrium:



Two associating chains with degrees r and r' , respectively, are in equilibrium with one chain of degree $r + r'$. This approach leads to a distribution of association chain lengths ranging from 1 to ∞ . Similar to chemical reactions, Browarzik⁶³ introduced the equilibrium association constant K_A , wherein the temperature dependence of the association is described by an Arrhenius approach:

$$K_A = K_{0,A} \exp\left(-\frac{\Delta h_A^{as}}{RT}\right) \quad (3-9)$$

In Eq. (3-9) Δh_A^{as} represents the association enthalpy and $K_{0,A}$ is a pre-exponential factor. Considering the mentioned distribution of association chain lengths, the contribution of CALM to the segment-molar Gibbs energy is defined by:

$$\frac{\Delta G_s^{CALM}}{RT} = -\frac{\phi_A}{N_A} \left(1 + \frac{1}{\tilde{K}_A \phi_A}\right) \ln(1 + \tilde{K}_A \phi_A) + \frac{\phi_A}{N_A} \left(1 + \frac{1}{\tilde{K}_A}\right) \ln(1 + \tilde{K}_A \phi_A); \quad (3-10)$$

$$\tilde{K}_A = K_A \exp(1)$$

3.1.4 Extended Chemical Association Lattice Model

When considering systems containing two associating components, like the investigated binary ethylene glycol (A) / ketone (B) mixtures, CALM is no longer suitable to describe the association of these systems because of an additional cross-association between the two polar components. Therefore, in order to calculate these systems properly, ECALM introduced by Browarzik⁶⁴ was applied. Just like CALM, ECALM also offers a straightforward calculation of the excess Gibbs energy without any iterative procedures. In this work, a modified version of ECALM was applied⁶⁰.

ECALM describes two types of associates, an ensemble of self-associates and an ensemble of cross-associates. The values $P_{AA} = k_{AA} x_A^2$, $P_{AB} = 2k_{AB} x_A x_B$ and $P_{BB} = k_{BB} x_B^2$ denote the probability that a pair of neighboring molecules within a cross-associate is of type ij ($ij = AA, AB, BB$). Based on the parameters k_{ij} the cross association parameters

$\eta_{AA} = k_{AA}/k_{BB}$, $\eta_{AB} = k_{AB}/k_{BB}$ and $\eta_{BB} = k_{BB}/k_{BB} = 1$ can be introduced. In this work, it was assumed that all cross-associates have got the same composition \bar{y}_B , which is given by⁶⁰:

$$\bar{y}_B = x_B \frac{x_A \eta_{AB} + x_B}{x_A^2 \eta_{AA} + 2x_A x_B \eta_{AB} + x_B^2}; \quad \bar{y}_A + \bar{y}_B = 1 \quad (3-11)$$

In Eq. (3-11) x_A and x_B are the mole fractions of the system. In case of $\eta_{AA} = \eta_{AB} = 1$ statistical cross-association occurs ($\bar{y}_B = x_B$). Thus, in this special case, there are no self-associates present in the system. For $\eta_{AA} < \eta_{AB} < 1$ it can be easily shown that the concentration of component (B) within the cross-associate is higher than the concentration in the system ($\bar{y}_B > x_B$). For the investigated ethylene glycol / ketone systems it was assumed that all molecules of the ketone are included in the ensemble of cross-associates. The remaining ethylene glycol forms self-associates.

The parameters η_{AA} and η_{AB} can be handled as adjustable parameters. Due to parameter reduction the following relation of these two quantities was assumed⁶⁰:

$$\eta_{AA} = \eta_{AB}^2 = \eta \quad (3-12)$$

Since ethylene glycol (A) as well as the ketone (B), are polar components, an association constant according to Eq. (3-9) can be defined for both components. These two association constants are then used for calculating the cross-association constant as proposed by Browarzik⁶⁴.

$$\ln \tilde{K}^{(ca)} = \bar{y}_A \ln K_A + \bar{y}_B \ln K_B \quad (3-13)$$

As the Gibbs free energy is defined in terms of the segment fraction, the cross-association constant has also to be written in terms of the segment fraction⁶⁰:

$$\ln \tilde{K}^{(ca)} = \frac{\phi_A N_A}{\phi_A N_B \eta + \phi_B N_A} \ln \tilde{K}_A + \frac{\phi_B N_A}{\phi_A N_B \eta + \phi_B N_A} \ln \tilde{K}_B \quad (3-14)$$

Based on the theory described above the contribution of the association to the Gibbs free energy can be expressed by:

$$\begin{aligned}
 \frac{\Delta G_s^{ECALM}}{RT} = & -\frac{\phi_A}{N_A}(1-\eta) \left[1 + \frac{1}{\tilde{K}_A \phi_A (1-\eta)} \right] \ln [1 + \tilde{K}_A \phi_A (1-\eta)] \\
 & - \left(\frac{\phi_A}{N_A} \eta + \frac{\phi_B}{N_B} \right) \left[1 + \frac{1}{\tilde{K}^{(ca)} (\phi_A \eta + \phi_B)} \right] \ln [1 + \tilde{K}^{(ca)} (\phi_A \eta + \phi_B)] \\
 & + \frac{\phi_A}{N_A} [\eta \ln \eta + (1-\eta) \ln (1-\eta)] + \frac{\phi_A}{N_A} C_A + \frac{\phi_B}{N_B} C_B \\
 & + \frac{\phi_A \phi_B \eta (Z_{OH} - 1)}{\phi_A N_B \eta + \phi_B N_A Z_{OH}} \ln \left(\frac{\tilde{K}_B}{\tilde{K}_A} \right)
 \end{aligned} \tag{3-15}$$

The parameters C_A and C_B are given by:

$$C_A = (1-\eta) \left\{ \left[1 + \frac{1}{\tilde{K}_A (1-\eta)} \right] \ln [1 + \tilde{K}_A (1-\eta)] - \ln (1-\eta) \right\} \tag{3-16}$$

$$+ \eta \left[\left(1 + \frac{1}{\tilde{K}_A \eta} \right) \ln (1 + \tilde{K}_A \eta) - \ln \eta \right]$$

$$C_B = \left(1 + \frac{1}{\tilde{K}_B} \right) \ln (1 + \tilde{K}_B) \tag{3-17}$$

3.1.5 Density Gradient Theory

The DGT is applied in this work for calculating the interfacial tension and interfacial concentration profiles of binary systems containing one of four hexane isomers and methanol. Within the DGT, the Helmholtz free energy is expanded having the molar density and its derivate as independent variables. The systems investigated in this work are assumed to be incompressible wherefore the Helmholtz free energy is replaced by the Gibbs free energy. For this case, concentration is the only variable changing over the interface. Therefore, the Gibbs

free energy is expanded in terms of concentration gradients. Assuming that the concentration only changes perpendicular to the interface, the series expansion (truncated at second order) reads as⁹⁶:

$$G = NI_0 \int_{-\infty}^{+\infty} \left[g_0(X) + \kappa \left(\frac{dX}{dz} \right)^2 \right] dz \quad (3-18)$$

The first contribution $g_0(X)$ corresponds to the Gibbs free energy of a homogeneous solution. The second contribution $\kappa \left(\frac{dX}{dz} \right)^2$ represents a gradient energy depending on the derivative of the local concentration, where κ is the so-called influence parameter. Applying this series expansion, reformulating the concentration into segment fractions, lead to Eq. (3-19) for the calculation of the interfacial tension⁹⁷, where $\Delta\Omega$ represents the grand thermodynamic potential (Eq. (3-20)).

$$\sigma = \int_{\phi_A^I}^{\phi_A^{II}} \sqrt{2\kappa\Delta\Omega(\phi_A)} d\phi_A \quad (3-19)$$

$$\Delta\Omega = \Delta G_s - \sum_{i=1}^2 (\mu_i \phi_i)^{Eq} \quad (3-20)$$

The interfacial concentration profile is defined by Eq. (3-21).

$$z - z_0 = \frac{1}{\Delta\rho^{Eq}} \int_{\phi_{A,0}}^{\phi_A} \sqrt{\frac{2\kappa}{\Delta\Omega}} d\phi_A \quad (3-21)$$

Within Eq. (3-21) $\Delta\rho^{Eq}$ represents the difference in density between the two bulk phases in equilibrium. z_0 denotes an arbitrarily selectable origin and $\phi_{A,0}$ represents the corresponding composition. In this work, $z_0 = 0$ related to $\phi_{A,0} = (\phi_A^I + \phi_A^{II})/2$ was selected. The influence parameter κ is fitted to one data point of the interfacial tension and remains constant for Eqs. (3-19) and (3-21). Since in this work a g^E-model was applied, $\Delta\rho^{Eq}$ is not accessible, wherefore Eq. (3-21) is solved for $z \cdot \Delta\rho^{Eq}$. This is done numerically for compositions ϕ_A lying in between the bulk concentrations of phase I and II.

3.2 Model development

3.2.1 Crystallization

In order to design a crystallization process for the separation of isomers dissolved in a solvent, it has to be known whether an oiling out will occur. Therefore, the LLE as well as the SLE of the system has to be known. Concerning the calculation of the SLE, it was assumed that the solid phase is composed of the pure substance. Differences in heat capacities of the solid and the liquid phase were neglected. Applying these assumptions the SLE can be calculated as follows¹³:

$$\frac{\Delta\mu_i(T, \phi_i)}{RT} = -\frac{\Delta h_i^{SL}}{RT} \left(1 - \frac{T}{T_i^{SL}} \right) \quad (3-22)$$

$\Delta\mu_i$ represents the difference in chemical potential of component i in solution and in its pure state. Δh_i^{SL} and T_i^{SL} denote the enthalpy of fusion and the melting temperature of component i , respectively, which can both be measured by differential scanning calorimetry (DSC).

In case of an oiling out during the crystallization process, an additional LLE between solvent and isomers has to be considered. The LLE can be calculated applying standard thermodynamics, meaning that the chemical potential of each component has to be the same in both phases:

$$\mu_i^I = \mu_i^{II} \quad (3-23)$$

For the calculation of the chemical potential within Eqs. (3-22) and (3-23), adjustable parameters of the LCT and the used association model have to be fitted to experimental data. In general, experimental LLE as well as SLE could be used for this adjustment. Since the LLE is more sensitive towards different model parameters, it was used for the adjustment in this work. While LLE data between the linear isomer and the solvent are usually available, experimental data of the branched isomers are often not available. To overcome this limitation, a methodology, which enables the prediction of LLE of systems containing branched isomers, was developed in this work. An overview of the methodology is shown in Figure 7.

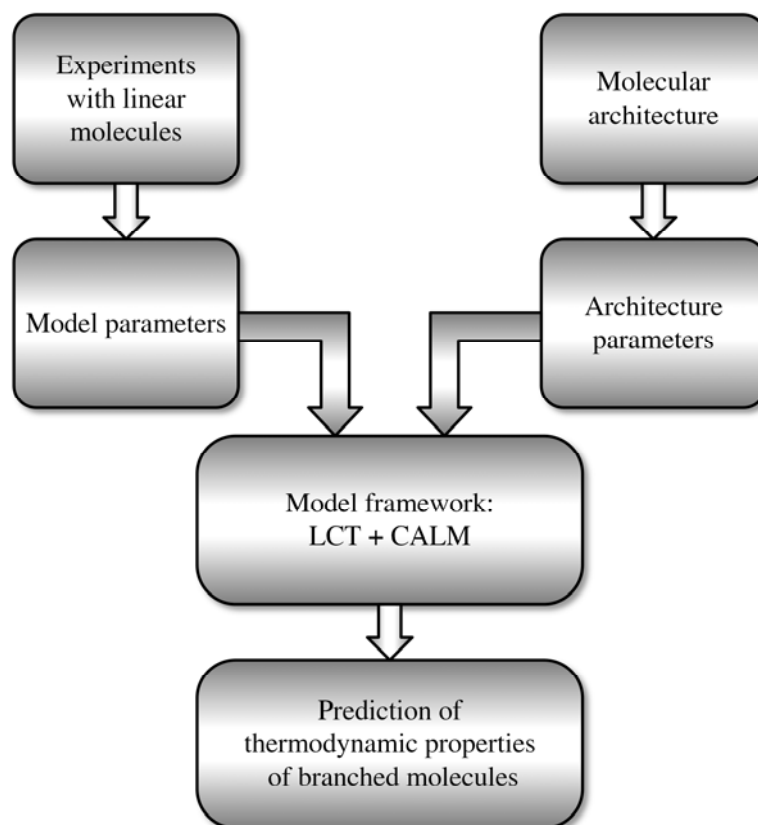


Figure 7: Overview of the methodology for the prediction of phase equilibria of branched molecules.

Basic idea of the developed methodology is to only perform experiments with linear molecules. The experimental results are then used to fit the necessary model parameters. Afterwards, the fitted model parameters are combined with the a-priori known architecture parameters, which were determined from the molecular architecture, in order to predict the LLE of systems containing the branched isomers.

For the prediction of a binary LLE between a branched non-polar molecule and a polar solvent showing self-association, three model parameters in total have to be known, i.e. the interaction energy $\Delta\varepsilon_{ij}/k_B$ defined within the LCT and the two association parameters Δh_i^{as} and K_{0i} of CALM. As the two association parameters of CALM only refer to the self-association of the solvent, they remain constant for all systems containing the same solvent regardless of whether the solute is linear or branched. Hence, Δh_i^{as} and K_{0i} can be adjusted to any binary LLE containing the desired solvent. According to investigations in literature, the interaction energy $\Delta\varepsilon_{ij}/k_B$ refers to the interaction between solvent and solute and is dependent on the chain length of the solute^{76,98}. Thus, the interaction energy $\Delta\varepsilon_{ij}/k_B$ between

a linear isomer and a solvent cannot be assigned to the corresponding branched isomer, which was mentioned in the introduction as one possibility. Second possibility mentioned is an extrapolation within a homologue series, where the dependence of chain length and interaction energy is used. Therefore, it was assumed that the interaction energy $\Delta\varepsilon_{ij}/k_B$ between a branched isomer and a solvent can be estimated by the length of the backbone of the branched isomer. So, the interaction energy $\Delta\varepsilon_{ij}/k_B$ between a linear molecule and a solvent can be assigned to any pair of branched molecule and solvent, where the backbone length of the branched molecule equals the length of the linear molecule. To reduce the experimental effort, an extrapolation function between interaction energy $\Delta\varepsilon_{ij}/k_B$ and chain length can be set up. Therefore, the interaction energy $\Delta\varepsilon_{ij}/k_B$ has to be fitted at least for three binary systems in order to give a reliable statement about the course of this extrapolation function.

For a ternary system containing solvent (1), branched isomer (2) and linear isomer (3), the following procedure was applied in this work (Figure 8).

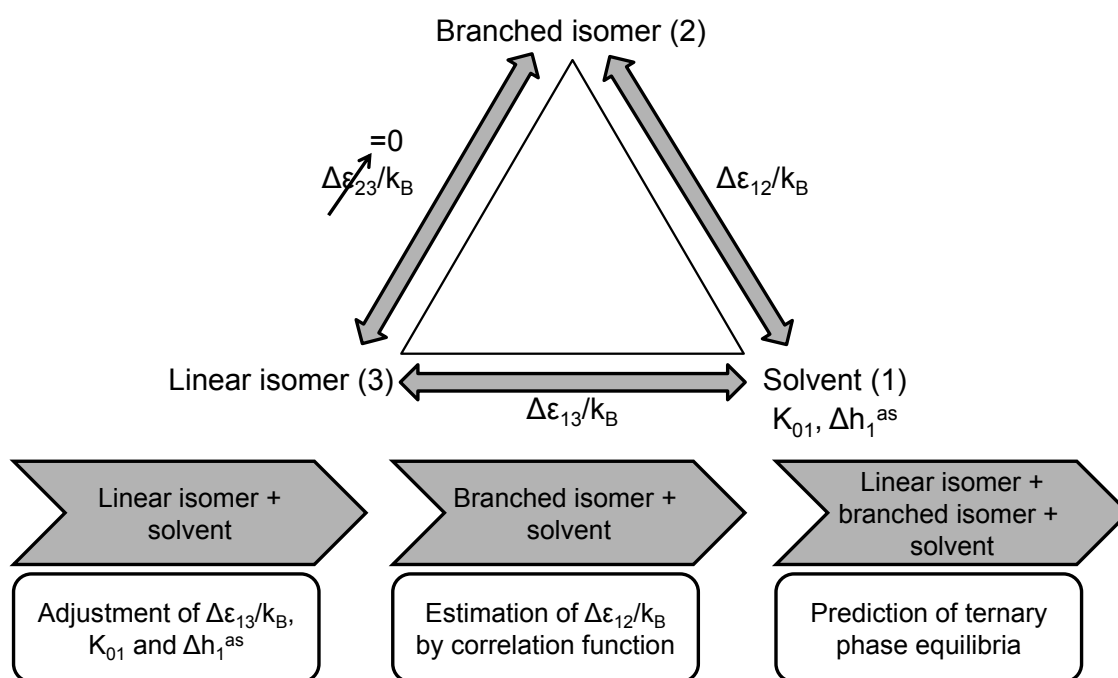


Figure 8: Procedure of defining model parameters for a ternary system containing solvent, branched isomer and linear isomer.

First of all, the two association parameters Δh_1^{as} and K_{01} of the solvent as well as the interaction energy $\Delta\varepsilon_{13}/k_B$ between solvent and linear isomer are simultaneously fitted to

LLE data of one binary system. Subsequently, the interaction energy is fitted for two more systems in order to set up an extrapolation function between interaction energy and chain length. Since the solvent is not switched in these systems, Δh_i^{as} and K_{0i} remain at the value that was obtained for the first system. The extrapolation function is then used in the second step to estimate the interaction energy $\Delta \varepsilon_{12} / k_B$ between solvent and branched isomer. Using the estimated interaction energy, the binary LLE between solvent and branched isomer can be predicted. The predicted LLE are compared with experimental data and evaluated in terms of mass fraction and temperature by the average relative deviation (*ARD*):

$$ARD[\%] = 100 \times \frac{1}{n_{data}} \sum_{i=1}^{n_{data}} \min \sqrt{\left(\frac{w_{exp,i} - w_{calc,i}}{w_{exp,i}} \right)^2 + \left(\frac{T_{exp,i} - T_{calc,i}}{T_{exp,i}} \right)^2} \quad (3-24)$$

In a third step, the ternary phase equilibria are predicted based on the binary subsystems. Thereby, the interaction energy $\Delta \varepsilon_{23} / k_B$ between linear and branched isomer is set to zero because both molecules belong to the same class of chemicals.

In case of predicting the binary LLE of systems showing cross-association, a slightly different procedure has to be applied. Here, six model parameters in total have to be known, i.e. the interaction energy $\Delta \varepsilon_{ij} / k_B$ defined within the LCT, the two association parameters Δh_i^{as} and K_{0i} for each of the two components and the parameter η , defining the ratio of cross-association to self-association. In this work, binary LLE between ketones and ethylene glycol were investigated. Since ketones are only slightly polar, it was assumed that their association enthalpy Δh_i^{as} is equal to zero. This means, that they are not able to perform self-association but in presence of a highly polar solvent like ethylene glycol, they are able to perform cross-association. A similar treatment of cross-association was also done in literature^{64,99}. Ethylene glycol contains hydroxyl groups. Since the association enthalpy is assumed to only refer to the hydroxyl group but not to the rest of the molecule, the value that was fitted before for alcohol molecules will be used also for ethylene glycol. The remaining 4 model parameters have to be fitted to LLE data of the linear ketone and ethylene glycol. Afterwards, the interaction energy $\Delta \varepsilon_{ij} / k_B$ between the branched ketone and ethylene glycol was determined by the length of the backbone as described above. The association parameters Δh_i^{as} and K_{0i} of ethylene glycol remain constant since the solvent was not switched. Regarding the association parameter K_{0i}

of the linear ketone and the cross-association parameter η , it was assumed that they can also be applied for the prediction of the binary LLE of the branched ketone.

3.2.2 Adsorption

For the calculation of liquid phase adsorption isotherms of binary mixtures containing a linear and a branched alkane, a new model was developed in this work. This model is based on the real adsorbed solution theory (RAST), where an activity coefficient is introduced for bulk phase and adsorbed phase. Contrary to earlier works^{100,101} applying RAST, this model also considers the swelling of the adsorbent in order to account for expansion or contraction of the adsorbent, which can be caused by solid-fluid interactions¹⁰². Commonly applied adsorption isotherms like Langmuir do not consider the individual structure of the present molecules. Therefore, the LCT is applied for the calculation of the liquid phase adsorption in order to take the molecular structure into account. The liquid phase adsorption takes place on porous adsorbents as shown in Figure 9.

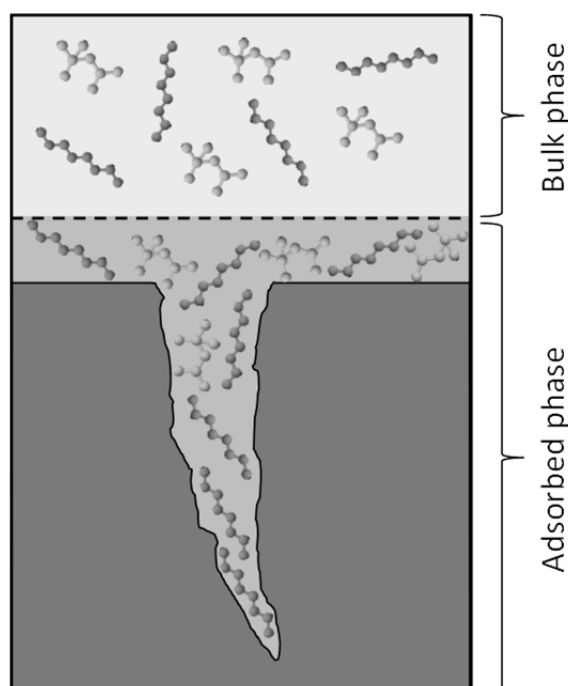


Figure 9: Concept of liquid phase adsorption on porous solids.

It can be seen in Figure 9 that the solid adsorbent is assumed to only be present in the adsorbed phase. Besides the solid adsorbent, the adsorbed phase contains all molecules adsorbed within the pores and on the surface of the adsorbent. The bulk phase is assumed to contain all molecules that are not adsorbed. Within the new model, the solid adsorbent is

treated as an additional component. Thus, for the calculation of the binary adsorption isotherm, the ternary system containing linear alkane (A), adsorbent (B) and branched alkane (C) is regarded. A similar approach, i.e. treating the adsorbent as additional component was already presented in literature¹⁰³. Regarding the calculation of the binary adsorption isotherms, it was assumed that bulk phase and adsorbed phase are in equilibrium. Thus, the chemical potentials of the components must be equal in both phases:

$$\mu_{linear}^{bulk\ phase} = \mu_{linear}^{adsorbed\ phase} + \Delta\mu_{Network} \quad (3-25)$$

$$\mu_{branched}^{bulk\ phase} = \mu_{branched}^{adsorbed\ phase} + \Delta\mu_{Network} \quad (3-26)$$

Because of the adsorption of molecules, the adsorbent will gain weight. In order to describe this mass uptake, the adsorbent is treated as a network, which is able to swell. This effect is considered in Eqs. (3-25) and (3-26) by the term $\Delta\mu_{Network}$. The gravimetric degree of swelling is defined as follows:

$$Degree\ of\ Swelling = \frac{m_{adsorbent}^{final}}{m_{adsorbent}^{begin}} \quad (3-27)$$

There are several approaches for describing swelling networks in literature. Two of the most widely used theories are the phantom network theory¹⁰⁴ and the affine network theory⁸⁴. The adsorbents investigated in this work are supposed to not swell that much, wherefore the affine network theory was applied in this work:

$$\Delta\mu_{Network} = RT \cdot c_{Network} \cdot \left(\phi_{Adsorbent}^{1/3} - \frac{\phi_{Adsorbent}}{2} \right) \quad (3-28)$$

$c_{Network}$ is an adjustable parameter, which has to be fitted to experimental swelling data. Additionally, a mass balance was included in the new model. For this purpose, the phase ratio PR between adsorbed phase and the feed was introduced:

$$PR = \frac{m^{adsorbed\ phase}}{m^{Feed}} \quad (3-29)$$

For a three component system, two component balances are sufficient to describe the overall mass balance:

$$w_{linear}^{Feed} = w_{linear}^{bulk\ phase} \cdot (1 - PR) + w_{linear}^{adsorbed\ phase} \cdot PR \quad (3-30)$$

$$w_{Adsorbent}^{Feed} = w_{Adsorbent}^{adsorbed\ phase} \cdot PR \quad (3-31)$$

Combining the condition of equal chemical potentials (Eqs. (3-25) and (3-26)) and the component balances (Eqs. (3-30) and (3-31)) lead to a system of 4 equations, which must be solved simultaneously. In addition to $c_{Network}$, the interaction energy $\Delta\varepsilon_{AB}/k_B$ between adsorbent and linear alkane as well as the interaction energy $\Delta\varepsilon_{BC}/k_B$ between adsorbent and branched alkane are two more adjustable parameters. The interaction energy $\Delta\varepsilon_{AC}/k_B$ between linear and branched alkane was set to zero. For the adjustment of the three adjustable parameters ($c_{Network}$, ε_{AB}/k_B , ε_{BC}/k_B) the following procedure was applied. All three model parameters were simultaneously fitted to experimental adsorption isotherm data as well as swelling data for the binary system n-octane + 2,2,4-trimethylpentane at one particular temperature. Afterwards, the network parameter $c_{Network}$ remained constant at this value for all other temperatures since it is assumed to not depend on temperature. In contrast to the network parameter $c_{Network}$, the interaction energies $\Delta\varepsilon_{ij}/k_B$ are dependent on temperature and were adjusted subsequently to adsorption isotherm data for different temperatures. When switching the system to n-hexane + 2,3-dimethylbutane, the network parameter $c_{Network}$ was still fixed to the adjusted value because it was assumed that the adsorbent behaves similar than for the system n-octane + 2,2,4-trimethylpentane. Thus, only the two interaction energies $\Delta\varepsilon_{ij}/k_B$ were adjusted for every temperature.

For the description of the adsorbent network, a segment number of 500 was assumed. This assumption was taken, because the influence of the chain length on the adsorption should be neglected and with this or higher chain lengths there is no impact on the modeled adsorption observed.

4 Materials and Methods

In this chapter, all materials that were used in this work will be introduced. After the materials section, the experimental procedures applied in this work will be mentioned. The last section of this chapter contains all analytical methods applied in this work.

The scientific work published in this chapter was performed by T. Goetsch and supported by R. van den Bongard, A. Köhler, J. Hönig, B. Scharzec and K. Kissing in the framework of a bachelor thesis or a master thesis. Scientific advice was given by T. Zeiner. Parts of this chapter have been published in:

T. Goetsch, P. Zimmermann, R. van den Bongard, S. Enders, T. Zeiner: "Superposition of Liquid-Liquid and Solid-Liquid Equilibria of Linear and Branched Molecules: Binary Systems" *Ind. Eng. Chem. Res.* 55 (2016) 11167.

T. Goetsch, P. Zimmermann, R. van den Bongard, S. Enders, T. Zeiner: "Superposition of Liquid-Liquid and Solid-Liquid Equilibria of Linear and Branched Molecules: Ternary Systems" *Ind. Eng. Chem. Res.* 56 (2017) 417.

T. Goetsch, A. Danzer, P. Zimmermann, A. Köhler, K. Kissing, S. Enders, T. Zeiner: "Liquid-Liquid Equilibrium and Interfacial Tension of Hexane Isomers-Methanol Systems" *Ind. Eng. Chem. Res.* 56 (2017) 9743.

Reprinted with permission from the American Chemical Society.

4.1 Materials

4.1.1 LLE and SLE experiments

In this work LLE and SLE experiments for different binary and ternary systems were performed. All chemicals that were used are listed in Table 4 including their CAS number, supplier, molar purity and the experiment they were used in. Ethanol and methanol were stored together with molecular sieves by Merck having pore sizes of 3 Å. All other chemicals were used without further purification.

Table 4: Chemicals used for LLE and SLE experiments.

Chemical Name	CAS #	Source	Molar purity	Used for
Ethanol	64-17-5	VWR	1.000*	Ternary LLE
Ethanol	64-17-5	Merck	0.990*	Binary SLE, ternary SLE
Methanol	67-56-1	Alfa Aesar	0.999*	Binary LLE
n-hexane	110-54-3	Merck	0.990	Binary LLE
2-methylpentane	107-83-5	Sigma Aldrich	0.990	Binary LLE
3-methylpentane	96-14-0	Sigma Aldrich	0.990	Binary LLE
2,3-dimethylbutane	79-29-8	Sigma Aldrich	0.980	Binary LLE
n-hexadecane	544-76-3	Sigma Aldrich	0.990	Binary SLE
n-hexadecane	544-76-3	Amresco	0.990	Ternary LLE
HMN [#]	4390-04-9	Sigma Aldrich	0.980	Ternary LLE, ternary SLE
Ethylene glycol	107-21-1	Sigma Aldrich	0.998	Binary LLE
2-pentanone	107-87-9	Alfa Aesar	0.990	Binary LLE
2-hexanone	591-78-6	Alfa Aesar	0.980	Binary LLE
3-methyl-2-butanone	563-80-4	Sigma Aldrich	0.990	Binary LLE
4-methyl-2-pentanone	108-10-1	Alfa Aesar	0.990	Binary LLE
Dibutyl ether	142-96-1	Alfa Aesar	0.990	Internal standard
Toluene	108-88-3	VWR	0.995	Internal standard

*Purity checked by Karl-Fischer titration

[#]2,2,4,4,6,8,8-heptamethylnonane

4.1.2 Interfacial tension

The interfacial tension of three binary systems containing a hexane isomer and methanol was measured with methanol purchased from Sigma Aldrich with a purity of 99.8% (checked by Karl-Fischer titration). The three hexane isomers were the same as for the investigation of binary LLE (Table 4). The pure components were degassed with an ultrasonic bath Bandelin Sonorex Super RK510 before measuring the interfacial tension.

4.1.3 Adsorption isotherms

Binary adsorption isotherms were determined for the systems n-hexane / 2,3-dimethylbutane and n-octane / 2,2,4-trimethylpentane. The chemicals used for these experiments as well as for the analysis are listed in Table 5.

Table 5: Chemicals used for adsorption experiments.

Chemical Name	CAS #	Source	Molar purity	Used for
n-hexane	110-54-3	Merck	0.990	Adsorption isotherm
2,3-dimethylbutane	79-29-8	Alfa Aesar	0.980	Adsorption isotherm
n-octane	111-65-9	Acros Organics	0.990	Adsorption isotherm
2,2,4-trimethylpentane	540-84-1	Sigma Aldrich	0.990	Adsorption isotherm
Dibutyl ether	142-96-1	Alfa Aesar	0.990	Internal standard
Toluene	108-88-3	VWR	0.995	Internal standard

As porous adsorbents, activated carbon, silica gel and zeolite were used. Activated carbon was purchased in form of pellets from VWR International. These pellets offer smaller surfaces in comparison to powder, however because of a better handling they were used in this work. Silica gel was purchased as a powder from Sigma Aldrich and the zeolite was purchased from Merck in spherical shape. A main property of the adsorbent influencing the separation efficiency is the pore size distribution. It was measured by TU Berlin for the three adsorbents by volumetric nitrogen adsorption technique.

4.2 Experimental procedures

4.2.1 Liquid-liquid equilibrium

Binary systems

The binary LLE of the investigated systems were measured by cloud-point experiments as well as by measuring tie lines. In order to perform the cloud-point experiments, binary mixtures were prepared and placed in a temperature-controlled water bath for 30 minutes. In a preliminary experiment it was shown that all systems possess an UCST behavior. In the beginning of the cloud-point experiments, the temperature, which can be adjusted with an accuracy of ± 0.1 K, was chosen higher than the UCST of the respective system so that all mixtures were clear at this point. Afterwards, the mixtures were cooled down by 0.5 K within 10 minutes and it was checked whether the mixtures stayed clear or became turbid. This procedure was repeated until all mixtures became turbid, which indicates the liquid-liquid phase transition. After all mixtures were turbid, the mixtures were heated up gradually by 0.5 K within 10 minutes until all mixtures were clear again. The principal of this measurement technique is illustrated in Figure 10.

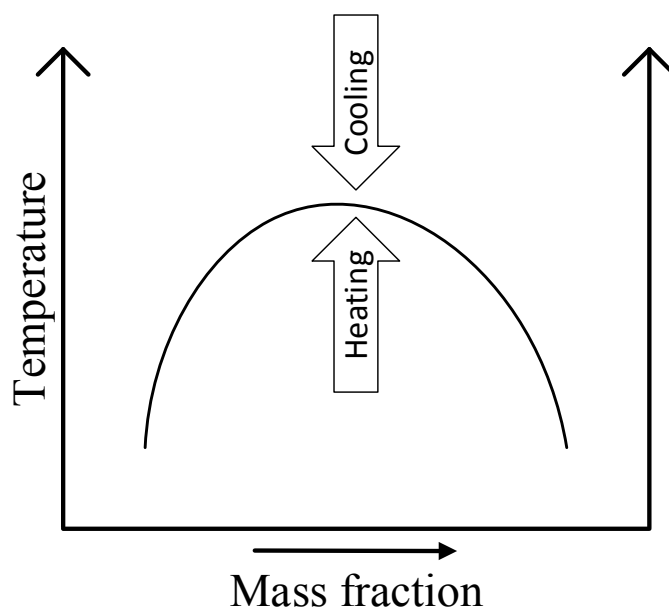


Figure 10: Principal of measuring cloud-points of binary systems.

Ideally, the temperature of phase transition should be the same in both cases. Here, the temperatures from the heating runs were always 0.5 K higher than the temperatures from the cooling runs. Having in mind that the temperature was changed in steps of 0.5 K, the measurements show a good accuracy. For further evaluation, the mean value of heating and cooling run was considered.

To approve the cloud-point experiments, tie lines of the binary system were measured for different temperatures additionally. Therefore, binary samples of known composition were prepared and placed in the temperature-controlled water bath. Here, they were first stirred for 1 hour. After stirring, the mixture separated into two phases. The equilibrium between the liquid phases was assumed to be reached after 24 hours, which was experimentally proven. Upper and lower phase were separated from each other using a syringe and were weighed afterwards. This procedure was done to check the phase ratio that is given by the gas chromatograph (GC). Then, samples of upper and lower phase were taken and the composition of both phases were analysed by GC as outlined in chapter 4.3.1.

Ternary systems

Also for the ternary systems investigated in this work, cloud-point experiments as well as GC analytics were performed, where the procedure of the cloud-point experiments was different in comparison to the procedure for binary systems. First, binary mixtures were prepared and placed in the temperature-controlled water bath for 30 minutes. All mixtures were clear at this point. Afterwards, an amount of 0.015 g of the third component was added to each mixture and it was checked after 2 minutes whether the mixtures became turbid or stayed clear. This procedure was repeated until all mixtures turned turbid, which indicates the liquid-liquid phase transition.

The measurement of ternary tie lines was basically performed in the same way as for binary samples. After preparing ternary samples of known composition and stirring for 1 hour, equilibration was reached after 24 hours. Then, samples of upper and lower phase were taken and analyzed by GC as described in chapter 4.3.1. Again, upper and lower phase were weighed in order to check the phase ratio that is given by the GC.

4.2.2 Solid-liquid equilibrium

Binary systems

In literature, no binary SLE data of the system n-hexadecane + methanol were available, wherefore this binary SLE was measured by DSC using a Seteram μ -DSCVII Evo in this work. The DSC plots were analyzed using the Calisto analyzing software. First of all, pure n-hexadecane was analyzed in order to determine the melting temperature and the enthalpy of fusion. An amount of 61.62 mg n-hexadecane was weighed with an accuracy of 0.01 mg into the DSC cell. The reference cell was filled with air for all measurements. After equilibration a heating run and a cooling with a temperature rate of 0.1 K min^{-1} was performed. The results of the heating and the cooling runs are shown in Figure 11.

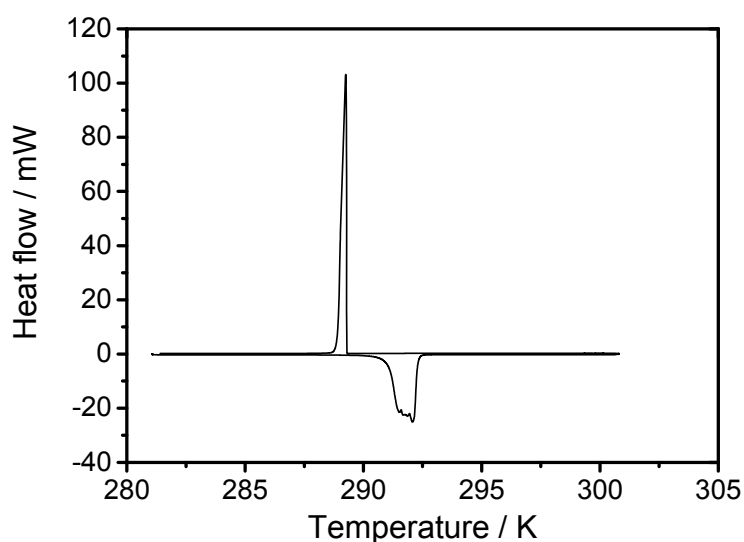


Figure 11: DSC heating (negative heat flows) and cooling (positive heat flows) curves of pure n-hexadecane.

The melting temperature can be read at the onset temperature, defined as the intersection of the tangent through the inflection point with the base line. A melting temperature of 291.07 K was determined in this work. This value corresponds well with values published in literature (291.34 K)¹⁰. The enthalpy of fusion was determined by integrating the corresponding melting peak to be 52433 J mol^{-1} . Again, this value agrees well with literature data (53359 J mol^{-1})¹⁰⁵.

After successfully validating the experimental procedure, the SLE of the binary system n-hexadecane + ethanol was determined. Mixtures of n-hexadecane and ethanol of different concentrations were prepared. Since within the cloud-point curve the temperature of the SLE does not change, the SLE of this system was only measured outside the already known LLE. Again, amounts of approximately 60 mg were weighed into the DSC cell and the same experimental procedure was applied to all samples.

Ternary systems

The ternary SLE was determined in a similar way than the determination of the ternary binodal curve. At first, binary mixtures of 2,2,4,4,6,8,8-heptamethylnonane + ethanol were prepared (Figure 12). Because the SLE does not change within the miscibility gap, the already known ternary LLE was exploited such that only mixtures with very high and very low concentrations of ethanol were prepared in order to measure the ternary SLE exclusively outside the miscibility gap.

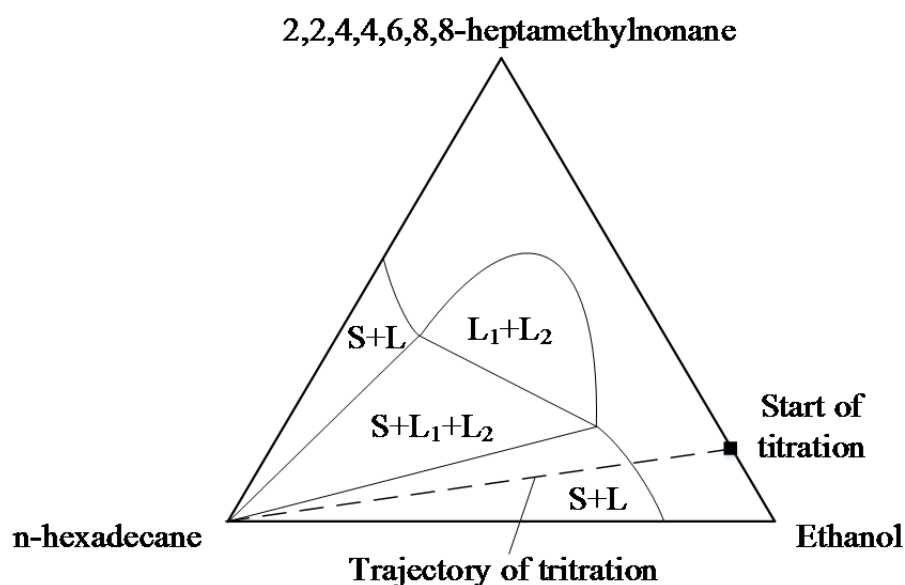


Figure 12: Experimental procedure for measuring the SLE of the ternary system ethanol + n-hexadecane + 2,2,4,4,6,8,8-heptamethylnonane by titration.

The mixtures were placed in the temperature-controlled water bath and stirred continuously. After 30 minutes, 0.015 g of n-hexadecane were added to the mixtures. After 5 minutes, it was checked whether there were precipitates visible or not, which denotes the solid-liquid phase transition. If there were no precipitates apparent, the procedure was repeated until there

where precipitates in every sample. To prove the quality of the gained results, the mixtures were heated up afterwards. If the precipitates disappear already at small temperature increases, then the measured SLE has a good accuracy. In this work, 0.2 K up to 0.4 K were required to make the precipitates disappear.

4.2.3 Interfacial tension

The interfacial tension between two coexisting liquid phases was measured with a Spinning-Drop Tensiometer. Therefore, the bulk phase densities have to be known. The bulk phase densities were measured using an oscillating u-tube Anton Paar DMA 38 Density Meter with an accuracy of $\pm 0.001 \text{ g cm}^{-3}$. The oscillating u-tube is a very simple but precise measurement technique, which is based on the law of harmonic oscillation. The measuring cell has got a volume of 2 ml. For each temperature, a calibration has to be done with substances of known density, e.g. water or air.

After determining the densities of the coexisting phases, the interfacial tension was measured with a Spinning-Drop Tensiometer SVT 20N from Data Physics having an accuracy of $\pm 0.001 \text{ g cm}^{-3}$. The measurement principle is based on the fact that the gravitational acceleration has only little effect on the shape of a droplet rotating at sufficient speed around its longitudinal axis. A temperature-controlled capillary (6.22 mm outer diameter; 4.00 mm inner diameter) was filled with the higher density phase. Subsequently, the capillary was rotated and some microliters of the lower density phase were injected in the rotating capillary tube forming a droplet (Figure 13).

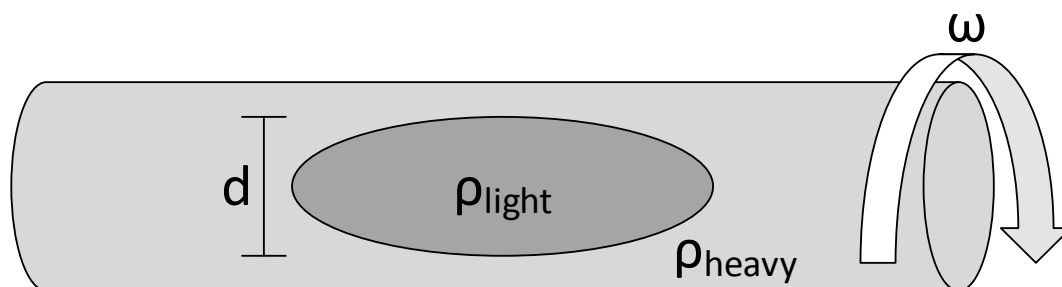


Figure 13: Principal of spinning-drop tensiometry.

Applying computer-aided tools, the size of the droplet was determined. The interfacial tension σ is dependent on the diameter of the droplet d , the rotating frequency of the capillary tube ω and the difference in density between both phases $\Delta\rho$ ¹⁰⁶:

$$\sigma = \frac{1}{32} d^3 \omega^2 \Delta\rho \quad (4-1)$$

In each measurement the rotating speed was varied from 4000 to 9000 rpm in order to obtain an accurate value of the interfacial tension. Additionally, the interfacial tension was measured twice for each temperature. The mean value out of these two measurements was afterwards used for further evaluation.

4.2.4 Pore Size Distribution

The pore size distribution was measured by TU Berlin using Belsorp-mini II (Bel, Japan, Inc.) by volumetric nitrogen adsorption technique. The measurement accuracy of the surface area has a resolution of 0.01 m² and a reproducibility of 1.5%. Naki et al.¹⁰⁷ provide more information on this experimental method. The evaluation of the pore size distribution function was performed by Non Localized Density Functional Theory. The software calculates the pore size distribution curve by fitting the integrated adsorption equation isotherms to the experimental ones minimizing the deviations. Integration over the pore size distribution results in the pore volume V_{Pore} .

4.2.5 Adsorption isotherms

The adsorption isotherms of binary systems containing a linear and a branched alkane were determined by a classical static batch method as described by Seidel-Morgenstern¹⁰⁸. Therefore, binary mixtures of known compositions were prepared and placed into a 10 ml glass vial. Afterwards, a known amount of solid adsorbent was added to the vial, which was then densely sealed with parafilm. The vial was placed in a temperature-controlled water bath as shown in Figure 14.

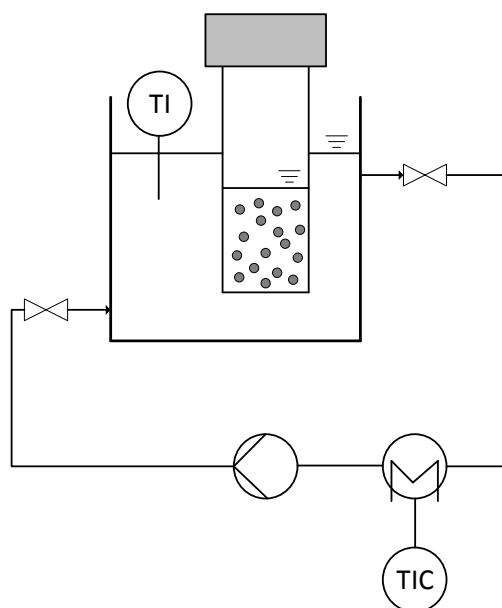


Figure 14: Experimental set-up for measuring adsorption isotherms

After storing the vial in the water bath it has to be waited for equilibration of bulk phase and adsorbed phase. According to literature¹⁰⁹, this can take a few hours or even several days. Therefore, it was checked what time is required to reach equilibrium by a preliminary experiment. The binary system n-octane + iso-octane was chosen for this investigation. Equimolar mixtures were prepared for each of the three adsorbents and the adsorption was investigated after 6, 24, 48 and 72 h, where an individual sample was prepared for each time. It could be observed, that 24 h is a suitable time for the samples to reach equilibrium. Since it was assumed that the system n-hexane + iso-hexane behaves similar to the C₈ system, a time of 24 h was selected for all adsorption experiments in this work. After equilibrium was reached, a sample of the bulk phase was drawn with a syringe. Regarding activated carbon and silica gel, an acetate membrane syringe filter holder was used in order to get pure samples. The composition of the liquid sample was then analyzed by GC as outlined in chapter 4.3.1.

In contrast to the bulk phase, the composition of the adsorbed phase in equilibrium is not accessible directly. However, by knowing the initial composition, the composition of the bulk phase in equilibrium and the total amount that is adsorbed the composition of the adsorbed phase in equilibrium can be determined. Regarding the three adsorbents, two different ways of determining the total amount adsorbed were applied. For activated carbon and zeolite, the adsorbent was separated from the remaining liquid by suction filtration. After filtration the total amount adsorbed was determined by weighing the adsorbent and calculating the

difference to the initial mass of the adsorbent. Zeolite achieved a constant mass after 1.5 minutes of filtration and could be weighed directly after filtration. In contrast, activated carbon achieved no constant mass after 1.5 minutes of filtration. A remaining liquid film on the surface of the activated carbon was observed. Since filtration for a longer time at ambient temperature can influence the reached equilibrium at other temperatures, the activated carbon was stored for 24 h at the adsorption temperature in order to achieve a constant mass. Silica gel as the third adsorbent was not appropriate for the described procedure since it could not be removed completely from the vial. Hence, the total amount adsorbed was determined via the pore volume of the silica gel. Both procedures are described in chapter 4.3.2. All adsorption measurements were performed twice and the mean value out of these two experiments was used for further evaluation.

4.3 Analytics

4.3.1 Gas chromatography

n-hexadecane + 2,2,4,4,6,8,8-heptamethylnonane + ethanol

In order to determine the compositions of lower and upper phase of the tie lines a gas chromatograph from Shimadzu (type GC-14A) was applied. The gas chromatograph was equipped with a non-polar column Innopeg-FFAP having a length of 25 m, an inner diameter of 0.32 mm and a film thickness of 0.48 μm . Helium with a velocity of 0.35 cm s^{-1} was used as carrier gas. At the end of the column, a flame ionization detector with a temperature of 573.15 K analyzed the contents of n-hexadecane and 2,2,4,4,6,8,8-heptamethylnonane. The content of ethanol was determined via a mass balance. Calibration curves with relative deviations of 1.29% and 0.91% were prepared for n-hexadecane and 2,2,4,4,6,8,8-heptamethylnonane, respectively. Dibutyl ether was used as internal standard in order to determine the mass fractions of the alkanes in the sample. Every sample was analyzed three times. The average mass fraction out of these three measurements was used for the further evaluation. In order to separate the peaks of the present components, the following method was applied: First, the column is heated up to a temperature of 353.15 K, which is held

constant for 3 minutes. Afterwards, the temperature is raised to a temperature of 503.15 K applying a heating rate of 30 K min⁻¹. After another 3 min, the column is cooled down to a temperature of 353.15 K. The method takes 11 min in total, typical retention times were 3.1 min for ethanol, 3.5 min for dibutyl ether, 7.2 min for 2,2,4,4,6,8,8-heptamethylnonane and 9.3 in for n-hexadecane.

Hexane isomers + methanol

For analysis of the composition of the binary system containing one of the for hexane isomers and methanol a GC from Shimadzu (type GC-14B) equipped with the column FS-Supreme-5mn HT having a length of 30 m, an inner diameter of 32 mm and a film thickness of 0.25 μm was applied. The content of methanol and the hexane isomers was analyzed by a flame ionization detector having a temperature of 543.15 K. Calibration curves were prepared for the pure substances resulting in relative deviations of 1.87% for n-hexane, 3.38% for 2-methylpentane, 1.81% for 3-methylpentane, 3.41% for 2,3-dimethylbutane and 0.66% for methanol. Toluene was used as internal standard. Every tie line was measured at least twice and every sample was analyzed three times. The average mass fraction out of all runs was used for further evaluation. The following GC method was applied: In the beginning, the column is heated up to a temperature of 313.15 K. The column is kept at this temperature for 140 s. Applying a heating rate of 30 K min⁻¹ the temperature is raised afterwards to 368.15 K. After reaching this temperature, the run is finished and the column is cooled down to 313.15 K. In total, the method lasts 4.2 min, typical retention times were 2.1 min for n-hexane, 2.0 min for 2-methylpentane, 2.0 min for 3-methylpentane, 2.0 min for 2,3-dimethylbutane, 1.7 min for methanol and 3.6 min for toluene.

Octane isomers + methanol

For the binary system n-octane + 2,2,4-trimethylpentane the same GC and the same method was applied as described in the previous section (“Hexane isomers / methanol”). Typical retention times were 2.3 min for iso-octane, 2.8 min for n-octane and 3.6 min for dibutyl ether. Regarding the binary system n-hexane + 2,3-dimethylbutane in adsorption experiments also the same GC but a different method was applied: After heating the column to a temperature of 343.15 K this temperature is held constant for 0.1 min. Then, the temperature

is raised to 355.15 K with a heating rate of 4 K min⁻¹. Afterwards, the temperature is raised to 373.15 K with 18 K min⁻¹. Typical retention times were 2.0 min for 2,3-dimethylbutane, 2.2 min for n-hexane and 3.6 min for toluene.

Ketones + ethylene glycol

In order to determine the concentrations of ketones and ethylene glycol, the same GC was applied as described in “n-hexadecane + 2,2,4,4,6,8,8-heptamethylnonane + ethanol” (GC-14A). Two different GC methods were applied in this work. The first method was used to determine the concentration of 2-pentanone and 3-methyl-2-butanone. Calibration curves with relative deviations of 1.91% for 2-pentanone, 1.22% for 3-methyl-2-butanone and 0.87% for ethylene glycol were prepared. Dibutyl ether was used as internal standard and ethanol was additionally used as solvent. Again, every sample was analyzed three times and the mean value was used for further evaluation. The method starts at a column temperature of 343.15 K, which was held constant for 5 minutes. Afterwards, the column temperature is raised to 503.15 K applying a heating rate of 30 K min⁻¹. After 2 minutes at this temperature, the method is finished and the column is cooled down to the starting temperature. The second method, which was used to analyze the concentration of 2-hexanone and 4-methyl-2-pentanone, is slightly different. It starts at a column temperature of 353.15 K, which was maintained for 4 minutes. Then, the temperature is raised to 503.15 K with a heating rate of 30 K min⁻¹. After additional 1.5 minutes the second method is finished. Calibration curves with relative deviations of 0.56% for 2-hexanone, 0.67% for 4-methyl-2-pentanone and 1.49% for ethylene glycol were prepared.

4.3.2 Total amount adsorbed

As already mentioned in chapter 4.2.5, two methods of determining the total amount adsorbed, an experimental and a calculative one, were applied in this work. All molecules adsorbed on the adsorbent and all molecules present within the pores are defined as total amount adsorbed. For the experimental method, the solid adsorbent is weighed before the adsorption experiment and after the experiment in the loaded equilibrium state. The difference in mass between these two states represents the total amount adsorbed:

$$m_{adsorbed} = m_{adsorbate} - m_{adsorbent} \quad (4-2)$$

For the calculative method, the pore volume of the adsorbent V_{pore} has to be known. It was assumed that the whole pore volume is accessible for the molecules. The total amount adsorbed can be calculated by Eq. (4-3), where $\rho_{adsorbed}$ represents the density of the adsorbed mixture.

$$m_{adsorbed} = V_{pore} \rho_{adsorbed} \quad (4-3)$$

The density of the binary alkane mixtures was measured for several compositions at temperatures between 283.15 K and 303.15 K applying a Densito 30PX oscillating tube densitometer from Mettler Toledo. Each density was measured three times and the average value was used for the calculation of the total amount adsorbed.

5 Results

In this chapter, the developed methodology will be applied to predict phase equilibria of systems containing branched molecules. In the first part, the underlying phase equilibria of crystallization processes were investigated. Different binary and ternary systems containing linear alkanes, branched alkanes as well as alcohols were used to predict binary and ternary LLE. Subsequently, systems showing cross-association were introduced. The methodology was applied to different systems containing linear and branched ketones dissolved in ethylene glycol. In the second part of this chapter, adsorption isotherms were investigated. For different binary systems containing a linear and a branched alkane and for three different adsorbents the liquid phase adsorption isotherms were calculated.

The scientific work published in this chapter was performed by T. Goetsch and supported by R. van den Bongard, A. Köhler, J. Hönig, B. Scharzec and K. Kissing in the framework of a bachelor thesis or a master thesis. LLE and SLE of the system methyl oleate + methanol as well as pore size distributions were measured by TU Berlin. Scientific advice was given by T. Zeiner. Parts of this chapter have been published in:

T. Goetsch, P. Zimmermann, R. van den Bongard, S. Enders, T. Zeiner: "Superposition of Liquid-Liquid and Solid-Liquid Equilibria of Linear and Branched Molecules: Binary Systems" *Ind. Eng. Chem. Res.* 55 (2016) 11167.

T. Goetsch, P. Zimmermann, R. van den Bongard, S. Enders, T. Zeiner: "Superposition of Liquid-Liquid and Solid-Liquid Equilibria of Linear and Branched Molecules: Ternary Systems" *Ind. Eng. Chem. Res.* 56 (2017) 417.

T. Goetsch, A. Danzer, P. Zimmermann, A. Köhler, K. Kissing, S. Enders, T. Zeiner: "Liquid-Liquid Equilibrium and Interfacial Tension of Hexane Isomers-Methanol Systems" *Ind. Eng. Chem. Res.* 56 (2017) 9743.

Reprinted with permission from the American Chemical Society.

5.1 Crystallization

The overall aim for this section is to predict the ternary superposition of LLE and SLE of the system n-hexadecane + 2,2,4,4,6,8,8-heptamethylnonane + ethanol. The prediction will be performed based on the binary subsystems. This means that all binary subsystems have to be known upfront. Thus, as a prerequisite the binary subsystem 2,2,4,4,6,8,8-heptamethylnonane + ethanol has to be predicted. As indicated in Figure 7, only experimental data of linear molecules will be used. In addition, more binary system containing a branched alkane and an alcohol will be investigated in order to prove the universality of the methodology. Before predicting the ternary phase equilibria, it will be also checked whether the superposition of LLE and SLE can be calculated simultaneously for binary systems.

5.1.1 Predicting binary LLE of systems containing branched molecules

The first system under consideration is ethanol (A) + 2,2,4,4,6,8,8-heptamethylnonane (B). According to Figure 7, the architecture parameters of the components have to be defined on the basis of the chemical formula. For 2,2,4,4,6,8,8-heptamethylnonane it was assumed that every carbon atom including its bonded hydrogen atoms represents an individual segment (see Figure 15).

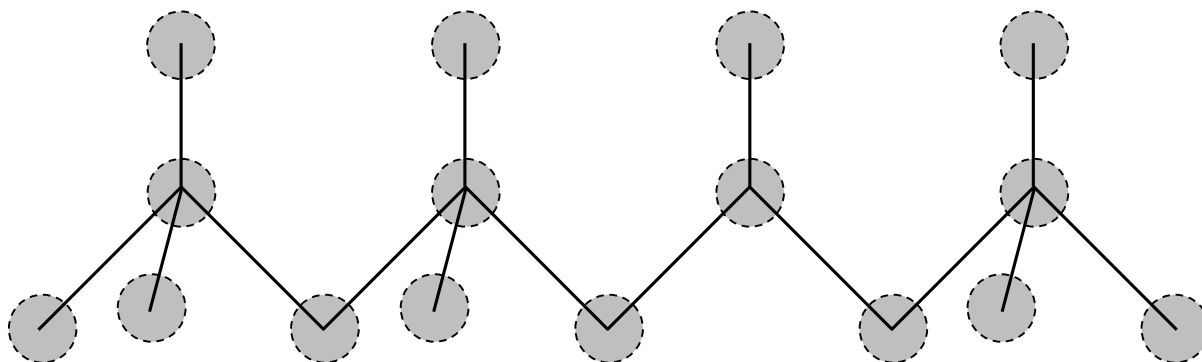


Figure 15: Definition of segments for the molecule 2,2,4,4,6,8,8-heptamethylnonane.

Regarding ethanol, also every carbon atom with its bonded hydrogen atoms is an individual segment as well as the hydroxyl group. This leads to architecture parameters listed in Table 6, where all molecules investigated in chapter 5.1.1-5.1.3 are shown.

Table 6: Architecture parameters defined within the LCT of all molecules investigated in chapter 5.1.1-5.1.3.

Molecule	N	N ₁	N ₂	N ₃
Methanol	2	1	0	0
Ethanol	3	2	1	0
n-hexane	6	5	4	3
2-methylpentane	6	5	5	3
3-methylpentane	6	5	5	4
2,3-dimethylbutane	6	5	6	4
n-heptane	7	6	5	4
n-octane	8	7	6	5
2,2,4-trimethylpentane	8	7	10	5
2,2,5-trimethylhexane	9	8	11	6
n-dodecane	12	11	10	9
n-tetradecane	14	13	12	11
n-hexadecane	16	15	14	13
HMN [#]	16	15	24	16

[#]2,2,4,4,6,8,8-heptamethylnonane

Besides the architecture parameters, all necessary model parameters for predicting the binary LLE of this system have to be defined, i.e. the two association parameters Δh_A^{as} and $K_{0,A}$ of ethanol as well as the interaction energy $\Delta \varepsilon_{ij}/k_B$ between 2,2,4,4,6,8,8-heptamethylnonane and ethanol. As already mentioned above, it was assumed that no experimental data of the system 2,2,4,4,6,8,8-heptamethylnonane + ethanol are available for the adjustment of model parameters. However, experimental data of systems containing ethanol and any other, linear alkane can be utilized. In this work, experimental LLE data of the three binary systems n-dodecane + ethanol, n-tetradecane + ethanol and n-hexadecane + ethanol were taken from literature¹¹⁰. The two association parameters Δh_A^{as} and $K_{0,A}$ of ethanol as well as the interaction energy $\Delta \varepsilon_{ij}/k_B$ between n-tetradecane and ethanol were simultaneously fitted to the LLE data of the system n-tetradecane + ethanol. Values of $\Delta h_A^{as} = -30685.5 \text{ J mol}^{-1}$, $K_{0,A} = \exp(-9.35)$ and $\Delta \varepsilon/k_B = 9.35 \text{ K}$ were found. In Figure 16 the result of the parameter adjustment is illustrated.

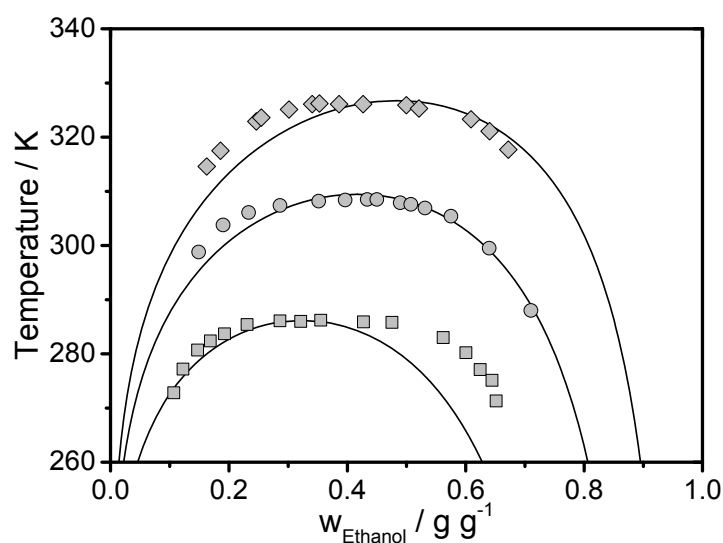


Figure 16: LLE of the binary systems n-dodecane (squares)¹¹⁰, n-tetradecane (circles)¹¹⁰ and n-hexadecane (diamonds)¹¹⁰ all with the solvent ethanol. The solid lines were calculated using the LCT in combination with CALM.

It can be seen that the combination of LCT and CALM is well-suited to describe the binary LLE of the system n-tetradecane + ethanol. Calculation and experimental data are in excellent agreement throughout the entire concentration range. Besides the already adjusted interaction energy between ethanol and n-tetradecane, two more chain lengths have to be investigated in order to set up the extrapolation function. Therefore, the interaction energy between ethanol and n-dodecane as well as n-hexadecane was adjusted (the two association parameters of ethanol remained constant). Values of $\Delta\varepsilon_{ij}/k_B = 7.40$ K and $\Delta\varepsilon_{ij}/k_B = 11.29$ K were fitted for the systems n-dodecane + ethanol and n-hexadecane + ethanol, respectively. Regarding these two binary systems, the interaction energy $\Delta\varepsilon_{ij}/k_B$ was the only adjustable parameter. For the binary system n-dodecane + ethanol the model slightly overestimates the solubility of the alkane in ethanol. The solubility of ethanol in n-dodecane as well as the UCST is well-described by the calculation. Regarding the binary system n-hexadecane + ethanol, small deviations on the ethanol-lean side can be noticed. A good agreement between experimental and calculated data can be found for the ethanol-rich side as well as for the UCST.

As described in chapter 3.2.1, the two association parameters Δh_A^{as} and $K_{0,A}$ can be directly applied for the system ethanol + 2,2,4,4,6,8,8-heptamethylnonane. The interaction energy $\Delta\varepsilon_{ij}/k_B$ between these two components has to be estimated by an extrapolation function. To set up the extrapolation function of the interaction energy depending on the chain length of

the alkanes, the three fitted interaction energies $\Delta\varepsilon_{ij}/k_B$ are plotted against the chain length of the corresponding alkane in Figure 17.

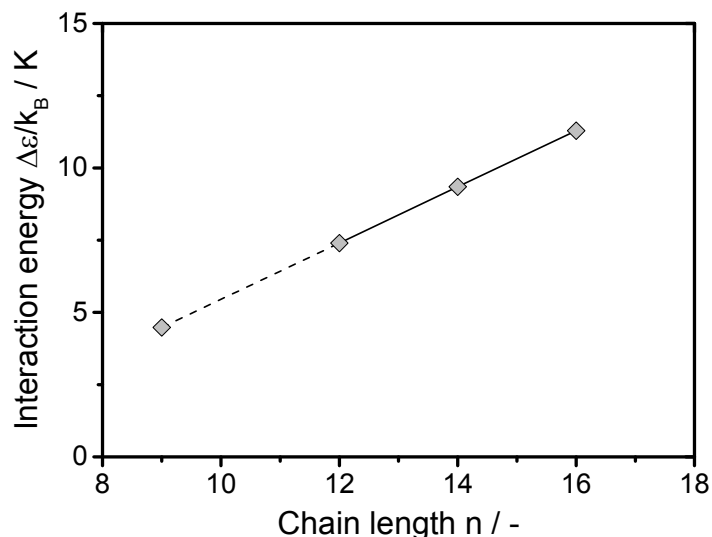


Figure 17: Interaction energy between alkane molecules and ethanol as a function of the chain length of the alkanes. The values for chain lengths of 12, 14 and 16 were fitted to experimental data, the value for a chain length of 9 was determined by extrapolation.

Within the investigated chain lengths of 12, 14 and 16, the fitted values show an almost linear trend. Using these three values, the following linear correlation of interaction energy and chain length can be set up:

$$\Delta\varepsilon_{ij}/k_B = 0.9725n - 4.2683 \quad (5-1)$$

This extrapolation function was then used for the determination of the interaction energy $\Delta\varepsilon_{ij}/k_B$ between 2,2,4,4,6,8,8-heptamethylnonane and ethanol. For a backbone of nine carbon atoms, like 2,2,4,4,6,8,8-heptamethylnonane, the interaction energy has a value of $\Delta\varepsilon_{ij}/k_B = 4.48$ K. This value, together with the two fitted association parameters of ethanol and the architecture parameters of 2,2,4,4,6,8,8-heptamethylnonane and ethanol (Table 6), was then used for the prediction of the LLE of the binary system 2,2,4,4,6,8,8-heptamethylnonane + ethanol (Figure 18).

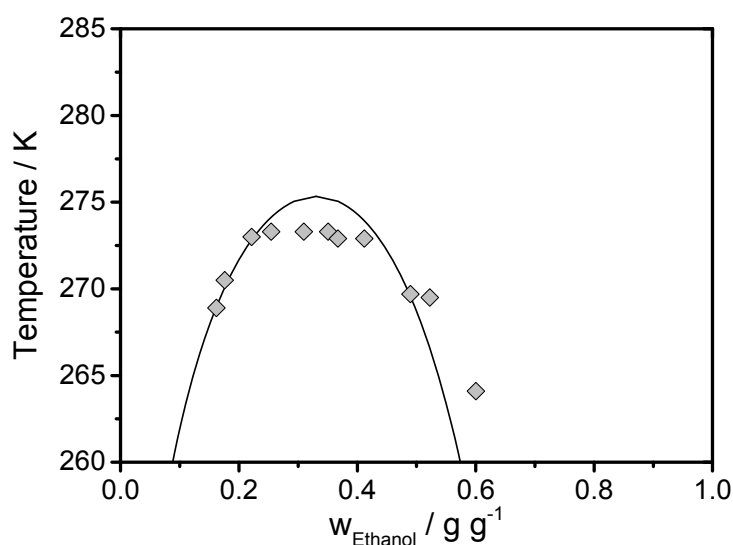


Figure 18: Predicted LLE of the binary system 2,2,4,4,6,8,8-heptomethylnonane + ethanol. Experimental data were taken from literature¹¹⁰, solid lines were calculated using the LCT in combination with CALM.

It can be seen that the predicted LLE of the binary system 2,2,4,4,6,8,8-heptomethylnonane + ethanol is in very good agreement with the experimental data reported by Dahlmann and Schneider¹¹⁰. The upper critical solutions temperature (UCST) is slightly overestimated, same as for the solubility of 2,2,4,4,6,8,8-heptomethylnonane in ethanol. The solubility of ethanol in 2,2,4,4,6,8,8-heptomethylnonane is perfectly described. Applying Eq. (3-24), an average relative deviation of $ARD=1.79\%$ was achieved. Thus, Figure 18 shows that the way of predicting the LLE of a system containing branched molecules as outlined in chapter 3.2.1 is suitable.

To validate this finding, additional two binary systems, i.e. methanol + 2,2,4-trimethylpentane as well as methanol + 2,2,5-trimethylhexane, were investigated. Again, architecture parameters as well as model parameters have to be defined. The architecture parameters were already listed in Table 6. The two association parameters Δh_A^{as} and $K_{0,A}$ of methanol as well as the interaction energy $\Delta \varepsilon_{ij}/k_B$ between methanol and the branched alkanes were defined similarly to the former binary system. The association enthalpy Δh_A^{as} is assumed to only refer to the hydroxyl group of the alcohol. Hence, the value of ethanol ($\Delta h_A^{as} = -30685.5 \text{ J mol}^{-1}$) was also applied for methanol. A similar treatment can be found in literature⁶⁰. In order to set up the extrapolation function between interaction energy and chain length, three binary systems were investigated, i.e. methanol + n-hexane, methanol + n-heptane and methanol + n-

octane. First, the association parameter $K_{0,A}$ of methanol and the interaction energy $\Delta\varepsilon_{ij}/k_B$ between methanol and n-hexane were simultaneously adjusted to experimental LLE data of this system reported by Matsuda et al.¹¹¹. Values of $K_{0,A} = \exp(-8.90)$ and $\Delta\varepsilon_{ij}/k_B = 17.40$ K were found. In Figure 19, calculated and experimental data are compared.

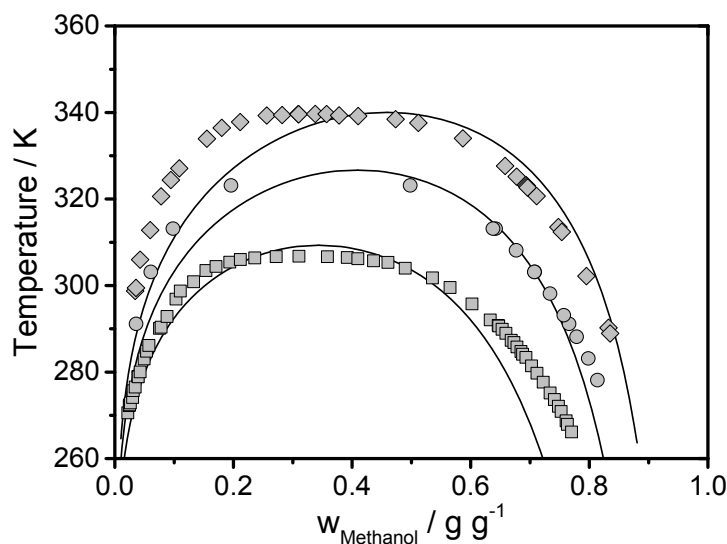


Figure 19: LLE of the binary systems n-hexane (squares)¹¹¹, n-heptane (circles)^{112,113} and n-octane (diamonds)¹¹⁴ all with the solvent methanol. The solid lines were calculated using the LCT in combination with CALM.

It can be seen that up to a mass fraction of methanol of 0.6 g g^{-1} the calculated binodal curve agrees excellent with the experimental data. For higher mass fractions of methanol, the model slightly overestimates the solubility of n-hexane in methanol. Afterwards, the interaction energy $\Delta\varepsilon_{ij}/k_B$ for the remaining two binary systems was fitted, keeping the association parameters of methanol constant. For both systems, deviations on the methanol-lean side, where the model overestimates the solubility of methanol in the corresponding alkane, arise. To set up the extrapolation function, the interaction energy $\Delta\varepsilon_{ij}/k_B$ is plotted against the chain length of the alkanes (Figure 20).

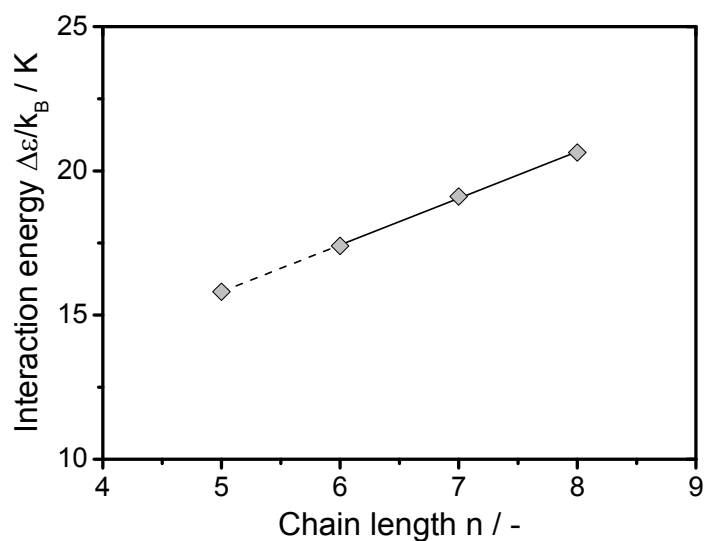


Figure 20: Interaction energy between alkane molecules and methanol as a function of the chain length of the alkanes. The values for chain lengths 6, 7 and 8 were fitted to experimental data, the value for a chain length of 5 was determined by extrapolation.

An almost perfect linear trend was also found for these systems resulting in the opportunity of extrapolating within a certain range of chain lengths by:

$$\Delta\varepsilon_{ij}/k_B = 1.62n + 7.71 \quad (5-2)$$

For predicting the LLE of the binary system 2,2,5-trimethylhexane + methanol, the interaction energy corresponding to a chain length of six is used ($\Delta\varepsilon_{ij}/k_B = 17.40 \text{ K}$). Since 2,2,4-trimethylpentane has a backbone of five carbon atoms, the extrapolation function is applied to calculate the respective value ($\Delta\varepsilon_{ij}/k_B = 15.81 \text{ K}$). Both predictions are illustrated in Figure 21.

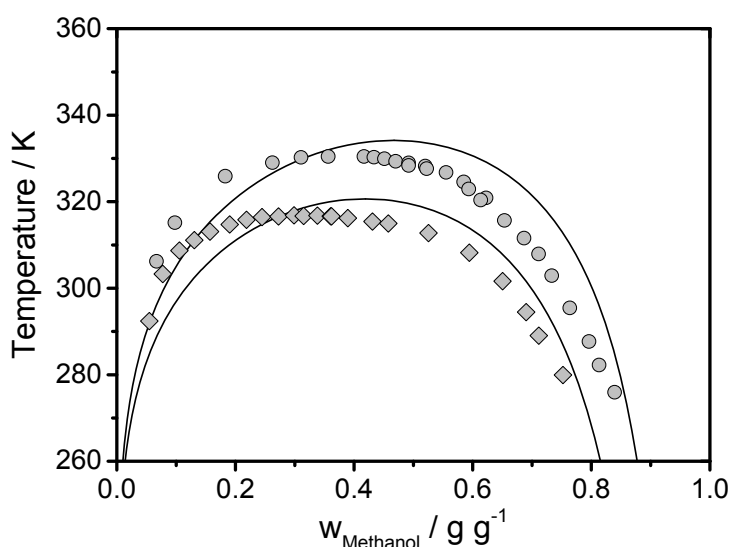


Figure 21: Predicted LLE of the binary systems 2,2,5-trimethylhexane + methanol (circles)¹¹³ and 2,2,4-trimethylpentane + methanol (diamonds)¹¹⁴. The solid lines were calculated using the LCT in combination with CALM.

Starting with the system 2,2,4-trimethylpentane + methanol, it can be seen that the predicted LLE is in good agreement with the experimental data reported by Kurihara et al.¹¹⁴, which results in an average relative deviation of $ARD=3.93\%$ (Eq. (3-24)). The UCST is slightly overestimated. On the methanol-lean side, the model overestimates the solubility of methanol in 2,2,4-trimethylpentane, whereas on the methanol-rich side the model underestimates the solubility of 2,2,4-trimethylpentane in methanol. For the system 2,2,5-trimethylhexane + methanol a comparably good agreement between experimental and predicted data can be found, leading to an average relative deviation of $ARD=3.50\%$. The same trends of deviation can be found as for the former system. Thus, Figure 21 confirms the conclusion drawn from Figure 18 that the developed methodology is well-suited for the prediction of binary LLE of systems containing a branched molecule.

However, in Figure 18 and Figure 21, the architecture of the branched alkane differed significantly from the architecture of the corresponding linear alkane. Hence, in a last step it was investigated whether the developed methodology is also able to consider small changes in the molecular architecture of the isomers. Therefore, binary systems containing methanol and one of the four hexane isomers n-hexane, 2-methylpentane, 3-methylpentane and 2,3-dimethylbutane were investigated. The architecture parameters listed in Table 6 display the ability of the LCT to also differentiate between these isomers. For the prediction of the binary LLE, the same association parameters of methanol were used as for the former two binary

systems. The interaction energies were estimated by the extrapolation function of Eq. (5-2), where 2-methylpentane and 3-methylpentane with a backbone of 5 carbon atoms have got an interaction energy of $\Delta\varepsilon_{ij}/k_B = 15.81$ K and 2,3-dimethylbutane with a backbone of 4 carbon atoms has got an interaction energy of $\Delta\varepsilon_{ij}/k_B = 14.19$ K. In Figure 22 the predicted LLE are compared with experimental cloud-points as well as with experimental tie lines. Experimental data are listed in Table 14 - Table 21.

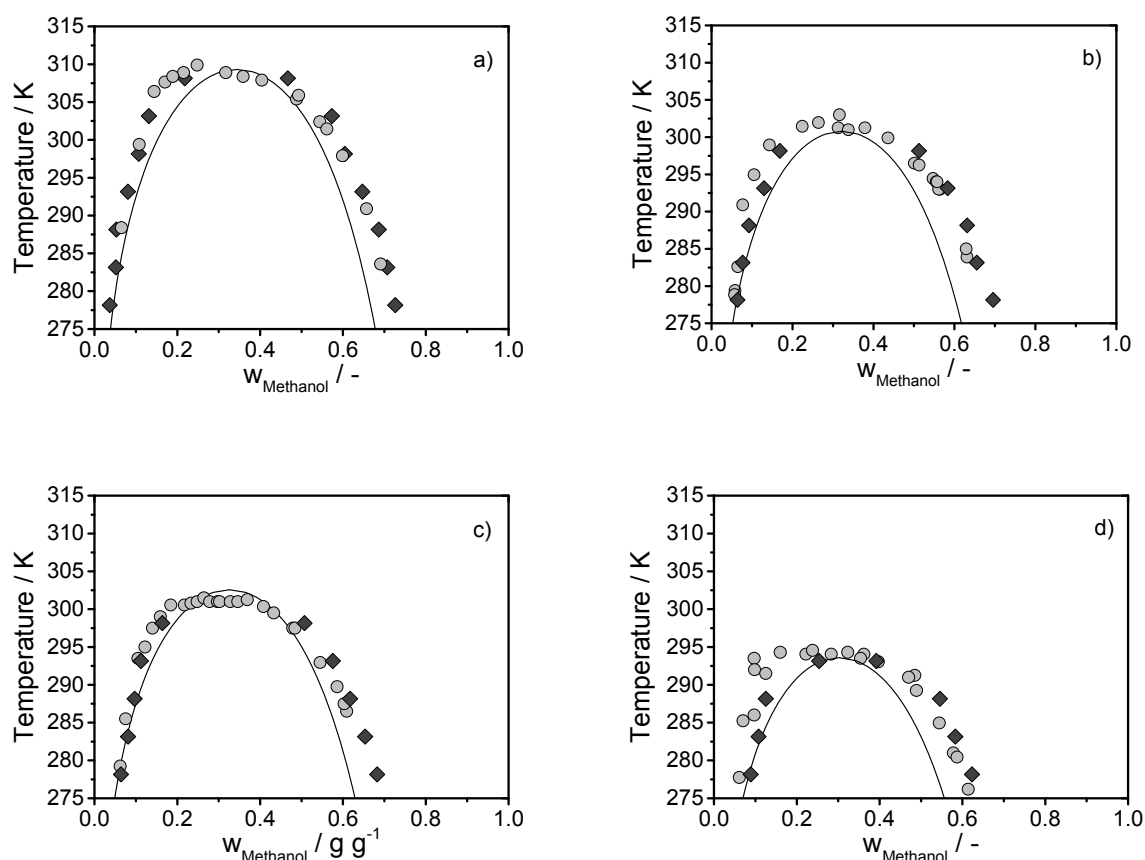


Figure 22: LLE of the binary systems methanol + n-hexane (a), methanol + 2-methylpentane (b), methanol + 3-methylpentane (c) and methanol + 2,3-dimethylbutane (d). Experimental cloud-points are shown as light grey circles; experimental tie lines are shown as grey diamonds. The solid line denote the fitted LLE for the system methanol + n-hexane and the predicted LLE for the three remaining systems; they were calculated using the LCT in combination with CALM.

In this case two different measuring techniques were applied in order to detect the effect of branching on the LLE precisely. Comparing the experimental cloud-points with the experimental tie lines, it can be seen that the agreement of both measuring techniques is excellent for all four binary systems so that definite trends can be observed within Figure 22. Regarding the different binary systems, it is obvious that the degree of branching of the

alkane has got a significant influence on the UCST. The higher the degree of branching of the hexane isomer the lower is the UCST ranging from approximately 308 K for the binary system methanol + n-hexane over 301 K for the binary systems methanol + 2-methylpentane and methanol + 3-methylpentane to an UCST of 294 K for the system methanol + 2,3-dimethylbutane. Comparing the two isomers 2-methylpentane and 3-methylpentane, no reliable statement can be given on whose UCST is higher, because the experimental data are comparable within the accuracy of the performed experiments.

Regarding the predicted LLE and the experimental data (Figure 22) both agree very well. Small deviations between predicted and measured data can be found for the methanol-rich phase for all systems. Average relative deviations of 2.17% for the binary system methanol + n-hexane (this LLE was not predicted but used for adjusting parameters), 2.40% for methanol + 2-methylpentane, 1.58% for methanol + 3-methylpentane and 2.73% for methanol + 2,3-dimethylbutane could be achieved. The deviations for the system methanol + 2,3-dimethylbutane are higher than for the other systems. A possible reason for this finding could be that 2,3-dimethylbutane had the lowest purity of all investigated substances (98% molar purity) and small amounts of impurities can already have a significant influence on the LLE. Moreover, it was already mentioned in literature⁷⁹ that the LCT is not perfectly accurate for small molecules. However, the overall agreement of predicted and experimentally determined LLE is very good. Therefore, it can be concluded that the developed methodology applying the LCT in combination with CALM is well-suited for predicting quantitatively the binary LLE for branched alkanes dissolved in an alcohol including small changes in the molecular architecture.

In addition to the LLE experiments, the interfacial tension of these four binary systems was also investigated. Data of the binary system methanol + n-hexane were taken from literature¹¹⁵, values for the remaining three systems were measured by spinning-drop tensiometry. The interfacial tension is a good opportunity for determining the UCST of a binary system since its value vanishes at the critical point. Besides measuring the interfacial tension, it was also calculated for all 4 systems as outlined in chapter 3.1.5. The experimentally determined interfacial tensions as well as the calculated ones are illustrated in Figure 23. Experimental data are listed in Table 39 - Table 41.

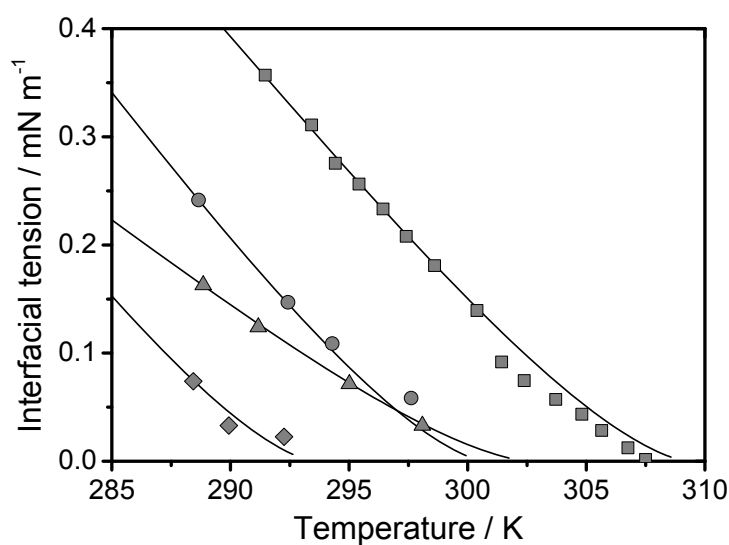


Figure 23: Interfacial tension as a function of temperature for the binary systems methanol + n-hexane (squares; exp. data from literature¹¹⁵), methanol + 2-methylpentane (circles), methanol + 3-methylpentane (triangles) and methanol + 2,3-dimethylbutane (diamonds). The solid lines were calculated by a DGT approach incorporating the LCT in combination with CALM.

By extrapolating the experimental data points, the UCST of the corresponding binary system can be estimated. It can be seen that the values obtained from the LLE experiments (308 K for methanol + n-hexane; 301 K for methanol + 2-methylpentane as well as for methanol + 3-methylpentane; 294 K for methanol + 2,3-dimethylbutane) are confirmed by the experimental interfacial tensions. For the calculation of the interfacial tension all model parameters of LCT and CALM remain constant. Additionally, the influence parameter κ of the DGT had to be fitted to one experimental data point for every binary system (Table 7). The point, which is furthest from the critical point, was used for this adjustment in order to get reliable results. Comparing calculated and experimental interfacial tension, a very good agreement can be found.

Table 7: Influence parameter κ adjusted to 4 binary systems.

Binary system	Influence parameter $\kappa / \text{J mol m}^{-4}$
Methanol + n-hexane	$1.13 \cdot 10^{-7}$
Methanol + 2-methylpentane	$1.85 \cdot 10^{-7}$
Methanol + 3-methylpentane	$0.58 \cdot 10^{-7}$
Methanol + 2,3-dimethylbutane	$2.43 \cdot 10^{-7}$

Measurements and calculations confirm the influence of the degree of branching on the UCST, which was observed in Figure 22, where the UCST decreases with increasing degree of branching. Again it can be seen that the binary systems methanol + 2-methylpentane and methanol + 3-methylpentane show similar UCSTs. But unlike the LLE experiments, a difference between both systems can be seen within the experiments. The system methanol + 2-methylpentane shows higher interfacial tension throughout the whole temperature range leading to the conclusion that its UCST must be higher than for the system methanol + 3-methylpentane. Regarding experimental and calculated interfacial tensions for the systems methanol + 2-methylpentane and methanol + 3-methylpentane, it can be seen that the calculated values intersect each other whereas the experimental data do not. This means that the LCT in combination with CALM predicts a higher UCST for the system methanol + 3-methylpentane. Since the measurement technique for determining the interfacial tension is very reliable, it is supposed that the combination of LCT and CALM gives a qualitatively wrong prediction for the UCST order of these two binary systems. In order to verify why the calculations of the interfacial tension of these two systems give a qualitatively wrong UCST order, a model calculation was conducted, where the binary LLE of the systems methanol + 2-methylpentane and methanol + 3-methylpentane were predicted, using solely the LCT applying the same model parameters as for the combination of LCT and CALM. The result of this model calculation is shown in Figure 24.

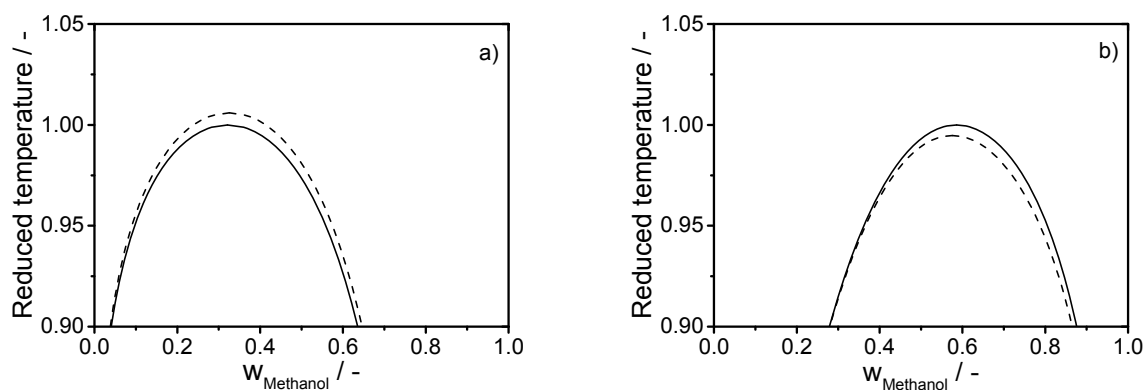


Figure 24: Predicted binary LLE of the systems methanol + 2-methylpentane (solid line) and methanol + 3-methylpentane (dashed line). The left side (a) was calculated using the LCT in combination with CALM, the right side (b) was calculated using solely the LCT. The reduced temperature T_r is related to the UCST of the system methanol + 2-methylpentane in both cases.

The predicted LLE are shown in terms of reduced temperatures, which are related to the UCST of the system methanol + 2-methylpentane in both cases. While the UCST of the system methanol + 2-methylpentane is lower applying LCT in combination with CALM, it is higher for the calculation applying only the LCT. Thus, it is obvious that the UCST order changes due to the omission of CALM. The LCT is able to take the molecular architecture into account. Therefore, it is able to give according to the interfacial tension measurements the qualitative correct order of UCST for these two binary systems (right side of Figure 24). The combination of LCT and CALM (left side of Figure 24) predicts the wrong UCST order, wherefore it is clear that the contribution of CALM to the Gibbs free energy ΔG^{LCT} is the reason for the different order in comparison with the experiments.

In addition to calculating the interfacial tension, the DGT approach was also applied to calculate the interfacial concentration profiles, which are shown in Figure 25.

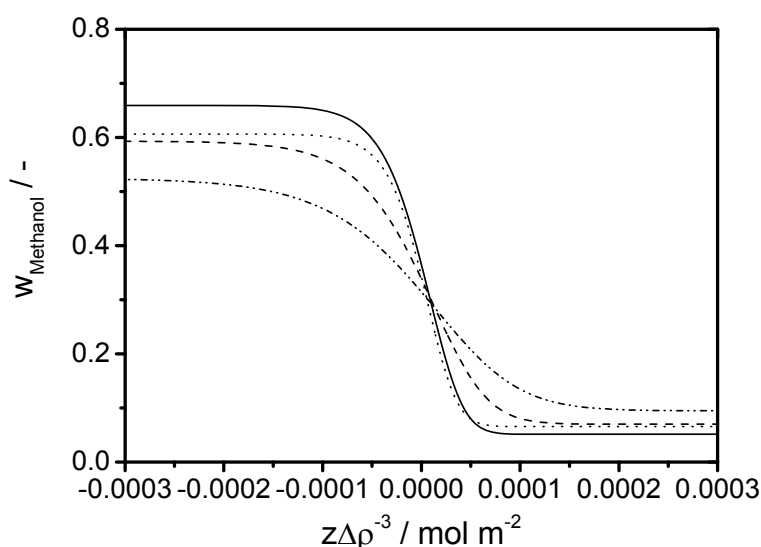


Figure 25: Interfacial concentration profile for the binary systems methanol + n-hexane (solid line), methanol + 2-methylpentane (dashed line), methanol + 3-methylpentane (dotted line) and methanol + 2,3-dimethylbutane (dash-dotted line). The lines were calculated for a temperature of 280 K by a DGT approach incorporating the LCT in combination with CALM.

Regarding the calculated interfacial concentration profiles, no enrichment of any component within the interfacial region can be found for all investigated systems. Since the degree of branching has got an influence on the UCST, it is clear that the thickness of the interfacial region changes for different degrees of branching. The binary system methanol + n-hexane shows the narrowest interfacial region whereas the binary system methanol + 2,3-dimethylbutane shows the broadest interfacial region. Comparing the systems methanol + 2-

methylpentane and methanol + 3-methylpentane, Figure 25 shows that the interfacial region of the system methanol + 2-methylpentane is broader. However, it cannot be proved whether the calculations for these two systems are qualitatively correct, because the interfacial region is not accessible experimentally.

In this chapter, the developed methodology was applied to predict binary LLE of systems containing an alcohol and a branched alkane. Regarding the difference in molecular architecture between linear and branched alkanes, large as well as very small differences were investigated. All predicted LLE were in very good agreement with the experimental data, wherefore it can be stated that the methodology is well-suited for quantitative predictions. However, it was also shown that a qualitative wrong UCST order for the two binary systems methanol + 2-methylpentane and methanol + 3-methylpentane was predicted. Reason for this finding is the contribution of CALM, which does not consider the molecular architecture like the LCT. Nonetheless, the developed methodology gives reliable predictions on the LLE which means that a possible oiling out during a crystallization process can be identified.

5.1.2 Simultaneous modelling of binary LLE and SLE

The first prerequisite for predicting the ternary superposition of systems containing branched molecules, i.e. predicting binary LLE of systems containing branched molecules, was demonstrated in the previous section. As an additional prerequisite, the model should be able to calculate the binary superposition of LLE and SLE by applying the same set of model parameters for both phase equilibria. In literature^{77,78}, this was already shown for large molecules. However, the LCT was not yet used for the simultaneous modeling of LLE and SLE of smaller molecules. For this reason, the LCT in combination with CALM will be applied to the two binary systems ethanol + n-hexadecane and ethanol + n-octadecane.

LLE data for the system ethanol + n-hexadecane as well as LLE and SLE data for the system ethanol + n-octadecane were available in literature^{110,116,117}. Since no experimental SLE data of the system n-hexadecane + ethanol were available in literature, own experiments were performed by DSC (Table 31). For the modelling of the binary LLE between n-hexadecane and ethanol, the same association parameters of ethanol and the same interaction energy between ethanol and n-hexadecane was used as in the previous section (chapter 5.1.1). Regarding the modelling of the binary SLE, the melting temperature and the enthalpy of fusion of n-hexadecane are needed additionally. Both values were determined by the DSC

experiments ($T^{SL} = 291.07 \text{ K}$; $\Delta h^{SL} = 52433 \text{ J mol}^{-1}$). The architecture parameters of ethanol and n-hexadecane defined within the LCT are listed in Table 6. In Figure 26, the calculated superposition of LLE and SLE of the system n-hexadecane + ethanol is compared with experimental data (Table 31).

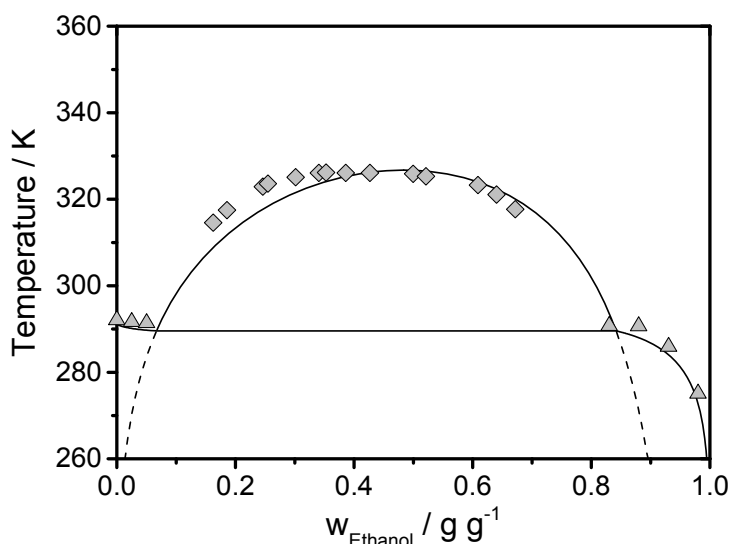


Figure 26: Superposition of LLE (diamonds)¹¹⁰ and SLE (triangles) of the binary system n-hexadecane + ethanol. The solid lines were calculated using the LCT in combination with CALM.

Comparing calculated and experimental LLE, only small deviations on the ethanol-lean side can be observed (as already seen in Figure 16). Regarding the SLE, an excellent agreement between experiments and calculations can be seen. Thus, both phase equilibria can be calculated in good accuracy applying the same set of model parameters. Below the SLE curve, the LLE is shown as a dashed line. According to Cahn³⁷, this is because the LLE is only metastable in this region.

For the calculation of the binary system n-octadecane + ethanol, the same association parameters of ethanol were used. The interaction energy between n-octadecane and ethanol was determined by the extrapolation function of Eq. (5-1) ($\Delta \varepsilon_{ij}/k_B = 13.26 \text{ K}$). Melting temperature¹¹⁸ and enthalpy of fusion¹¹⁹ of n-octadecane were taken from literature. n-octadecane was treated as linear chain of 18 segments ($N_1 = 17$; $N_2 = 16$; $N_3 = 15$). The calculated superposition of binary LLE and SLE for the system n-octadecane + ethanol is compared with experimental data in Figure 27.

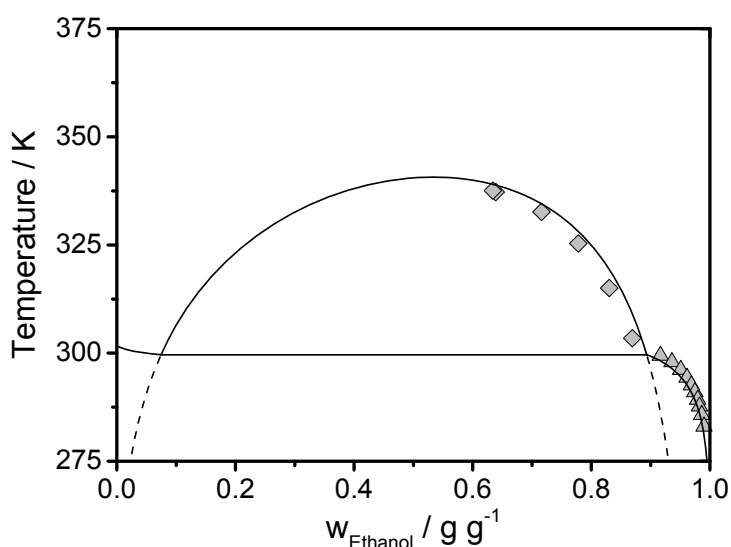


Figure 27: Superposition of LLE (diamonds)¹¹⁶ and SLE (triangles)¹¹⁷ of the binary system n-octadecane + ethanol. The solid lines were calculated using the LCT in combination with CALM.

Because the literature data of Chang et al.¹¹⁶ and Domanska¹¹⁷ only present the ethanol-rich side of LLE and SLE, it cannot be proved whether the calculated data agree with the experimental ones for the whole range of concentrations. However, for high concentrations in ethanol, it can be seen that the agreement of calculated and experimental LLE and SLE data is excellent. Having in mind that no model parameter was fitted to these experimental data, Figure 27 confirms the methodology of extrapolating the interaction energy within a homologue series.

This section proved that it is possible to apply the LCT in combination with CALM for simultaneously modelling LLE and SLE of binary systems. Together with the results of chapter 5.1.1, it can now be proven whether the developed methodology is able to predict ternary phase equilibria of systems containing branched molecules based on the binary subsystems.

5.1.3 Prediction of ternary phase behavior including linear and branched molecules

After successfully showing the possibility of predicting binary LLE of systems containing a branched molecule and the possibility of simultaneously calculating LLE and SLE of binary systems, the aim of this section is the prediction of ternary phase equilibria of systems containing branched molecules. This implies that no experimental data of the ternary system

was used for adjusting model parameters. All necessary model parameters were determined as described in the previous two sections. The ternary system n-hexadecane + 2,2,4,4,6,8,8-heptamethylnonane + ethanol was chosen for the prediction. First of all it was investigated whether the ternary LLE of this system can be predicted based on the binary subsystems. Therefore, the binodal curve and three tie lines were predicted at a temperature of 298.15 K. This temperature is higher than the melting temperature of n-hexadecane assuring that no SLE will arise. In order to validate the ternary prediction, binodal curve as well as tie lines were also measured at this temperature (Table 33 and Table 34). In Figure 28 the predicted LLE is compared with experimental data.

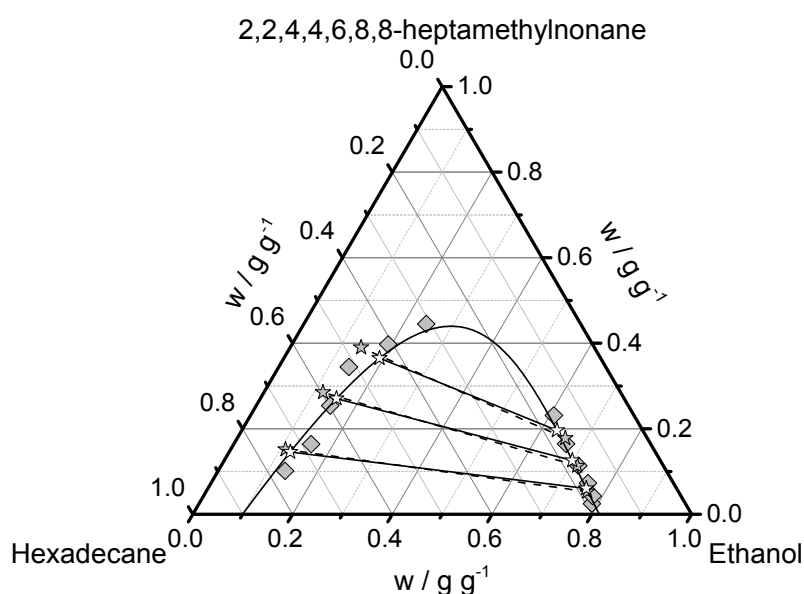


Figure 28: LLE of the ternary system n-hexadecane + 2,2,4,4,6,8,8-heptamethylnonane + ethanol at a temperature of 298.15 K. Experimental points on the binodal curve are shown as diamonds; experimental tie lines are shown as grey stars connected by dashed lines. The binodal curve as well as the tie lines (white stars connected by solid lines) was calculated using the LCT in combination with CALM.

Comparing experimental cloud-points with tie lines, it can be seen that both measuring techniques lead to the same results. Regarding predicted binodal curve and tie lines, an excellent agreement with the experimental data can be found for the compositions on the ethanol-rich side. Likewise, the slope of the tie lines is predicted in excellent agreement with the experimental data. Small deviations between predicted and calculated data arise on the ethanol-lean side. This finding is not surprising, since the calculations also show small deviations for the binary system n-hexadecane + ethanol (Figure 26). Nevertheless, it can be stated that the prediction of the ternary LLE based on the binary subsystems is in very good agreement with the experimental data so that no further adjustment of model parameters is

necessary. Same was found for further systems shown in appendix A. Having gained trust in the prediction based on the binary subsystems, it can be checked whether the superposition of ternary LLE and SLE, which is essential for the design of crystallization processes, can be predicted correctly. The already determined model parameters were used for the prediction of both phase equilibria and the same melting temperature und enthalpy of fusion as in chapter 5.1.2 were used. It was assumed that the solid phase only contains n-hexadecane. Figure 29 shows the predicted superposition of ternary LLE and SLE for a temperature of 283.15 K. The predicted phase equilibria are compared with experimental data listed in Table 37.

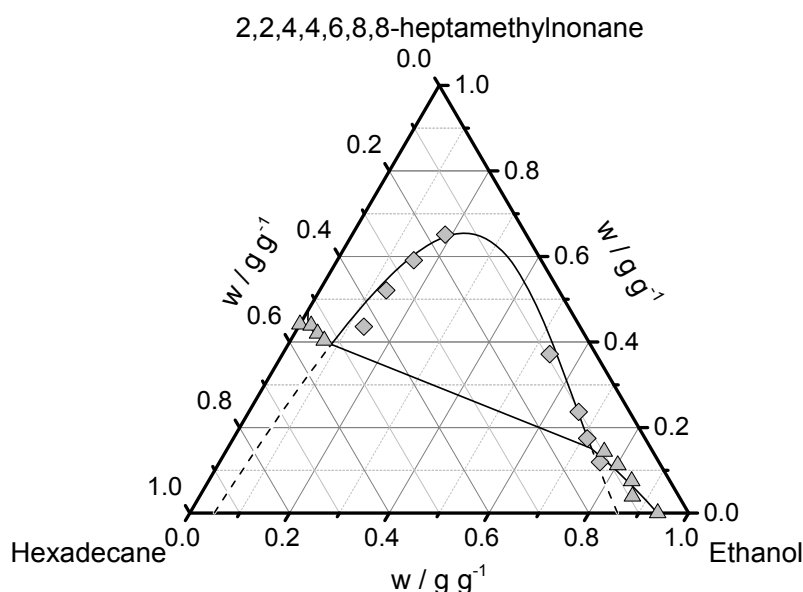


Figure 29: Superposition of LLE (diamonds) and SLE (triangles) of the ternary system n-hexadecane + 2,2,4,4,6,8,8-heptamethylnonane + ethanol at a temperature of 283.15 K. Lines were calculated using the LCT in combination with CALM. The dashed lines denote the metastable LLE.

Below the SLE curve, the LLE is shown as a dashed line. Like in chapter 5.1.2 this indicates that the LLE is only metastable in this region. The SLE was only determined outside the LLE, because a mixture within the miscibility gap would directly separate into two phases. Comparing predicted and measured SLE data, an excellent agreement can be seen. Regarding the binodal curve, a very good agreement between predicted and measured data can be seen. Only the lowest point on the ethanol-lean side shows a small deviation to the predicted binodal curve. In order to prove the capability of the developed methodology to consider the temperature dependency of the system, the superposition of ternary LLE and SLE was also predicted for a temperature of 278.15 K (Figure 30) and compared with experimental data (Table 38).

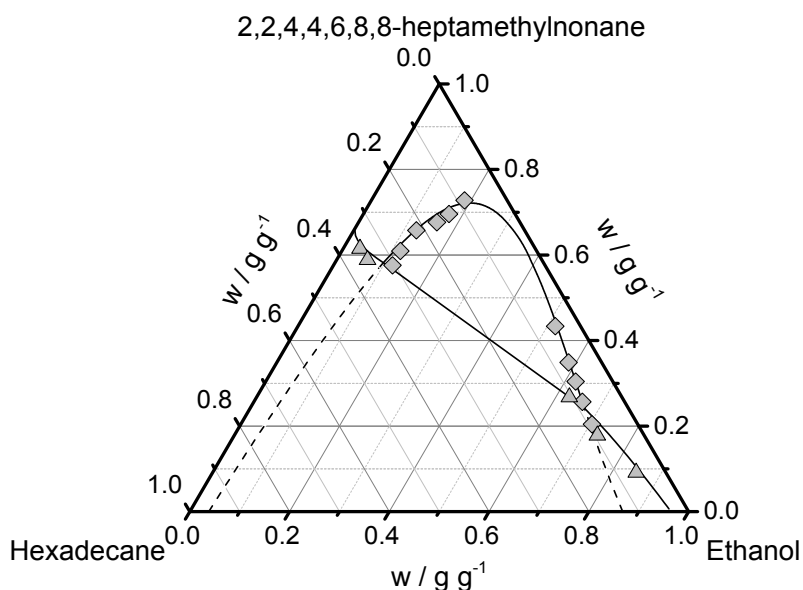


Figure 30: Superposition of LLE (diamonds) and SLE (triangles) of the ternary system n-hexadecane + 2,2,4,4,6,8,8-heptamethylnonane + ethanol at a temperature of 278.15 K. Lines were calculated using the LCT in combination with CALM. The dashed lines denote the metastable LLE.

Again, the agreement of predicted and measured data is excellent for the ternary LLE as well as for the ternary SLE. Therefore, the model is able to consider the influence of temperature on the superposition of ternary LLE and SLE. By predicting the superposition of ternary LLE and SLE over a broad temperature range, a 4-dimensional phase diagram can be constructed (Figure 31), which can be used for defining suitable operating windows for a crystallization process.

It can be seen that the region of the ternary SLE is growing with decreasing temperature. This leads to a bigger region where a crystallization process is possible. However, also the region where an oiling out can occur is growing, which has to be considered within process design. Concluding, this section impressively shows the possibility of predicting ternary phase equilibria of systems containing branched molecules based on model parameters that were fitted to experimental data of linear molecules. Having in mind Figure 8, only experimental data of the binary subsystem ethanol + n-hexadecane were available for parameter adjustment out of this ternary system. Therefore, the developed methodology makes phase equilibria of systems containing branched molecules accessible and, additionally, it contributes to a shorter period of process design.

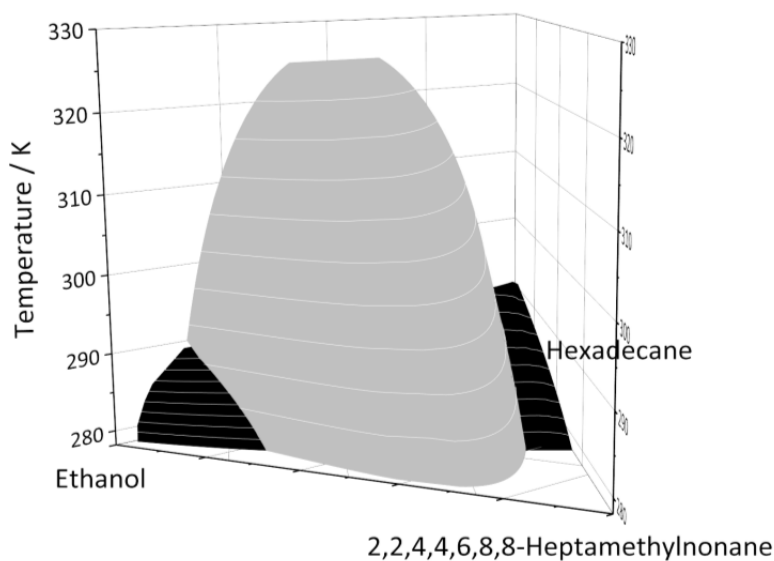


Figure 31: Superposition of LLE (light grey) and SLE (black) of the ternary system n-hexadecane + 2,2,4,4,6,8,8-heptamethylnonane + ethanol

5.1.4 Extension to systems showing cross association

In the previous section, systems containing a polar solvent and one or two non-polar solutes were investigated. It was shown that binary and ternary LLE of these systems as well as the superposition of LLE and SLE can be predicted accurately. Because of only one polar component within these systems, only self-association of the solvent had to be considered. In this section, the methodology will be applied to binary systems containing a polar solvent and a polar solute. Besides the self-association of the solvent, a possible cross-association between solvent and solute has to be considered at this time. At first, it will be proved whether the superposition of LLE and SLE can be calculated accurately. Secondly, it will be proved whether binary LLE of systems containing a branched polar component can be predicted by the developed methodology.

Superposition of LLE and SLE

Before proving the capability of predicting phase equilibria of systems containing branched polar molecules, it will be checked whether the superposition of LLE and SLE can be calculated correctly. As model substances, methanol + methyl oleate were chosen as solvent and solute, respectively. Methyl oleate is an amphiphilic component, containing a polar part

and a non-polar part. As can be seen in Figure 32, the non-polar part is much larger than the polar one, wherefore methyl oleate can be characterized as slightly polar.

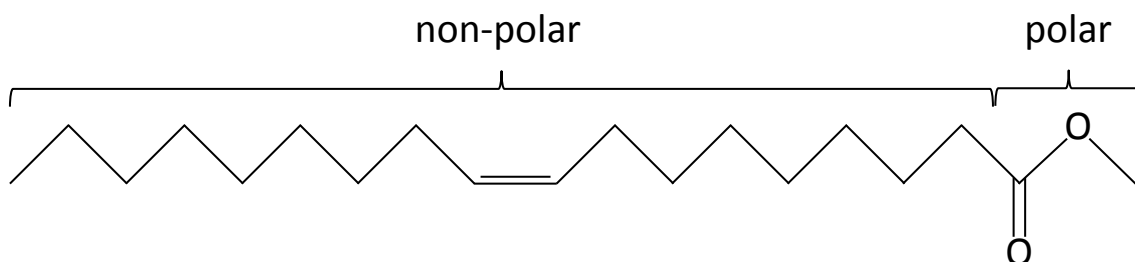


Figure 32: Molecular architecture of methyl oleate.

According to Figure 7, architecture parameters as well as model parameters have to be defined for the calculation of LLE and SLE. Regarding methanol, the same architecture parameters as listed in Table 6 were applied. For methyl oleate, every carbon atom including bonded hydrogen atoms as well as both oxygen atoms were defined as individual segments. This leads to a segment number of 21, a number of bonds of 20, a number of two consecutive bonds of 20 and a number of three consecutive bonds of 19. After defining the architecture parameters, all necessary model parameters have to be determined. While the LCT was combined with CALM in order to describe the self-association of the solvent for the alkane/alcohol systems, it has now to be combined with ECALM to additionally describe cross-association between methanol and methyl oleate. Thus, 6 model parameters have to be defined in total, i.e. the two association parameters Δh_i^{as} and K_{oi} for methanol as well as for methyl oleate, the interaction energy $\Delta \varepsilon_{ij}/k_B$ between methanol and methyl oleate and the parameter η describing the ratio of cross-association and self-association (chapter 3.2.1). The association parameters Δh_i^{as} and K_{oi} of methanol were taken from chapter 5.1.1. Methyl oleate as only slightly polar component is assumed to not be able of performing self-association, wherefore its association enthalpy Δh_i^{as} was set to zero⁶⁴. The remaining three parameters, i.e. interaction energy $\Delta \varepsilon_{ij}/k_B$ between methanol and methyl oleate, association parameter K_{oi} of methyl oleate and the cross-association parameter η , were simultaneously adjusted to binary LLE data of this system. Values of $\Delta \varepsilon_{ij}/k_B = 1.00$ K, $K_{oi} = \exp(-1.90)$ and $\eta = 0.034$ were found. Additionally, the melting temperature and heat of fusion of methyl oleate is needed. Values of $T_i^{SL} = 254.9$ K and $\Delta h_i^{SL} = 48031$ J mol⁻¹ were measured by TU

Berlin. In Figure 33 LLE and SLE were calculated applying the adjusted parameters and compared with experimental data. Experimental data are listed in Table 30 and Table 32.

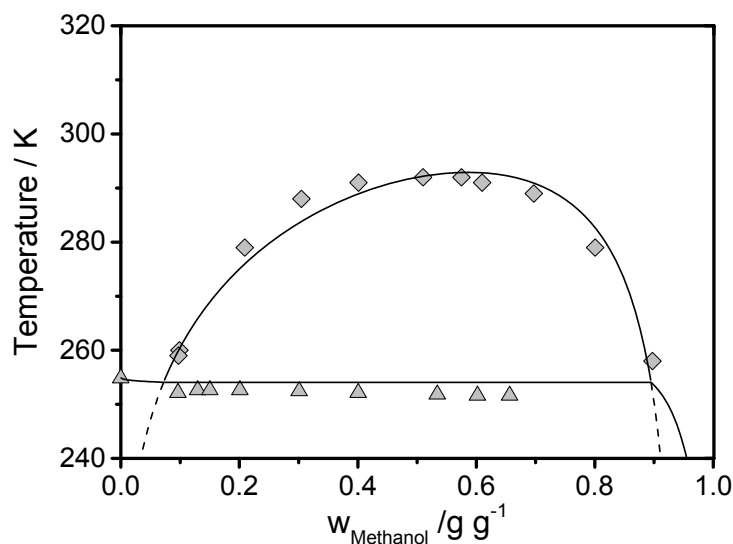


Figure 33: Superposition of LLE (diamonds) and SLE (triangles) of the binary system methyl oleate + methanol. The solid lines were calculated using the LCT in combination with ECALM. Measurements were performed by TU Berlin.

Regarding the binary LLE, it can be seen that the calculated phase equilibrium agrees very well with the experimental data for the whole concentration range. Within the two-phase region the calculated SLE is a few degrees higher than the experimental data. However, having in mind that no SLE data were used for parameter adjustment, this also represents a very good agreement between calculations and experiments. The cross-association parameter η was adjusted to 0.034. This means that the self-association of methanol is predominant to the cross-association between methanol and methyl oleate, proving the assumption that methyl oleate is only slightly polar. Thus, it can be stated that the LCT in combination with ECALM is well-suited for the simultaneous calculation of LLE and SLE of systems showing self-association as well as cross-association.

Prediction of binary LLE

After successfully calculating the superposition of LLE and SLE, it will be checked whether phase equilibria of systems containing a branched polar component can be accurately predicted with the developed methodology. Therefore, two linear ketones, i.e. 2-pentanone

and 2-hexanone, as well as two branched ketones, i.e. 3-methyl-2-butanone and 4-methyl-2-pentanone were investigated as polar components. Ethylene glycol was chosen as solvent. As aim, LLE of the binary systems containing ethylene glycol and one of the branched ketones should be predicted based on model parameters that were fitted to experimental data of the linear ketones.

For the prediction of binary LLE, the same concept was applied as for the alkane/alcohol systems (see Figure 7). For the definition of the architecture parameters of the ketones, every carbon atom including its bonded hydrogen atoms was treated as individual segment. Additionally, the oxygen was defined as individual segment. Regarding ethylene glycol, every carbon atom including bonded hydrogen atoms as well as every hydroxyl group was defined as individual segments. This leads to architecture parameters of ketones and ethylene glycol listed in Table 8.

Table 8: Architecture parameters defined within the LCT of ethylene glycol and four different ketones.

Molecule	N	N ₁	N ₂	N ₃
Ethylene glycol	4	3	2	1
2-pentanone	6	5	5	3
2-hexanone	7	6	6	4
3-methyl-2-butanone	6	5	6	4
4-methyl-2-pentanone	7	6	7	5

Next, the necessary model parameters have to be defined. The ketones are amphiphilic molecules like methyl oleate. However, their non-polar part is smaller, which should lead to more cross-association between ethylene glycol and the ketones in comparison to methanol and methyl oleate. According to literature^{64,99}, it was assumed that the ketones are not able to perform self-association wherefore their association enthalpy Δh_i^{as} was set to zero. The value of the association enthalpy of ethylene glycol was assumed to be the same as for ethanol and methanol because it only refers to the hydroxyl group ($\Delta h_i^{as} = 30685.5 \text{ J mol}^{-1}$). The remaining 4 model parameters, i.e. interaction energy $\Delta \varepsilon_{ij}/k_B$, K_{0i} of ethylene glycol, K_{0i} of the ketone and the cross-association parameter η have to be adjusted to experimental LLE data as described in chapter 3.2.1. All systems were investigated by cloud-point experiments as well as by GC analysis. While for the alkane/alcohol systems both techniques led to the

same results (see Figure 22), differences arose for the ketone/ethylene glycol systems as exemplarily shown for the system 2-pentanone + ethylene glycol in Figure 34.

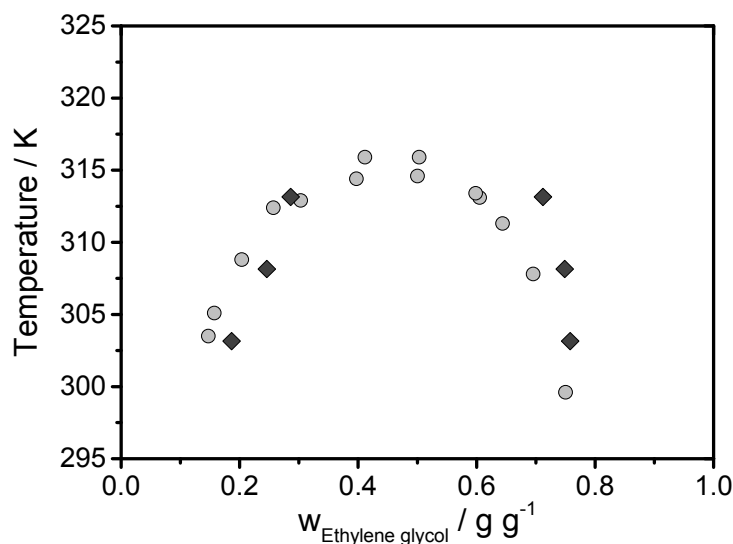


Figure 34: LLE of the binary system ethylene glycol + 2-pentanone. Cloud-points are shown as circles, tie lines are shown as diamonds.

On the ethylene glycol-lean side it can be seen that both techniques agree well. However, on the ethylene glycol-rich side considerable differences are noticeable. The GC analysis leads to a higher weight fraction of ethylene glycol for the complete temperature range, where the difference between cloud-point measurements and GC analysis increases with increasing temperature. The same results were observed for the remaining three systems of ketone + ethylene glycol (see appendix A). The analytical procedure described in chapter 4.3.1 seems not to be the reason for the differences, because it agrees well with the cloud-point experiments on the ethylene glycol-lean side. Moreover, the same differences were observed in experiments performed by different persons, eliminating the possibility of an individual experimental error. Therefore, it was supposed that a reaction could take place between ethylene glycol and the ketones. According to literature^{120,121} a polyol like ethylene glycol can react with aldehydes or ketones to cyclic acetals, where water is produced as a by-product:

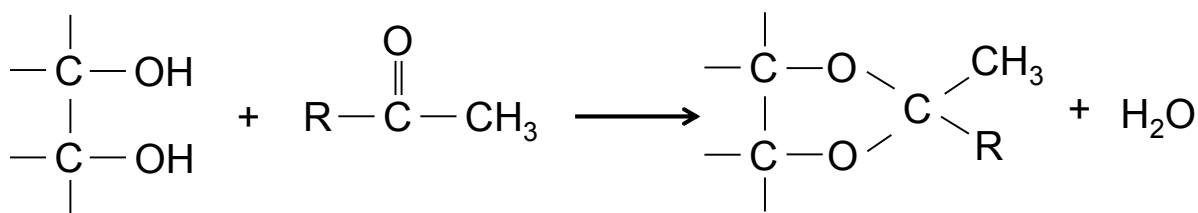


Figure 35: Reaction mechanism of ethylene glycol and ketone adapted from Chopade and Sharma¹²⁰.

Usually, the reaction shown in Figure 35 is catalyzed by an acidic catalyst. However, Mota et al.¹²² could show that the reaction takes also place without catalyst in smaller extend. Thus, within the approximately 24 hour duration of the tie line experiments small amounts of water could have been produced influencing the LLE. In order to proof this hypothesis, tie lines were measured for the binary system ethylene glycol + 2-pentanone as well as for ethylene glycol + 2-hexanone applying the same procedure as described in chapter 4.2.1. The water content was analyzed by Karl-Fischer titration before and after the experiment. It could be shown that water is produced during the experiment (Appendix A). Comparing the water content of both phases, the majority of water was localized in the ethylene glycol-rich phase. This finding is not surprising because ethylene glycol is much more hygroscopic than the ketones. Even though only small amounts of water were produced, this could be an explanation why the GC analysis fails on the ethylene glycol-rich side. Stephenson¹²³ investigated the mutual solubilities of binary water/ketone systems for all 4 ketones investigated in this work. In all cases, the mutual solubility was considerably below 10w-%. Thus, this small amount of water heavily influences the LLE between ethylene glycol and the ketones, wherefore it was decided to not take the GC data but the cloud-point data for parameter adjustment. Although, the reaction can also take place during the cloud-point experiments, its extend will be much smaller because of the shorter duration of the experiment.

Starting with the binary system ethylene glycol + 2-pentanone the remaining 4 model parameters were simultaneously adjusted to the corresponding LLE data shown in Figure 36. The association parameter K_{oi} of ethylene glycol was adjusted to $K_{oi} = \exp(-9.90)$. The values of the other model parameters are listed in Table 9. Regarding the binary system ethylene glycol + 2-hexanone, the association parameters of ethylene glycol remained constant. The remaining model parameters were adjusted to experimental LLE of the corresponding system. Because of technical and safety reasons, there are only data available

up to a temperature of around 340 K (Figure 36). In Table 9 the adjusted values of the model parameters are shown.

Table 9: Adjusted model parameters for the binary systems ethylene glycol + 2-pentanone and ethylene glycol + 2-hexanone.

Parameter	2-pentanone	2-hexanone
$\Delta\varepsilon_{ij}/k_B / \text{K}$	29.1	36.0
$\Delta h_i^{as} / \text{J mol}^{-1}$	0	0
$K_{0i} / -$	$\exp(-2.7)$	$\exp(-1.6)$
$\eta / -$	0.06	0.05

Regarding the values of the cross-association parameter η , it can be seen that they are larger than for methyl oleate ($\eta=0.034$). Thus, the presumption that the ketones perform more cross-association than methyl oleate because of the smaller non-polar part is confirmed. In Figure 36 the adjusted model parameters were applied for calculating the binary LLE of both systems (experimental data are listed in Table 22 and Table 24). Although, there is only a limited number of experimental data available for the system ethylene glycol + 2-hexanone, these data can be represented by the calculation. The same good agreement between experimental data and calculation can be seen for the binary system ethylene glycol + 2-pentanone. Only small deviations can be seen on the ethylene glycol-rich side.

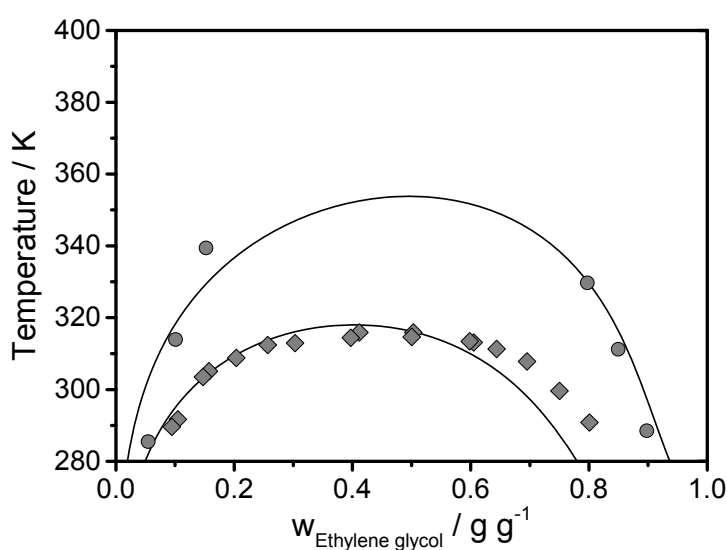


Figure 36: LLE of the binary systems ethylene glycol + 2-pentanone (diamonds) and ethylene glycol + 2-hexanone (circles). The solid lines were calculated using the LCT in combination with ECALM.

In the next step, model parameters adjusted to experimental data of linear ketones and architecture parameters of the branched ketones will be combined in order to predict the binary LLE between ethylene glycol and one of the branched ketones. The association parameters of ethylene glycol remained constant since they only refer to the solvent. Regarding the association parameters of the branched ketone, a similar association behavior than of the linear ketone is assumed, wherefore the association parameters of the linear ketone will be used also for the corresponding branched isomer. Same is assumed for the cross-association parameter η . For the estimation of the interaction energy between ethylene glycol and the branched ketones, the same methodology as for the alkane/alcohol systems was applied meaning that only the linear backbone of the branched ketones is considered. Therefore, an extrapolation function of the interaction energy as a function of the chain length has to be set up. In Figure 37, the two adjusted interaction energies are shown with their corresponding chain length.

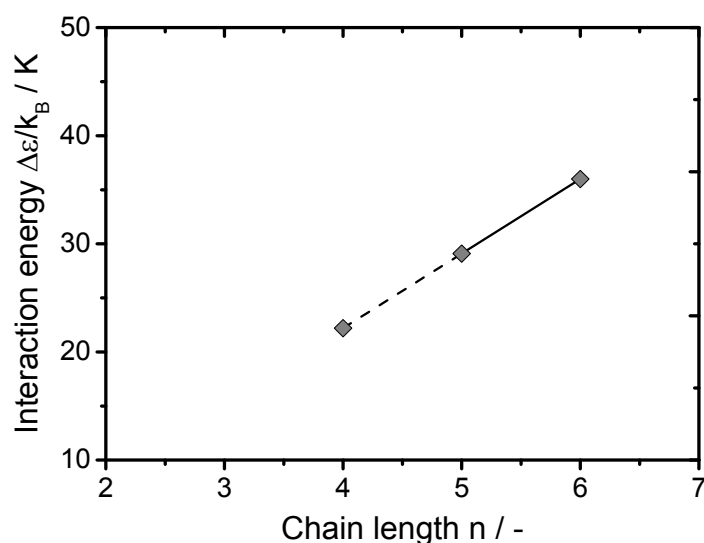


Figure 37: Interaction energy between 2-ketone molecules and ethylene glycol as a function of the chain length of the ketone. The values for chain lengths 5 and 6 were fitted to experimental data, the value for a chain length of 4 was determined by extrapolation.

Even though two data points are not perfectly suited to decide on the course of the function, a linear dependence as was found for the alkanes (Figure 17 and Figure 20) was also assumed for the ketones. This leads to the following extrapolation function:

$$\Delta\varepsilon_{ij}/k_B = 6.9 n - 5.4 \quad (5-3)$$

For 4-methyl-2-pentanone, with a backbone of 5 carbon atoms, the adjusted value for 2-pentanone can be directly applied ($\Delta\varepsilon_{ij}/k_B = 29.1\text{ K}$). Applying the extrapolation function (5-3), the interaction energy between ethylene glycol and 3-methyl-2-butanone, having a backbone of 4 carbon atoms, was estimated to $\Delta\varepsilon_{ij}/k_B = 22.2\text{ K}$. These values were then applied in order predict the binary LLE for both systems. The predicted phase equilibria are compared with the experimental data in Figure 38. Experimental data are listed in Table 26 and Table 28.

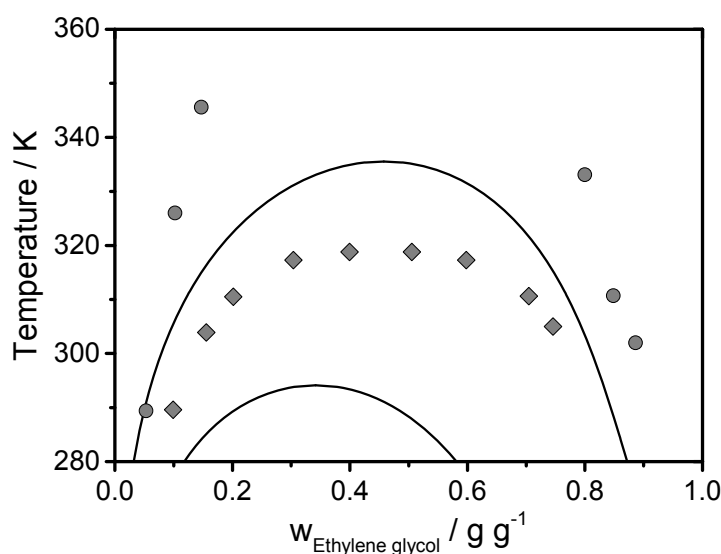


Figure 38: Predicted LLE of the binary systems ethylene glycol + 3-methyl-2-butanone (diamonds) and ethylene glycol + 4-methyl-2-pentanone (circles). The solid lines were calculated using the LCT in combination with ECALM.

Comparing the predicted LLE with the experimental data, considerable differences can be observed for both systems. In both cases, the model predicts a much better solubility than the experimental data. For the system ethylene glycol + 3-methyl-2-butanone the binodal curve is predicted around 30 K below the experimental one. Similar deviations can be seen for the system ethylene glycol + 4-methyl-2-pentanone. Thus, it has to be concluded that the developed methodology cannot be applied directly for the prediction of binary LLE containing a branched polar component. In Figure 33 and Figure 36 it was shown that the model framework of LCT and ECALM is in general able to describe self-association of the solvent and cross-association between solvent and solute simultaneously. However, in both figures only linear molecules were investigated. Thus, the large differences in Figure 38 must

be caused by the branched polar component. In Figure 39 the configuration of ethylene glycol with 2-hexanone and 4-methyl-2-pentanone is shown graphically.

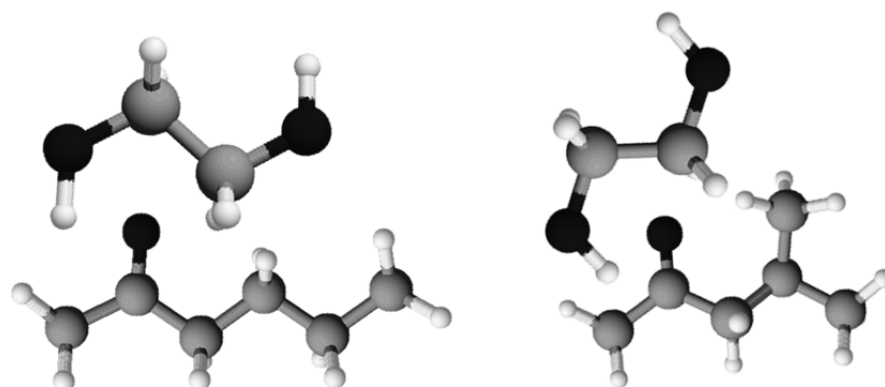


Figure 39: Configuration of ethylene glycol with 2-hexanone (left side) and 4-methyl-2-pentanone (right side).

On the left side, it can be seen that the keto-group is well-accessible for the ethylene glycol leading to no sterically hindrance of cross-association between both molecules. On the right side, the configuration of ethylene glycol with 4-methyl-2-pentanone is shown. As can be seen, the methylene group of the branched ketone is located near the keto-group. This makes it more complicated for the ethylene glycol to interact with the functional group because it can only be reached from a certain direction. Thus, the methylene group of the branched ketone causes a sterically hindrance of the cross-association. Since the calculation of activity coefficients within ECALM is based on FH, it cannot account for molecular architecture and therefore such a sterically hindrance is not covered within the prediction of the binary LLE, which leads to significant deviations to the experimental data.

This section proved that the developed methodology cannot be applied directly to predict phase equilibria of systems showing self-association as well as cross-association. The reason for this is a sterically hindrance caused by the methylene side group. In order to describe the binary LLE, a readjustment of model parameters is possible. However, this would be no prediction and since experimental data of systems containing branched molecules are often not available, this procedure is often not applicable. A possible solution for this shortcoming would be the use of an association model, where the activity coefficients of the chemical equilibrium are calculated by the LCT.

5.2 Adsorption

In this section, the separation of isomers by means of adsorption will be investigated. Two binary systems containing a linear and a branched alkane were considered. In order to calculate the liquid phase adsorption isotherms, a new model based on the LCT was developed. Besides calculating adsorption isotherms, this model also considers a swelling of the adsorbent and the overall mass balance between bulk phase and adsorbed phase. First, the experimental results including pore size distributions and separation efficiencies of the different adsorbents will be discussed. Afterwards, the developed adsorption model will be applied to calculate the liquid phase adsorption isotherms of the two binary alkane systems.

5.2.1 Pore size distribution

As shown in Figure 9, porous adsorbents are used for the separation of isomers, because linear molecules can more easily enter the pores than the branched ones. Thus, the pore size distribution of the adsorbent is a main influencing parameter for the separation efficiency. In this work, three different porous adsorbents were investigated, i.e. activated carbon, silica gel and zeolite. The pore size distributions of these three adsorbents were determined as described in chapter 4.2.4. The results of the measurements are illustrated in Figure 40.

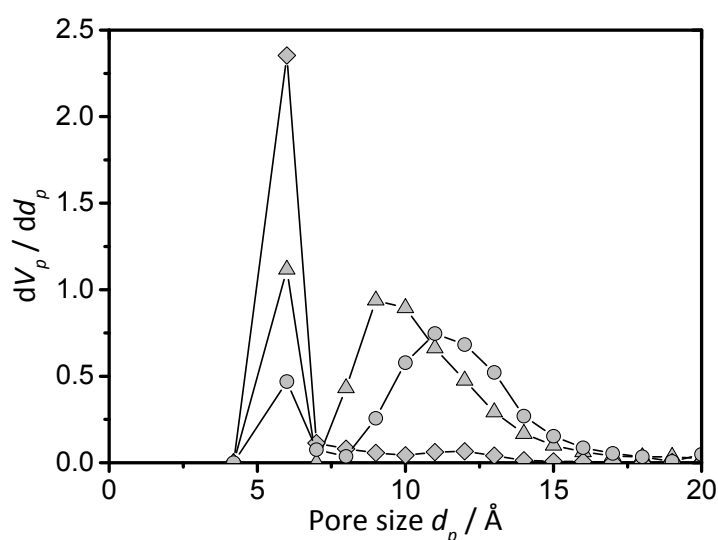


Figure 40: Pore size distributions of zeolite (diamonds), activated carbon (triangles) and silica gel (circles). Measurements were performed by TU Berlin.

It can be seen that the pore size distributions differ for all three adsorbents. Zeolite shows a very sharp pore size distribution with pores having a size of approximately 5 Å. This pore size is larger than the kinetic diameter of n-hexane and n-octane but smaller than the kinetic diameter of 2,3-dimethylbutane and 2,2,4-trimethylpentane²¹. Hence, only the linear alkanes are able to enter the pores, wherefore zeolite should achieve an almost perfect separation of linear and branched alkanes. Activated carbon and silica gel also offer pores with a size of approximately 5 Å. However, there are fewer pores with this size in comparison to zeolite. Additionally, Figure 40 shows that activated carbon as well as silica gel possesses a bimodal pore size distribution with pores having much larger sizes than 5 Å. This allows the branched alkanes to also enter the pores of the adsorbent leading to a poorer separation of linear and branched alkanes. Regarding activated carbon and silica gel, it is obvious that silica gel has fewer pores with 5 Å and more pores with larger sizes. Thus, silica gel should lead to the worst separation efficiency of the three investigated adsorbents. In the next section it will be proved whether these considerations on separation efficiency based on the experimental pore size distributions agree with the experimentally observed separation efficiencies.

5.2.2 Binary system n-octane + 2,2,4-trimethylpentane

In the last section, it was supposed that zeolite achieves an almost perfect separation of linear and branched alkanes, whereas silica gel should lead to a bad separation efficiency. This hypothesis will be checked for the binary system n-octane + 2,2,4-trimethylpentane. The separation efficiency for the three different adsorbents was determined at a temperature of 293.15 K. The results are shown in Figure 41.

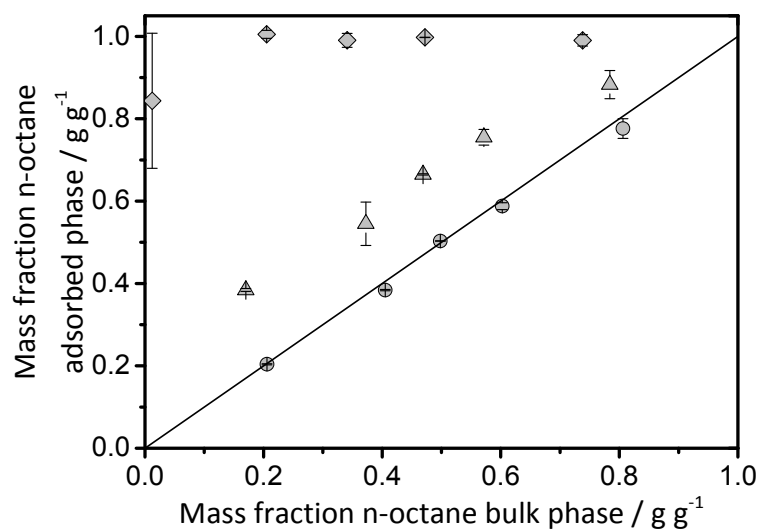


Figure 41: Adsorption isotherms of the binary system n-octane + 2,2,4-trimethylpentane on zeolite (diamonds), activated carbon (triangles) and silica gel (circles) at a temperature of 293.15 K.

Here, the mass fraction of n-octane in the bulk phase is shown on the x-axis and the mass fraction of n-octane in the adsorbed phase is shown on the y-axis. This means that data points lying on the diagonal (black line) lead to no separation between linear and branched alkanes. Regarding Figure 41, it can be seen that the use of silica gel leads to this poor separation. The experimental data of all investigated compositions are located on the diagonal. Data points lying away from the diagonal achieve a separation of linear and branched alkanes. The more the points are away from the diagonal the better is the separation efficiency. As can be seen, zeolite achieves an almost perfect separation with n-octane mass fractions of approximately one in the adsorbed phase throughout the whole concentration range. The separation efficiency of activated carbon lies in between zeolite and silica gel. Therefore, the experimental data confirm the theoretical considerations made from the pore size distributions. Thus, for an industrial adsorption process zeolite would be the best adsorbent. However, the aim of this chapter was not to achieve a perfect separation of linear and branched alkanes but the development of a new adsorption model. This adsorption model should be able to cover all kinds of separation efficiencies ranging from no separation to an almost perfect separation. Hence, all three adsorbents were further investigated. In the upcoming paragraphs, the adsorption isotherms of the system n-octane + 2,2,4-trimethylpentane were measured and calculated for all three adsorbents at different temperatures.

First, the adsorption of n-octane + 2,2,4-trimethylpentane on activated carbon was investigated. Liquid phase adsorption isotherms were measured for 283.15 K, 293.15 K and 303.15 K. Regarding the calculation, the LCT was used without an association model since both molecules are non-polar. The architecture parameters of the alkanes are listed in Table 6. As already described in chapter 3.2.2, the system is treated as a ternary one: n-octane (A), porous adsorbent (B), 2,2,4-trimethylpentane (C). Thus, three model parameters in total have to be defined, i.e. the network parameter $c_{Network}$ of the adsorbent and the interaction energy $\Delta\varepsilon_{ij}/k_B$ between adsorbent and both alkanes. As described in chapter 3.2.2 all three model parameters were simultaneously fitted to adsorption isotherm data of one particular temperature. Afterwards, the network parameter was fixed to this value and the interaction energies were adjusted for the remaining two temperatures. The network parameter $c_{Network}$ of activated carbon was adjusted to 2.2. The adjusted interaction energies $\Delta\varepsilon_{ij}/k_B$ between activated carbon and each of the octane isomers are listed in Table 10. In Figure 42, the calculated adsorption isotherms of this system as well as the calculated swelling behavior of activated carbon are compared with experimental data (Table 42 and Table 43).

Table 10: Adjusted interaction energies between n-octane (A) and adsorbent (B) ($\Delta\varepsilon_{AB}/k_B$) as well as between adsorbent (B) and 2,2,4-trimethylpentane (C) ($\Delta\varepsilon_{BC}/k_B$) for three different adsorbents at three different temperatures.

T / K	283.15	293.15	303.15
Activated carbon			
$\Delta\varepsilon_{AB}/k_B$ / K	-61	-58	-51
$\Delta\varepsilon_{BC}/k_B$ / K	-48	-41	-20
Silica gel			
$\Delta\varepsilon_{AB}/k_B$ / K	-11	-11	-11
$\Delta\varepsilon_{BC}/k_B$ / K	-13	-13	-14
Zeolite			
$\Delta\varepsilon_{AB}/k_B$ / K	-135	-135	-135
$\Delta\varepsilon_{BC}/k_B$ / K	0	0	0

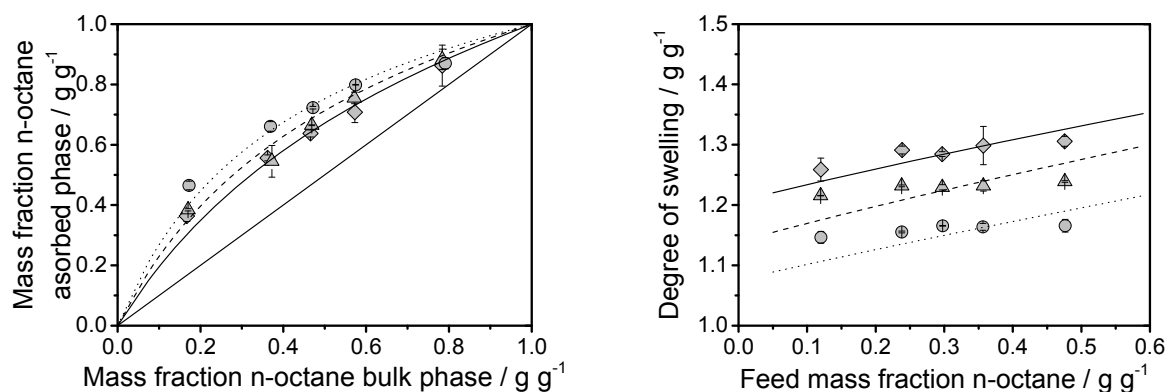


Figure 42: Left side: Adsorption isotherms of the binary system n-octane + 2,2,4-trimethylpentane on activated carbon at temperatures of 283.15 K (diamonds; solid line), 293.15 K (triangles; dashed line) and 303.15 K (circles; dotted line). The lines were calculated by the adsorption model. Right side: Degree of swelling of activated carbon for the binary system n-octane + 2,2,4-trimethylpentane at temperatures of 283.15 K (diamonds; solid line), 293.15 K (triangles; dashed line) and 303.15 K (circles; dotted line). The mass fraction of activated carbon was 0.40 in each case.

Regarding the experimental adsorption isotherms, it is obvious that the temperature has an effect on the separation efficiency. The higher the temperature the better is the separation efficiency indicated by a larger distance to the diagonal (Left side of Figure 42). Within the model, the separation efficiency is expressed by the difference of the two interaction energies. While the difference is 13 K for a temperature of 283.15 K, a difference of 31 K can be found for a temperature of 303.15 K (Table 10). The fact that the separation efficiency increases with increasing temperature was also predicted by the DFT in combination with the LCT-EOS⁴³. The comparison of the experimental adsorption isotherms and the calculated isotherms shows that the model is able to describe the different separation efficiencies in good agreement with the experimental data. The degree of swelling of activated carbon is also dependent on temperature. It can be seen on the right side of Figure 42 that for higher temperatures the degree of swelling decreases. This means that in total fewer molecules are adsorbed at higher temperatures. This finding is covered within the calculations by lowering the individual interaction energies of linear and branched alkane with rising temperatures (Table 10). Comparing the experimental swelling data with the calculated ones, it can be seen that the model calculates lower degrees of swelling for higher temperatures, where the difference between the three temperatures agrees well with the difference between the experimental data. However, as can be seen in Figure 42, the slopes of experimental and calculated data are slightly different.

The same binary system was then investigated on silica gel (experimental data are listed in Table 44 and Table 45). In Figure 41 it was observed that no separation between n-octane and 2,2,4-trimethylpentane was achieved for a temperature of 293.15 K. As can be seen in Figure 43, also no separation is possible for temperatures of 283.15 K and 303.15 K meaning that linear and branched alkanes can enter the pores equally good for all temperatures.

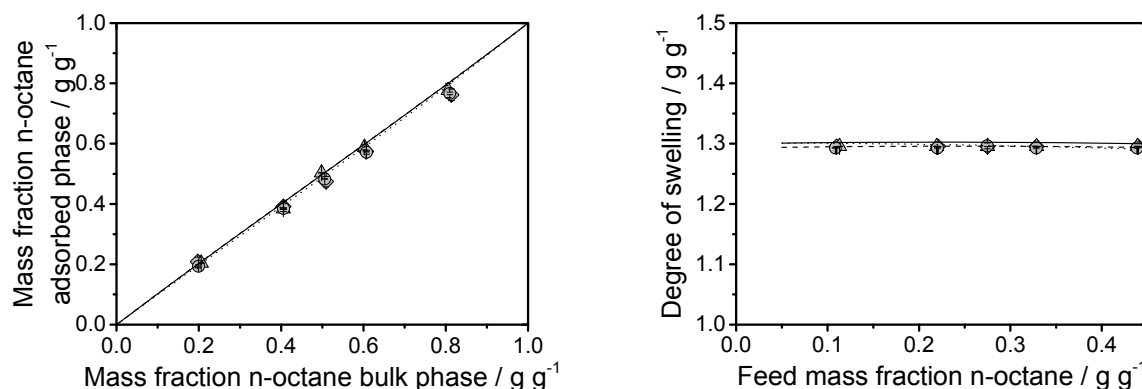


Figure 43: Left side: Adsorption isotherms of the binary system n-octane + 2,2,4-trimethylpentane on silica gel at temperatures of 283.15 K (diamonds; solid line), 293.15 K (triangles; dashed line) and 303.15 K (circles; dotted line). The lines were calculated by the adsorption model. Right side: Degree of swelling of silica gel for the binary system n-octane + 2,2,4-trimethylpentane at temperatures of 283.15 K (diamonds; solid line), 293.15 K (triangles; dashed line) and 303.15 K (circles; dotted line). The mass fraction of silica gel was 0.55 in each case.

This finding is covered within the calculations by nearly equal interaction energies between silica gel and the octane isomers for all temperatures (Table 10). A slightly higher adsorption was measured for 2,2,4-trimethylpentane wherefore its interaction energy with silica gel is a bit higher than for n-octane. Since the ability of the molecules for entering the pores is not dependent on temperature, it is clear that the degree of swelling is also not dependent on temperature, which can be seen on the right side of Figure 43. The calculations were performed with a network parameter $c_{Network}$ of 0.9. Comparing experimental data with the calculations, a very good agreement can be observed for the adsorption isotherms as well as for the degree of swelling. In contrast to activated carbon, the adsorption model is this time able to calculate the right slope of the swelling data.

Finally, the adsorption of the binary system n-octane + 2,2,4-trimethylpentane was investigated on zeolite (Table 46 and Table 47). Because of the very sharp pore size distribution (Figure 40), an almost perfect separation of linear and branched alkane was

observed for a temperature of 293.15 K (Figure 41). The same separation efficiency was also achieved for temperatures of 283.15 K and 303.15 K (Figure 44).

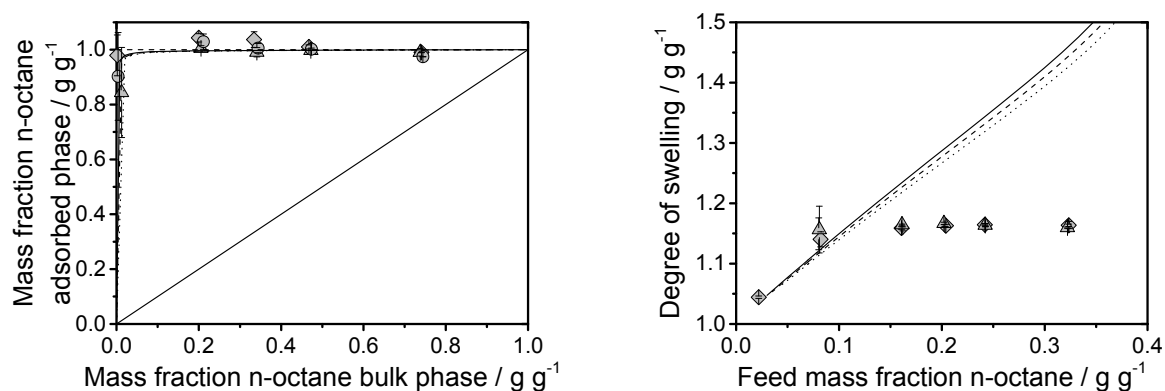


Figure 44: Left side: Adsorption isotherms of the binary system n-octane + 2,2,4-trimethylpentane on zeolite at temperatures of 283.15 K (diamonds; solid line), 293.15 K (triangles; dashed line) and 303.15 K (circles; dotted line). The lines were calculated by the adsorption model. Right side: Degree of swelling of zeolite for the binary system n-octane + 2,2,4-trimethylpentane at temperatures of 283.15 K (diamonds; solid line), 293.15 K (triangles; dashed line) and 303.15 K (circles; dotted line). The mass fraction of zeolite was 0.60 in each case.

Almost over the whole composition range a mass fraction of one was measured within the adsorbed phase for the linear alkane for all investigated temperatures. This means that the linear alkane shows a very strong preferential adsorption on zeolite, which is covered by a large interaction energy between linear alkane and zeolite (Table 10). The branched alkane on the other hand is not able to enter the pores and is therefore not able to adsorb onto the zeolite because of its larger kinetic diameter, wherefore its interaction energy with zeolite was set to zero. Regarding the experimental swelling data, it can be seen that the degree of swelling rapidly increases for low n-octane mass fractions and remains at a constant value for mass fractions of n-octane in the feed larger than 0.08. Comparing experimental data and calculations, which were performed with a network parameter $c_{Network}$ of 3.4, a very good agreement can be seen for the adsorption isotherms. Some experimental data with mass fractions larger than one were measured because of uncertainties within the analytics. Of course, the calculations are restricted to mass fractions not larger than one, leading to a not perfect match with these experimental data. However, all reasonable data points agree very well with the calculations. Regarding the degree of swelling of zeolite, it is obvious that the

model is not able to describe the constant value but calculates increasing degrees of swelling for increasing mass fractions of n-octane in the feed.

This finding shows the limitation of the developed model, especially the assumption underlying Eqs. (3-25), (3-26) and (3-28). In comparison to the swelling of crosslinked polymers, for instance hydrogels, the degree of swelling is very small and therefore the applied swelling model (Eq. (3-28)) must be very precise, especially for small degrees of swelling. On the other hand, the introduced chemical potential for the swelling equilibria in Eqs. (3-25) and (3-26) covers different effects related to the adsorbent. Such effects are pore size distribution, pore geometry, accessibility of the pores for the molecules, energetic heterogeneity of the pores. These effects are not directly included in the model but indirectly covered within the adjustable parameters. In the case of zeolite, the accessibility of the pores is the most important quantity because the pore size distribution is quite narrow (Figure 40). Here, the inclusion of this effect into the interaction energy does obviously not work for the description of the degree of swelling. Nevertheless, the extreme sharp separation represented by the adsorption isotherm can be covered by the model. In contrast, regarding activated carbon and silica gel all mentioned factors are relevant. Here, the procedure of representing these effects by the adjustable parameters is justified.

5.2.3 Binary system n-hexane + 2,3-dimethylbutane

Besides the binary system n-octane + 2,2,4-trimethylpentane also the binary system n-hexane + 2,3-dimethylbutane was investigated. For the calculations of adsorption isotherms and degree of swelling all network parameters $c_{Network}$ adjusted to the system n-octane + 2,2,4-trimethylpentane remained constant for the binary system n-hexane + 2,3-dimethylbutane. The individual interaction energies $\Delta\epsilon_{ij}/k_B$ for n-hexane and 2,3-dimethylbutane were adjusted for every temperature (see Table 11). The first adsorbent investigated was activated carbon. The calculated adsorption isotherms as well as the calculated degree of swelling are compared with experimental data in Figure 45. Experimental data are listed in Table 48 and Table 49.

Table 11: Adjusted interaction energies between n-hexane (A) and adsorbent (B) (ε_{AB}/k_B) as well as between adsorbent (B) and 2,3-dimethylbutane (C) (ε_{BC}/k_B) for three different adsorbents at three different temperatures.

T / K	283.15	293.15	303.15
Activated carbon			
$\Delta\varepsilon_{AB}/k_B$ / K	-64	-51	-41
$\Delta\varepsilon_{BC}/k_B$ / K	-52	-30	-10
Silica gel			
$\Delta\varepsilon_{AB}/k_B$ / K	-13	-13	-13
$\Delta\varepsilon_{BC}/k_B$ / K	-15	-15	-16
Zeolite			
$\Delta\varepsilon_{AB}/k_B$ / K	-135	-135	-135
$\Delta\varepsilon_{BC}/k_B$ / K	0	0	0

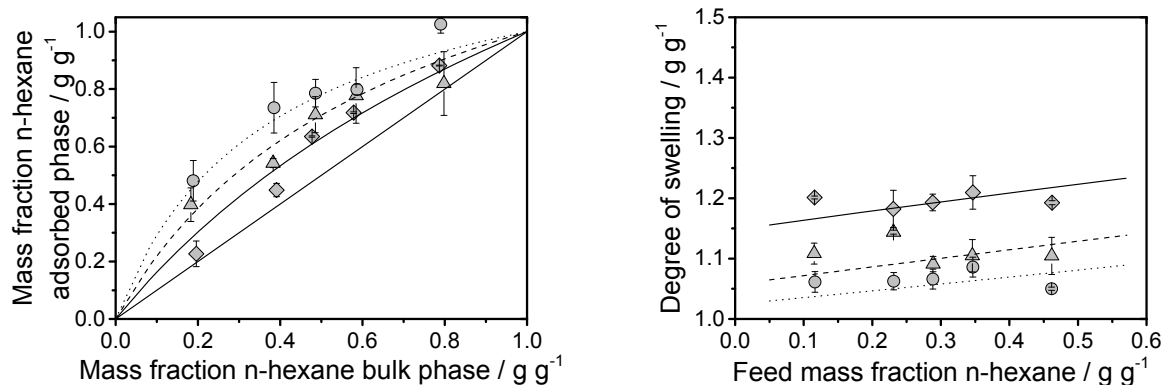


Figure 45: Left side: Adsorption isotherms of the binary system n-hexane + 2,3-dimethylbutane on activated carbon at temperatures of 283.15 K (diamonds; solid line), 293.15 K (triangles; dashed line) and 303.15 K (circles; dotted line). The lines were calculated by the adsorption model. Right side: Degree of swelling of activated carbon for the binary system n-hexane + 2,3-dimethylbutane at temperatures of 283.15 K (diamonds; solid line), 293.15 K (triangles; dashed line) and 303.15 K (circles; dotted line). The mass fraction of activated carbon was 0.42 in each case.

Similarly to the system n-octane + 2,2,4-trimethylpentane, it can be seen that the adsorption is temperature dependent. The highest separation efficiency was achieved for the highest temperature (Left side of Figure 45). Comparing the experimental adsorption isotherms with data measured for the binary system n-octane + 2,2,4-trimethylpentane (Figure 42), it can be seen that the data for the system n-hexane + 2,3-dimethylbutane are more scattered. As described in chapter 4.2.5 the loaded activated carbon was stored for 24 h after suction filtration in order to remove the liquid film on the activated carbon. The hexane isomers have got a lower vapor pressure than the octane isomers. This could lead to a worse reproducibility during the drying process. On the right side of Figure 45, it can be seen that the degree of swelling decreases with increasing temperature, same as was observed for the binary system n-octane + 2,2,4-trimethylpentane.

Comparing the adjusted interaction energies of Table 10 and Table 11, it can be seen that the individual values only differ slightly, which proves that both binary systems behave quite similar. Hence, the assumption of using the same network parameter $c_{Network}$ for both binary systems was justified. The agreement of experimental and calculated adsorption isotherms is not that good as for the former system, which is caused by the more scattered data. Regarding the degree of swelling, the model is able to describe the experimental data as good as for the system n-octane + 2,2,4-trimethylpentane. Again the temperature dependency can be described quite well; however, the slope of the calculations does not perfectly agree with the experimental data.

The next adsorbent investigated was silica gel. Again it can be seen that the system n-hexane + 2,3-dimethylbutane behaves similar to the system n-octane + 2,2,4-trimethylpentane (Figure 46; Table 50 and Table 51).

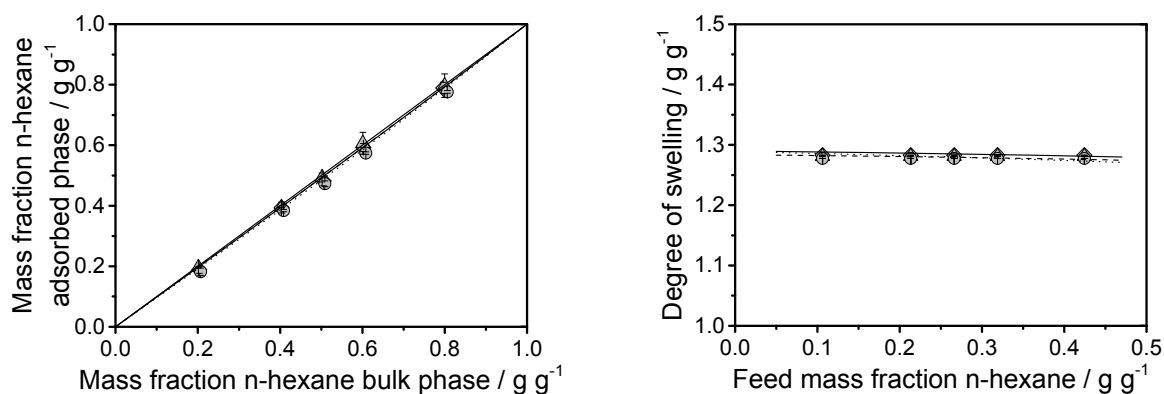


Figure 46: Left side: Adsorption isotherms of the binary system n-hexane + 2,3-dimethylbutane on silica gel at temperatures of 283.15 K (diamonds; solid line), 293.15 K (triangles; dashed line) and 303.15 K (circles; dotted line). The lines were calculated by the adsorption model. Right side: Degree of swelling of silica gel for the binary system n-hexane + 2,3-dimethylbutane at temperatures of 283.15 K (diamonds; solid line), 293.15 K (triangles; dashed line) and 303.15 K (circles; dotted line). The mass fraction of silica gel was 0.53 in each case.

Regarding the adsorption isotherms, it can be seen that no separation of linear and branched alkane was achieved for all investigated temperatures. Linear as well as branched hexane isomers are equally able to enter the pores. Thus, the degree of swelling is also constant for all temperatures. Comparing calculations with the experimental data, it can be seen that the developed model is again able to describe adsorption isotherms as well as degree of swelling in excellent agreement with the experimental data.

The last adsorbent investigated was zeolite. Likewise the system n-octane + 2,2,4-trimethylpentane, an almost perfect separation was observed for the system n-hexane + 2,3-dimethylbutane at all investigated temperatures (Figure 47; Table 52 and Table 53). Already for a low equilibrium mass fraction of n-hexane in the bulk phase, a mass fraction of n-hexane in the adsorbed phase of one was measured.

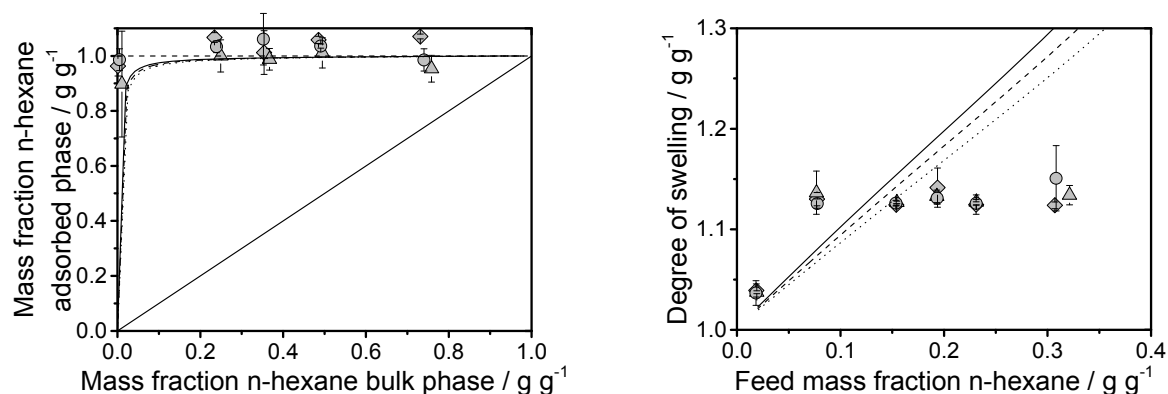


Figure 47: Left side: Adsorption isotherms of the binary system n-hexane + 2,3-dimethylbutane on zeolite at temperatures of 283.15 K (diamonds; solid line), 293.15 K (triangles; dashed line) and 303.15 K (circles; dotted line). The lines were calculated by the adsorption model. Right side: Degree of swelling of zeolite for the binary system n-hexane + 2,3-dimethylbutane at temperatures of 283.15 K (diamonds; solid line), 293.15 K (triangles; dashed line) and 303.15 K (circles; dotted line). The mass fraction of zeolite was 0.62 in each case.

Again some n-octane mass fractions larger than one were determined in the adsorbed phase because of uncertainties within the analytics. Regarding the degree of swelling of zeolite (right side of Figure 47), a fast increase was observed for small feed mass fractions of n-hexane. For mass fractions larger than 0.08 a constant degree of swelling was determined. Comparing the experimental data with the calculations, a very good agreement can be found for the adsorption isotherm considering the reasonable data points, whereas the degree of swelling is not describable with the developed model.

5.2.4 Analysis of adsorption model

All in all, it was shown that the developed adsorption model is well-suited to describe the separation of isomers by means of adsorption. All kinds of separation efficiencies were described in very good agreement with the experimental data. Additionally, it was shown that the developed model is able to cover the temperature dependency of the adsorption, i.e. less overall adsorption for higher temperatures and better separation efficiency for higher temperatures. Besides the network parameter $c_{Network}$ two interaction energies $\Delta\epsilon_{ij}/k_B$, one between adsorbent and linear isomer and one between adsorbent and branched isomer, have to be defined for the calculation, where the network parameter $c_{Network}$ describes the swelling

behavior of the adsorbent and the interaction energies $\Delta\varepsilon_{ij}/k_B$ describe the strength of adsorption of the corresponding isomer. Regarding Figure 48, it can be seen that the adjusted values for the interaction energies are reasonable.

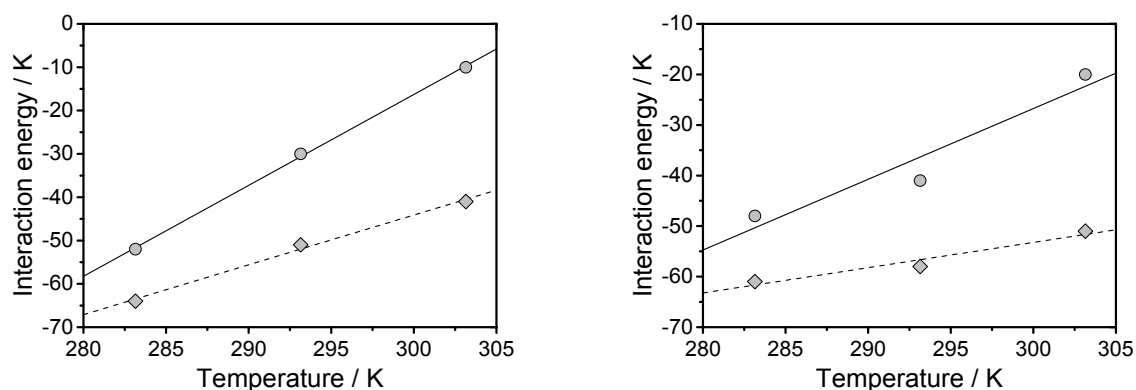


Figure 48: Adjusted interaction energies between activated carbon and linear alkane (diamonds) as well as between activated carbon and branched alkanes (circles). Left side: Binary system n-hexane + 2,3-dimethylbutane. Right side: Binary system n-octane + 2,2,4-trimethylpentane. The lines denote linear fits based on the corresponding data.

The values are negative in all cases. Having in mind the definition of the interaction energy

$\Delta\varepsilon_{ij}/k_B$ (Eq. (3-6)), this means that the attractive forces between adsorbent and isomer are stronger than the sum of the individual energies leading to an adsorption of the isomer. The higher the magnitude of the interaction energy between adsorbent and isomer the more of the isomer will be adsorbed. Hence, for decreasing temperatures the magnitude of the interaction energies increases in order to cover the higher overall adsorption. In Figure 48, it can be seen that the difference between the individual interaction energies is not constant but increasing with increasing temperatures in order to describe the temperature dependency of the separation efficiency. Since the model parameters were adjusted to experimental adsorption isotherm data, the calculations are not predictive. However, it can be seen for both binary systems that the interaction energies show a quite linear relationship to temperature. Thus, the adjusted values could be used to set up an extrapolation function between interaction energy and temperature. This extrapolation function could then be used to calculate adsorption isotherms at different temperatures without having experimental data at this temperature.

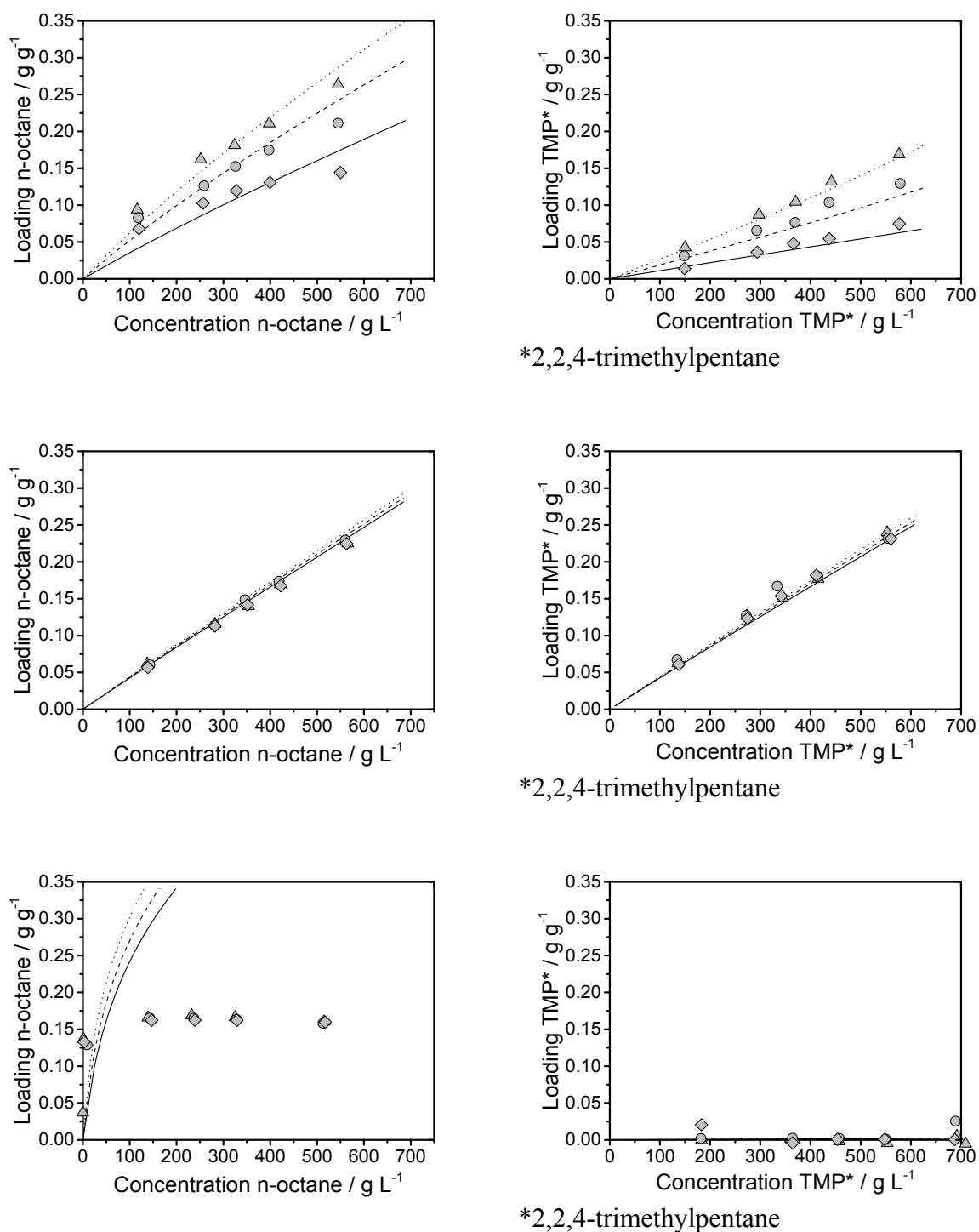


Figure 49: Quasi-pure-component adsorption isotherms of the binary system n-octane (left side) + 2,2,4-trimethylpentane (right side). The adsorption on activated carbon is shown in the first row, on silica gel in the second row and on zeolite in the third row.

While the separation efficiency could be described in very good agreement with the experimental data, it was also obvious that the degree of swelling of the adsorbent could only

partially be described in good agreement with the experimental data. To analyze this finding, the experimental data of the binary system n-octane + 2,2,4-trimethylpentane were reinvestigated in a different way, showing quasi-pure-component adsorption isotherms of linear and branched isomers (Figure 49).

Comparing the data for the three different adsorbents, it can be seen that activated carbon and silica gel are not completely covered, which can be seen by rising values of the loading throughout the whole concentration range. Zeolite on the other hand shows already at low concentrations a complete coverage of its surface. Regarding the calculated loadings, it is evident that they agree with the experimental data for activated carbon and silica gel. In other words, they agree in cases where the adsorbent is not completely covered. For zeolite, where a complete coverage of the surface was achieved, calculations and experimental data differ significantly. Thus, it can be supposed that the developed model is not able to describe a complete coverage of the adsorbent's surface. Since there is no model parameter that contains information of the capacity of the adsorbent, this finding is not surprising. All the model knows, is a different affinity to linear and branched isomers integrated into the two interaction energies.

5.3 Application in process design

In this section, the developed models for crystallization and adsorption are evaluated for designing a possible isomer separation process. Within the collaborative research center InPROMPT, reactions of long-chain unsaturated oleochemicals like hydroesterification are of special interest. As described by Gaide et al.⁴, the reaction is preferably performed in a thermomorphic multicomponent solvent system (TMS). This means that the reaction is performed at a temperature where the reaction mixture is homogeneous. Afterwards, the temperature is switched such that two liquid phases arise. According to Dreimann et al.¹²⁴, this phase separation can be utilized in order to efficiently recycle the homogeneous catalyst. To further decrease catalyst loss, an additional organophilic solvent nanofiltration is possible. For the subsequent purification of linear and branched isomers produced in the mentioned reactions, the developed models can be applied. Unfortunately, the esters produced in the mentioned reaction were not available in high purity. Therefore, no reliable phase equilibrium data could be measured for these systems. Thus, the separation of isomers for the reference

system n-hexadecane + 2,2,4,4,6,8,8-heptamethylnonane + ethanol was investigated in this chapter. It was assumed that the same key performance parameters like conversion can be assumed as for the mentioned ester systems. Process design depends on whether the linear isomer, the branched isomer or both isomers are of interest. Here, a process concept is introduced, where both isomers are captured (Figure 50).

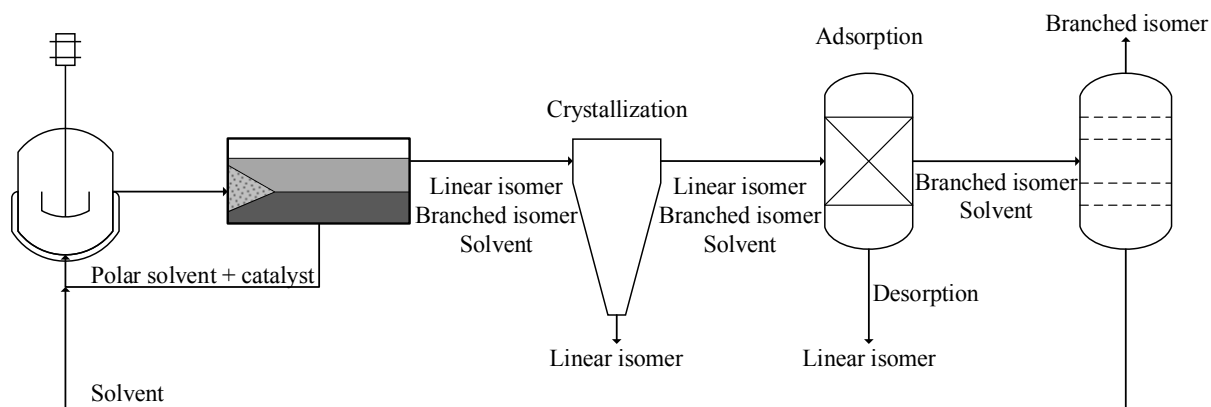


Figure 50: Process flowsheet for purifying linear as well as branched isomer.

In process design, it is crucial to always focus on the overall process meaning that reaction and separation have to be optimized simultaneously. As described by Gaide et al.⁴, high conversion can be achieved for a ratio of linear and branched isomer of 75:25. In order to reach higher l/b ratios (up to 96:4 was achieved), a loss in conversion has to be taken. Regarding Figure 50, it can be seen that a crystallization step follows the recycle of polar solvent and catalyst. As shown in Figure 51, only the shaded regions are suitable for crystallization because the region in between will lead to oiling out.

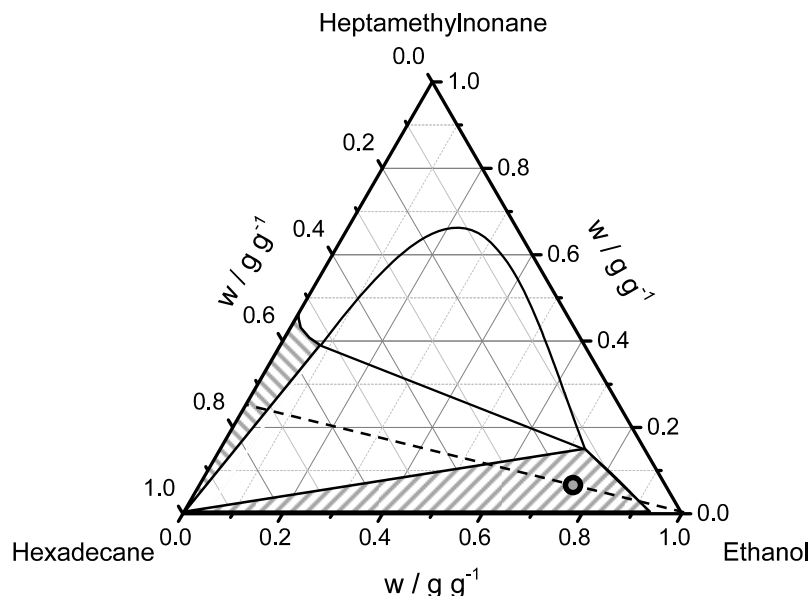


Figure 51: Superposition of ternary LLE and SLE for a temperature of 283.15 K. The shaded regions denote possible operating windows for crystallization. The marked concentration is achieved by adding ethanol to a 75:25 mixture of linear and branched isomer.

Because an operational point can vary to a certain extent, the right region is preferred. Hence, a l/b ratio of 75:25 after the reaction in combination with a large excess of solvent is sufficient in order to reach a suitable concentration for crystallization while keeping the conversion of the reaction at a high level. Then, the linear isomer can be separated from the mixture with a theoretical purity of 100% (in real operation, the purity is usually slightly lower³). However, according to the lever rule, the linear isomer cannot be separated completely.

After crystallization, the mixture is fed to an adsorption step. As described in chapter 5.2, the linear isomer can be perfectly separated from the mixture by application of the right porous adsorbent. Thus, after the adsorption, the reaction mixture only contains the branched isomer and the solvent and the porous adsorbent is loaded with linear isomer. It depends on the amount of adsorbed linear isomer, its value and the overall costs of a subsequent desorption step whether desorption should be performed for capturing the adsorbed linear isomer. In case of a very cheap desorption, it is also imaginable to capture the linear isomer exclusively by adsorption. An exact answer to this question can only be given by a detailed process optimization including all investment and operational costs. Since this was not in the scope of this work, a flexible flowsheet with crystallization and adsorption is proposed.

In a last process step, branched isomer and solvent have to be separated for example by rectification. Here, it can be again seen that the complete process has to be in focus all the

time. On the one hand the solvent has to build a suitable TMS with the polar solvent and on the other hand the separation of solvent and branched isomer has to be performed with low effort, e.g. no azeotrope between branched isomer and solvent. After separating branched isomer and solvent, the solvent can be recycled to the reaction step.

All in all, it could be shown that the developed models are well-suited for the process design of isomer separation. The underlying phase equilibria of crystallization and adsorption are calculated by a minimum amount of experimental data. This leads to a fast and efficient definition of suitable operating windows. A possible process was introduced, where linear as well as branched isomer can be captured. Processes where only one of these isomers are of interest are also imaginable. The developed models offer a moderate numerical effort, wherefore they are applicable in process optimization. This was not in the scope of this work and has to be evaluated in the future.

6 Conclusion and outlook

The separation of isomers is still challenging in chemical industry. After non-regiospecific reactions like hydroformylation or hydroesterification, normally only a specific isomer is of interest. Crystallization and adsorption are suitable unit operations for this separation task. However, there are several challenges arising while designing these unit operations. For example, when crystallization is performed from solution, a possible oiling out, which has often a negative impact on the final product properties, has to be avoided. Thus, the underlying phase equilibria have to be known in order to design a suitable crystallization process.

First objective of this work was the development of a methodology for predicting phase equilibria of systems containing branched molecules. This methodology, which is based on an incompressible version of the Lattice Cluster Theory (LCT) in combination with a chemical association model, is necessary because branched molecules are often not available in high purity for experiments. The LCT was chosen for this task since it considers the molecular architecture within the Helmholtz free energy, where the molecular architecture is defined by architecture parameters based on the chemical formula. Basic idea of the developed methodology is to combine model parameters that were adjusted to experimental data of linear molecules with architecture parameters of the branched molecules. Within the incompressible version of the LCT, one interaction energy has to be defined for a binary system. While this parameter is usually adjusted to experimental data, another procedure is necessary for systems containing branched molecules. An adjustment of this parameter for the corresponding linear isomer and a subsequent use also for the branched isomer is not applicable. Therefore, the possibility of extrapolating within a homologue series was checked. For different binary systems containing linear alkanes and an alcohol it could be shown that the interaction energy shows a linear dependence of the chain length within a certain range of chain lengths. It was assumed that the interaction energy related to the branched isomer can be estimated based on the linear backbone. First, this methodology was tested for predicting LLE of different binary systems containing a branched alkane and an alcohol, wherefore the LCT was combined with the Chemical Association Lattice Model (CALM). In literature it was shown that small differences in molecular architecture can have a significant influence on phase equilibria. Therefore, special attention was drawn to the question whether the

methodology can cover these small differences in molecular architecture correctly. All predicted LLE showed a very good agreement with the experimental data including molecules, which only differ in the position of one methylene group. Subsequently, it was checked whether LLE and SLE of ternary systems containing a linear alkane, a branched alkane and an alcohol can be predicted correctly by the developed methodology. The prediction was based on the binary subsystems, where the binary subsystem containing branched alkane and alcohol itself was already predicted. Both predicted phase equilibria, ternary LLE as well as ternary SLE, agreed very well with the experimental data, where the temperature dependence of both phase equilibria is covered quantitatively. Moreover, it was demonstrated that the distribution behavior within the ternary LLE can be predicted in very good agreement with experimental data. Afterwards, the methodology was applied to binary systems showing self-association as well as cross association. Therefore, binary LLE of two systems containing a branched ketone and ethylene glycol were predicted applying the LCT in combination with the Extended Chemical Association Lattice Model (ECALM). Here, it was shown that the predicted binary LLE differ significantly from the experimental data. Reason for this finding is the position of the methylene group of the branched ketone. It is located next to the functional group leading to a sterically hindrance of the cross-association. Such a sterically hindrance cannot be described by the applied association model, wherefore the prediction failed for these systems.

Second objective of this work was to check whether the LCT is able to describe oiling out during crystallization. Thus, LLE and SLE have to be calculated simultaneously meaning that the same set of model parameters is applied. In order to prove this, different binary and ternary systems consisting of alcoholic alkane solutions were investigated. To consider the self-association of the alcohol, the LCT was combined with CALM. First, model parameters of LCT and CALM were adjusted to binary LLE data. Afterwards, the binary SLE was predicted based on the adjusted parameters. It could be shown that both phase equilibria can be described in very good agreement with experimental data. Subsequently, ternary LLE and SLE were predicted based on the binary subsystems without further adjustment of model parameters. Again, a very good agreement of experimental and calculated data was observed for both phase equilibria. Lastly, the system methyl oleate + methanol was investigated to prove whether the superposition of LLE and SLE can also be calculated for systems showing self-association and cross-association. Therefore, the LCT was combined with ECALM. Once again, the calculations agreed very well with the experiments, wherefore it can be stated that

the LCT in combination with a chemical association model is well-suited for simultaneously calculating LLE and SLE.

In the last part of this work, a new model based on an incompressible version of the LCT was developed for the liquid phase adsorption of isomers on porous adsorbents. Besides calculating the liquid phase adsorption isotherms, the model also considers the swelling of the porous adsorbent, which can be caused by solid-fluid interactions. Therefore, the adsorbent is treated as individual component. Within the new model, different interaction energies between isomers and the adsorbent can be defined to describe preferential adsorption of one isomer. An additional contribution to the chemical potential accounts for the swelling of the adsorbent. The model was applied to two binary systems containing a linear alkane and a branched alkane and to three porous adsorbents. The adsorbents were chosen to have significantly different pore size distributions in order to prove whether the adsorption model can describe all kinds of different separation efficiencies. Model parameters were directly adjusted to experimental adsorption isotherms as well as to experimental swelling data. It could be observed that the adsorption isotherms agreed very well with the experimental data for all systems. Thus, the new model is able to describe all kinds of different separation efficiencies ranging from an almost perfect separation to no separation. Regarding the swelling behavior, only two adsorbents could be described in good accuracy. The swelling behaviour of the third adsorbent could not be described by the adsorption model. By further evaluating the available data, it was obvious that this adsorbent was fully loaded while the remaining two were not completely loaded by the alkanes. Thus, it seems that the developed model is only applicable to porous adsorbents not completely loaded.

In the future, a more detailed analysis on predicting phase equilibria of systems showing self-association as well as cross-association should be performed. First, a branched polar component not leading to a sterically hindrance of cross-association should be searched in order to prove the applicability of the developed methodology. For systems where a sterically hindrance of cross-association occurs, an association model is needed, which takes the molecular architecture into account. The calculation of activity coefficients within CALM and ECALM is based on FH. If they were calculated by the LCT instead, this could offer a possibility to overcome the stated shortcomings. Regarding the developed adsorption model, no prediction of adsorption isotherms is possible. Reason for this is that the pore size distribution of the porous adsorbent is only considered indirectly. In order to predict adsorption isotherms of systems containing branched molecules, the developed model should

be combined with an existing density functional theory approach. This hybrid model would be predictive while assuring a reasonable numerical effort.

References

- (1) **Zagajewski, M.; Dreimann, J.; Thönes, M.; Behr, A.** Rhodium catalyzed hydroformylation of 1-dodecene using an advanced solvent system: Towards highly efficient catalyst recycling. *Chem. Eng. Process.* **2016**, *99*, 115–123.
- (2) **Behr, A.; Vorholt, A. J.; Rentmeister, N.** Recyclable homogeneous catalyst for the hydroesterification of methyl oleate in thermomorphic solvent systems. *Chem. Eng. Sci.* **2013**, *99*, 38–43.
- (3) **Beierling, T.; Osiander, J.; Sadowski, G.** Melt crystallization of isomeric long-chain aldehydes from hydroformylation. *Sep. Purif. Technol.* **2013**, *118*, 13–24.
- (4) **Gaide, T.; Behr, A.; Arns, A.; Benski, F.; Vorholt, A. J.** Hydroesterification of methyl 10-undecenoate in thermomorphic multicomponent solvent systems—Process development for the synthesis of sustainable polymer precursors. *Chem. Eng. Process.* **2016**, *99*, 197–204.
- (5) **Mohameed, H. A.; Jdayil, B. A.; Takroui, K.** Separation of para-xylene from xylene mixture via crystallization. *Chem. Eng. Process.* **2007**, *46*, 25–36.
- (6) **Gu, Z.-Y.; Jiang, D.-Q.; Wang, H.-F.; Cui, X.-Y.; Yan, X.-P.** Adsorption and Separation of Xylene Isomers and Ethylbenzene on Two Zn–Terephthalate Metal–Organic Frameworks. *J. Phys. Chem. C* **2010**, *114*, 311–316.
- (7) **Schenk, M.; Vidal, S. L.; Vlugt, T. J. H.; Smit, B.; Krishna, R.** Separation of Alkane Isomers by Exploiting Entropy Effects during Adsorption on Silicalite-1: A Configurational-Bias Monte Carlo Simulation Study. *Langmuir* **2001**, *17*, 1558–1570.
- (8) **Ott, J. B.; Goates, J. R.** (Solid + liquid) phase equilibria in binary mixtures containing benzene, a cycloalkane, an n-alkane, or tetrachloromethane. An equation for representing (solid + liquid) phase equilibria. *J. Chem. Thermodyn.* **1983**, *15*, 267–278.
- (9) **Petrov, A. A.; Sergienko, S. R.; Nechitailo, N. A.; Tsedilina, A. L.** Synthesis and properties of monomethyl alkanes of composition C₁₂-16. *Izvestiya Akademii Nauk SSSR, Seriya Khimicheskaya* **1959**, 1091–1097.
- (10) **Snow, R. L.; Ott, J. B.; Goates, J. R.; Marsh, K. N.; O'Shea, S.; Stokes, R. H.** (Solid + liquid) and (vapor + liquid) phase equilibria and excess enthalpies for (benzene + n-tetradecane), (benzene + n-hexadecane), (cyclohexane + n-tetradecane),

- and (cyclohexane + n-hexadecane) at 293.15, 298.15, and 308.15 K. Comparison of GE calculated from (vapor + liquid) and (solid + liquid) equilibria. *J. Chem. Thermodyn.* **1986**, *18*, 107–130.
- (11) **Terres, E.; Gebert, F.; Fischer, D.; Modak, G.** Determination of a foaming point above the solidification point of paraffinic hydrocarbons. *Brennstoff-Chemie* **1954**, *35*, 263–269.
- (12) **Ulrich, J.; Bierwirth, J.; Henning, S.** Solid Layer Melt Crystallization. *Sep. Purif. Methods* **2006**, *25*, 1–45.
- (13) *Crystallization: Basic concepts and industrial applications*; **Beckmann, W.**, Ed.; Wiley-VCH Verlag GmbH & Co. KGaA: Weinheim, 2013.
- (14) **Mullin, J. W.; Nyvlt, J.** Programmed cooling of batch crystallizers. *Chem. Eng. Sci.* **1971**, *26*, 369–377.
- (15) **Micovic, J.; Beierling, T.; Lutze, P.; Sadowski, G.; Górak, A.** Entwurfsmethode zur Auslegung hybrider Trennverfahren aus Rektifikation und Schmelzekristallisation für die Aufreinigung engsiedender Gemische. *Chem. Ing. Tech.* **2012**, *84*, 2035–2047.
- (16) **Bravo-Bravo, C.; Segovia-Hernández, J. G.; Hernández, S.; Gutiérrez-Antonio, C.; Briones-Ramírez, A.** Design and Optimization of a Hybrid Distillation/Melt Crystallization Process using Genetic Algorithms. *Chem. Eng. Trans.* **2011**, *24*, 427–432.
- (17) **Bastiaensen, E.; Eck, B.; Thiel, J.** Method for purifying acrylic acid or methacrylic acid by crystallization and distillation, Jun 30, 1999.
- (18) **Herm, Z. R.; Wiers, B. M.; Mason, J. A.; van Baten, J. M.; Hudson, M. R.; Zajdel, P.; Brown, C. M.; Masciocchi, N.; Krishna, R.; Long, J. R.** Separation of hexane isomers in a metal-organic framework with triangular channels. *Science* **2013**, *340*, 960–964.
- (19) **Maloney, M. L.; Maschmeyer, T.; Jansen, J. C.** Technical and economical evaluation of a zeolite membrane based heptane hydroisomerization process. *Chem. Eng. J.* **2005**, *106*, 187–195.
- (20) **Barcia, P. S.; Zapata, F.; Silva, J. A. C.; Rodrigues, A. E.; Chen, B.** Kinetic separation of hexane isomers by fixed-bed adsorption with a microporous metal-organic framework. *J. Phys. Chem. B* **2007**, *111*, 6101–6103.
- (21) **Funke, H. H.; Argo, A. M.; Falconer, J. L.; Noble, R. D.** Separations of Cyclic, Branched, and Linear Hydrocarbon Mixtures through Silicalite Membranes. *Ind. Eng. Chem. Res.* **1997**, *36*, 137–143.

- (22) **Doki, N.; Yokota, M.; Sasaki, S.; Kubota, N.** Simultaneous Crystallization of d - and l -Asparagines in the Presence of a Tailor-Made Additive by Natural Cooling Combined with Pulse Heating. *Cryst. Growth Des.* **2004**, *4*, 1359–1363.
- (23) **Lim, B.-G.; Ching, C.-B.; Tan, R. B.; Ng, S.-C.** Recovery of (–)-praziquantel from racemic mixtures by continuous chromatography and crystallisation. *Chem. Eng. Sci.* **1995**, *50*, 2289–2298.
- (24) **Lorenz, H.; Perlberg, A.; Sapoundjiev, D.; Elsner, M. P.; Seidel-Morgenstern, A.** Crystallization of enantiomers. *Chem. Eng. Process.* **2006**, *45*, 863–873.
- (25) **Kaspereit, M.; Swernath, S.; Kienle, A.** Evaluation of Competing Process Concepts for the Production of Pure Enantiomers. *Org. Process Res. Dev.* **2012**, *16*, 353–363.
- (26) **Maier, N. M.; Franco, P.; Lindner, W.** Separation of enantiomers: needs, challenges, perspectives. *J. Chromatogr. A* **2001**, *906*, 3–33.
- (27) **Muynck, C. de; Beauprez, J.; Soetaert, W.; Vandamme, E. J.** Boric acid as a mobile phase additive for high performance liquid chromatography separation of ribose, arabinose and ribulose. *J. Chromatogr. A* **2006**, *1101*, 115–121.
- (28) **Kaspereit, M.; Jandera, P.; Skavrada, M.; Seidel-Morgenstern, A.** Impact of adsorption isotherm parameters on the performance of enantioseparation using simulated moving bed chromatography. *J. Chromatogr. A* **2002**, *944*, 249–262.
- (29) **Lorenz, H.; Sheehan, P.; Seidel-Morgenstern, A.** Coupling of simulated moving bed chromatography and fractional crystallization for efficient enantioseparation. *J. Chromatogr. A* **2001**, *908*, 201–214.
- (30) **Gedicke, K.; Beckmann, W.; Brandt, A.; Sapoundjiev, D.; Lorenz, H.; Budde, U.; Seidel-Morgenstern, A.** Coupling Chromatography and Crystallization for Efficient Separations of Isomers. *Adsorption* **2005**, *11*, 591–596.
- (31) **Kaspereit, M.; Gedicke, K.; Zahn, V.; Mahoney, A. W.; Seidel-Morgenstern, A.** Shortcut method for evaluation and design of a hybrid process for enantioseparations. *J. Chromatogr. A* **2005**, *1092*, 43–54.
- (32) **Kaspereit, M.** *Separation of enantiomers by a process combination of chromatography and crystallisation*; Forschungsberichte aus dem Max-Planck-Institut für Dynamik Komplexer Technischer Systeme Bd. 14; Shaker: Aachen, 2006.
- (33) **Kiesow, K.; Tumakaka, F.; Sadowski, G.** Experimental investigation and prediction of oiling out during crystallization process. *J. Cryst. Growth* **2008**, *310*, 4163–4168.

- (34) **Kiesow, K.; Ruether, F.; Sadowski, G.** Solubility, crystallization and oiling-out behavior of PEGDME: 1. Pure-solvent systems. *Fluid Phase Equilib.* **2010**, *298*, 253–261.
- (35) **Yang, H.; Rasmuson, Å. C.** Investigation of Batch Cooling Crystallization in a Liquid–Liquid Separating System by PAT. *Org. Process Res. Dev.* **2012**, *16*, 1212–1224.
- (36) **Yang, H.; Rasmuson, Å. C.** Phase equilibrium and mechanisms of crystallization in liquid–liquid phase separating system. *Fluid Phase Equilib.* **2015**, *385*, 120–128.
- (37) **CAHN, J. W.** The Metastable Liquidus and Its Effect on the Crystallization of Glass. *J. Am. Ceram. Soc.* **1969**, *52*, 118–121.
- (38) **Lu, J.; Li, Y.-P.; Wang, J.; Ren, G.-B.; Rohani, S.; Ching, C.-B.** Crystallization of an active pharmaceutical ingredient that oils out. *Sep. Purif. Technol.* **2012**, *96*, 1–6.
- (39) **Hofman, T.; Reda, M.; Gliński, M.** Liquid–liquid equilibrium in binary systems of isomeric C8 aliphatic monoethers with nitromethane. *Fluid Phase Equilib.* **2013**, *356*, 271–276.
- (40) **Reda, M.; Ruszczyński, L.; Gliński, M.; Hofman, T.** (Liquid+liquid) equilibrium in binary systems of isomeric C8 aliphatic monoethers with acetonitrile and its interpretation by the COSMO-SAC model. *J. Chem. Thermodyn.* **2015**, *85*, 42–48.
- (41) **Weidlich, U.; Gmehling, J.** A Modified UNIFAC Model. 1. Prediction of VLE, hE, and gamma. *Ind. Eng. Chem. Res.* **1987**, *26*, 1372–1381.
- (42) **Lin, S.-T.; Sandler, S. I.** A Priori Phase Equilibrium Prediction from a Segment Contribution Solvation Model. *Ind. Eng. Chem. Res.* **2002**, *41*, 899–913.
- (43) **Zimmermann, P.; Goetsch, T.; Zeiner, T.; Enders, S.** Modelling of adsorption isotherms of isomers using density functional theory. *Mol. Phys.* **2016**, *115*, 1389–1407.
- (44) **Fredenslund, A.; Jones, R. L.; Prausnitz, J. M.** Group-contribution estimation of activity coefficients in nonideal liquid mixtures. *AIChE J.* **1975**, *21*, 1086–1099.
- (45) **Wilson, G. M.; Deal, C. H.** Activity coefficients and molecular structure: Activity coefficients in changing environments - Solution of groups. *Ind. Eng. Chem. Fundam.* **1962**, *1*.
- (46) **Ronc, M.; Ratcliff, G. A.** Prediction of excess free energies of liquid mixtures by an analytical group solution model. *Can. J. Chem. Eng.* **1971**, *49*, 825–830.

-
- (47) **Abrams, D. S.; Prausnitz, J. M.** Statistical thermodynamics of liquid mixtures: A new expression for the excess Gibbs energy of partly or completely miscible systems. *AIChE J.* **1975**, *21*, 116–128.
- (48) **Magnussen, T.; Rasmussen, P.; Fredenslund, A.** UNIFAC parameter table for prediction of liquid-liquid equilibria. *Ind. Eng. Chem. Proc. Des. Dev.* **1981**, *20*, 331–339.
- (49) **Gupte, P. A.; Danner, R. P.** Prediction of Liquid-Liquid Equilibria with UNIFAC: A Critical Evaluation. *Ind. Eng. Chem. Res.* **1987**, *26*, 2036–2042.
- (50) **Klamt, A.; Schüürmann, G.** COSMO: A New Approach to Dielectric Screening in Solvents with Explicit Expressions for the Screening Energy and its Gradient. *J. Chem. Soc. Perkin Trans. 2* **1993**, 799–805.
- (51) **Onsager, L.** Electric Moments of Molecules in Liquids. *J. Am. Chem. Soc.* **1936**, *58*, 1486–1493.
- (52) **Klamt, A.** Conductor-like Screening Model for Real Solvents: A New Approach to the Quantitative Calculation of Solvation Phenomena. *J. Phys. Chem.* **1995**, *99*, 2224–2235.
- (53) **Klamt, A.; Jonas, V.; Bürger, T.; Lohrenz, J. C. W.** Refinement and Parametrization of COSMO-RS. *J. Phys. Chem. A* **1998**, *102*, 5074–5085.
- (54) **Freed, K. F.** New lattice model for interacting, avoiding polymers with controlled length distribution. *J. Phys. A: Math. Gen.* **1985**, *18*, 871–887.
- (55) **Bawendi, M. G.; Freed, K. F.; Mohanty, U.** A lattice model for self-avoiding polymers with controlled length distributions. II. Corrections to Flory–Huggins mean field. *J. Chem. Phys.* **1986**, *84*, 7036–7047.
- (56) **Nemirovsky, A. M.; Bawendi, M. G.; Freed, K. F.** Lattice models of polymer solutions: Monomers occupying several lattice sites. *J. Chem. Phys.* **1987**, *87*, 7272–7284.
- (57) **Freed, K. F.; Bawendi, M. G.** Lattice Theories of Polymeric Fluids. *J. Phys. Chem.* **1989**, *93*, 2194–2203.
- (58) **Pesci, A. I.; Freed, K. F.** Lattice models of polymer fluids: Monomers occupying several lattice sites. II. Interaction energies. *J. Chem. Phys.* **1989**, *90*, 2003–2016.
- (59) **Dudowicz, J.; Freed, K. F.; Madden, W. G.** Role of Molecular Structure on the Thermodynamic Properties of Melts, Blends, and Concentrated Polymer Solutions. Comparison of Monte Carlo Simulations with the Cluster Theory for the Lattice Model. *Macromolecules* **1990**, *23*, 4803–4819.

- (60) **Zeiner, T.; Browarzik, C.; Browarzik, D.; Enders, S.** Calculation of the (liquid+liquid) equilibrium of solutions of hyperbranched polymers with the lattice-cluster theory combined with an association model. *J. Chem. Thermodyn.* **2011**, *43*, 1969–1976.
- (61) **Browarzik, C.; Browarzik, D.; Enders, S.** Liquid–liquid phase equilibria of hyperbranched polymers—Experimental study and modeling. *Fluid Phase Equilib.* **2012**, *328*, 49–60.
- (62) **Kulaguin Chicaroux, A.; Górak, A.; Zeiner, T.** Demixing behavior of binary polymer mixtures. *J. Mol. Liq.* **2015**, *209*, 42–49.
- (63) **Browarzik, D.** Calculation of excess functions and phase equilibria in binary and ternary mixtures with one associating component. *J. Mol. Liq.* **2009**, *146*, 95–104.
- (64) **Browarzik, D.** Extension of the chemical associating lattice model (CALM) to cross association. *J. Mol. Liq.* **2010**, *156*, 171–178.
- (65) **van Durme, K.; Loozen, E.; Nies, E.; van Mele, B.** Phase Behavior of Poly(vinyl methyl ether) in Deuterium Oxide. *Macromolecules* **2005**, *38*, 10234–10243.
- (66) **van Durme, K.; van Assche, G.; Nies, E.; van Mele, B.** Phase transformations in aqueous low molar mass poly(vinyl methyl ether) solutions: theoretical prediction and experimental validation of the peculiar solvent melting line, bimodal LCST, and (adjacent) UCST miscibility gaps. *J. Phys. Chem. B* **2007**, *111*, 1288–1295.
- (67) **Zeiner, T.; Schrader, P.; Enders, S.; Browarzik, D.** Phase- and interfacial behavior of hyperbranched polymer solutions. *Fluid Phase Equilib.* **2011**, *302*, 321–330.
- (68) **Enders, S.; Browarzik, D.** Modeling of the (liquid+liquid) equilibrium of polydisperse hyperbranched polymer solutions by lattice-cluster theory. *J. Chem. Thermodyn.* **2014**, *79*, 124–134.
- (69) **Zeiner, T.; Enders, S.** Phase behavior of hyperbranched polymer solutions in mixed solvents. *Chem. Eng. Sci.* **2011**, *66*, 5244–5252.
- (70) **Enders, S.; Langenbach, K.; Schrader, P.; Zeiner, T.** Phase Diagrams for Systems Containing Hyperbranched Polymers. *Polymers* **2012**, *4*, 72–115.
- (71) **Schrader, P.; Zeiner, T.; Browarzik, C.; Puyan, M. J.; Enders, S.** Phase behaviour of hyperbranched polymers in demixed solvents. *Mol. Phys.* **2012**, *110*, 1359–1373.
- (72) **Kulaguin-Chicaroux, A.; Zeiner, T.** Novel aqueous two-phase system based on a hyperbranched polymer. *Fluid Phase Equilib.* **2014**, *362*, 1–10.

- (73) **Kulaguin Chicaroux, A.; Plath, M.; Zeiner, T.** Hyperbranched polymers as phase forming components in aqueous two-phase extraction. *Chem. Eng. Process.* **2016**, *99*, 167–174.
- (74) **Chicaroux, A. K.; Zeiner, T.** Investigation of interfacial properties of aqueous two-phase systems by density gradient theory. *Fluid Phase Equilib.* **2016**, *407*, 135–142.
- (75) **Fischlschweiger, M.; Enders, S.; Zeiner, T.** Solubility calculations of branched and linear amino acids using lattice cluster theory. *Mol. Phys.* **2014**, *112*, 2282–2296.
- (76) **Fischlschweiger, M.; Enders, S.** Solid–liquid phase equilibria of binary hydrocarbon mixtures predicted by Lattice Cluster Theory. *J. Mol. Liq.* **2015**, *212*, 436–443.
- (77) **Langenbach, K.; Fischlschweiger, M.; Enders, S.** Prediction of the solid–liquid–liquid equilibria of linear and branched semi-crystalline poly-ethylene in solutions of diphenyl ether by Lattice Cluster Theory. *Mol. Phys.* **2016**, *114*, 2717–2723.
- (78) **Goetsch, T.; Zimmermann, P.; Enders, S.; Zeiner, T.** Tuneable extraction systems based on hyperbranched polymers. *Chem. Eng. Process.* **2016**, *99*, 175–182.
- (79) **Langenbach, K.; Enders, S.** Development of an EOS based on lattice cluster theory for pure components. *Fluid Phase Equilib.* **2012**, *331*, 58–79.
- (80) **Langenbach, K.; Enders, S.; Browarzik, C.; Browarzik, D.** Calculation of the high pressure phase equilibrium in hyperbranched polymer systems with the lattice-cluster theory. *J. Chem. Thermodyn.* **2013**, *59*, 107–113.
- (81) **Langenbach, K.; Browarzik, D.; Sailer, J.; Enders, S.** New formulation of the lattice cluster theory equation of state for multi-component systems. *Fluid Phase Equilib.* **2014**, *362*, 196–212.
- (82) **Flory, P. J.** Thermodynamics of High Polymer Solutions. *J. Chem. Phys.* **1942**, *10*, 51–61.
- (83) **Huggins, M. L.** Solutions of Long Chain Compounds. *J. Chem. Phys.* **1941**, *9*, 440.
- (84) **Flory, P. J.** *Principles of Polymer Chemistry*; Cornell University Press: Ithaca, 1953.
- (85) **Koningsveld, R.** Liquid-liquid equilibria in multicomponent polymer systems. *Discuss. Faraday Soc.* **1970**, *49*, 144.
- (86) **Koningsveld, R.; Stockmayer, W. H.; Kennedy, J. W.; Kleintjens, L. A.** Liquid-Liquid Phase Separation in Multicomponent Polymer Systems. XI. Dilute and Concentrated Polymer Solutions in Equilibrium. *Macromolecules* **1974**, *7*, 73–79.
- (87) **Russel, T. P.; Hjelm, R. P., JR.; Seeger, P. A.** Temperature Dependence of the Interaction Parameter of Polystyrene and Poly(methyl methacrylate). *Macromolecules* **1990**, *23*, 890–893.

- (88) **Koningsveld, R.; Kleintjens, L. A.** Liquid-Liquid Phase Separation in Multicomponent Polymer Systems. X. Concentration Dependence of the Pair-Interaction Parameter in the System Cyclohexane-Polystyrene. *Macromolecules* **1971**, *4*, 637–641.
- (89) **Dudowicz, J.; Freed, K. F.** Effect of Monomer Structure and Compressibility on the Properties of Multicomponent Polymer Blends and Solutions: 1. Lattice Cluster Theory of Compressible Systems. *Macromolecules* **1991**, *24*, 5076–5095.
- (90) **Kulaguin-Chicaroux, A.; Zeiner, T.** Novel aqueous two-phase system based on a hyperbranched polymer. *Fluid Phase Equilib.* **2014**, *362*, 1–10.
- (91) **Dudowicz, J.; Freed, K. F.; Douglas, J. F.** Modification of the Phase Stability of Polymer Blends by Diblock Copolymer Additives. *Macromolecules* **1995**, *28*, 2276–2287.
- (92) **Nemirovsky, A. M.; Dudowicz, J.; Freed, K. F.** Dense self-interacting lattice trees with specified topologies: From light to dense branching. *Physical Review A* **1992**, *45*, 7111–7127.
- (93) **Langenbach, K.; Enders, S.; Browarzik, C.; Browarzik, D.** Calculation of the high pressure phase equilibrium in hyperbranched polymer systems with the lattice-cluster theory. *J. Chem. Thermodyn.* **2013**, *59*, 107–113.
- (94) **Wertheim, M. S.** Fluids with highly directional attractive forces. I. Statistical thermodynamics. *J. Stat. Phys.* **1984**, *35*, 19–34.
- (95) **Wertheim, M. S.** Fluids with highly directional attractive forces. III. Multiple attraction sites. *J. Stat. Phys.* **1986**, *42*, 459–476.
- (96) **Enders, S.; Quitzsch, K.** Calculation of Interfacial Properties of Demixed Fluids Using Density Gradient Theory. *Langmuir* **1998**, *14*, 4606–4614.
- (97) **Grunert, T.; Enders, S.** Prediction of interfacial properties of the ternary system water+benzene+butan-1-ol. *Fluid Phase Equilib.* **2014**, *381*, 46–50.
- (98) **Goetsch, T.; Zimmermann, P.; van den Bongard, R.; Enders, S.; Zeiner, T.** Superposition of Liquid–Liquid and Solid–Liquid Equilibria of Linear and Branched Molecules: Binary Systems. *Ind. Eng. Chem. Res.* **2016**, *55*, 11167–11174.
- (99) **Kleiner, M.; Sadowski, G.** Modeling of Polar Systems Using PCP-SAFT: An Approach to Account for Induced-Association Interactions. *J. Phys. Chem. C* **2007**, *111*, 15544–15553.

- (100) **E. Costa; J. L. Sotelo; G. Calleja; C. Marrón.** Adsorption of binary and ternary hydrocarbon gas mixtures on activated carbon: Experimental determination and theoretical prediction of the ternary equilibrium data. *AIChE J.* **1981**, *27*, 5–12.
- (101) **Lisec, O.; Hugo, P.; Seidel-Morgenstern, A.** Frontal analysis method to determine competitive adsorption isotherms. *J. Chromatogr. A* **2001**, *908*, 19–34.
- (102) **Gor, G. Y.; Paris, O.; Prass, J.; Russo, P. A.; Ribeiro Carrott, M Manuela L; Neimark, A. V.** Adsorption of n-pentane on mesoporous silica and adsorbent deformation. *Langmuir* **2013**, *29*, 8601–8608.
- (103) **Berti, C.; Ulbig, P.; Schulz, S.** Correlation and Prediction of Adsorption from Liquid Mixtures on Solids by Use of GE-Models. *Adsorption* **2000**, *6*, 79–91.
- (104) **James, H. M.; Guth, E.** Statistical Thermodynamics of Rubber Elasticity. *J. Chem. Phys.* **1953**, *21*, 1039–1049.
- (105) **Mondieig, D.; Rajabalee, F.; Metivaud, V.; Oonk, H. A. J.; Cuevas-Diarte, M. A.** n -Alkane Binary Molecular Alloys. *Chem. Mater.* **2004**, *16*, 786–798.
- (106) **Vonnegut, B.** Rotating Bubble Method for the Determination of Surface and Interfacial Tensions. *Rev. Sci. Instrum.* **1942**, *13*, 6–9.
- (107) **Nakai, K.; Sonoda, J.; Iegami, H.; Naono, H.** High Precision Volumetric Gas Adsorption Apparatus. *Adsorption* **2005**, *11*, 227–230.
- (108) **Seidel-Morgenstern, A.** Experimental determination of single solute and competitive adsorption isotherms. *J. Chromatogr. A* **2004**, *1037*, 255–272.
- (109) **Kipling, J. J.** *Adsorption from solutions of non-electrolytes*; Academic Press: London, 1965.
- (110) **Dahlmann, U.; Schneider, G. M.** (Liquid + liquid) phase equilibria and critical curves of (ethanol + dodecane or tetradecane or hexadecane or 2,2,4,4,6,8,8-heptamethylnonane) from 0.1 MPa to 120.0 MPa. *J. Chem. Thermodyn.* **1989**, *21*, 997–1004.
- (111) **Matsuda, H.; Kurihara, K.; Ochi, K.; Kojima, K.** Prediction of liquid-liquid equilibria at high pressure for binary systems using EOS-GE models: methanol + hydrocarbon systems. *Fluid Phase Equilib.* **2002**, *203*, 269–284.
- (112) **Tagliavini, G.; Arich, G.** Liquid-liquid equilibrium in the system methanol-heptane-morpholine. *Ricerca sci.* **1958**, *28*, 1902–1910.
- (113) **Kiser, R. W.; Johnson, G. D.; Shetlar, M. D.** Solubilities of Various Hydrocarbons in Methanol. *J. Chem. Eng. Data* **1961**, *6*, 338–341.

- (114) **Kurihara, K.; Midorikawa, T.; Hashimoto, T.; Kojima, K.; Ochi, K.** Liquid-Liquid Solubilities for the Binary Systems of Methanol with Octane and 2, 2, 4-Trimethylpentane. *J. Chem. Eng. Japan / JCEJ* **2002**, *35*, 360–364.
- (115) **Abbas, S.; Satherley, J.; Penfold, R.** The liquid-liquid coexistence curve and the interfacial tension of the methanol-n-hexane system. *J. Chem. Soc. Faraday Trans.* **1997**, *93*, 2083–2089.
- (116) **Chang, S. S.; Maurey, J. R.; Pummer, W. J.** Solubilities of two n-alkanes in various solvents. *J. Chem. Eng. Data* **1983**, *28*, 187–189.
- (117) **Domańska, U.** Solubility of n-paraffin hydrocarbons in binary solvent mixtures. *Fluid Phase Equilib.* **1987**, *35*, 217–236.
- (118) **Domanska, U.; Lachwa, J.; Morawski, P.; Malanowski, S. K.** Phase Equilibria and Volumetric Properties in Binary Mixtures Containing Branched Chain Ethers (Methyl 1,1-Dimethylethyl Ether or Ethyl 1,1-Dimethylethyl Ether or Methyl 1,1-Dimethylpropyl Ether or Ethyl 1,1-Dimethylpropyl Ether). *J. Chem. Eng. Data* **1999**, *44*, 974–984.
- (119) **Domalski, E.** Heat capacities and entropies of organic compounds in the condensed phase. Volume III. *J. Phys. Chem. Ref. Data* **1996**, *25*, 1–525.
- (120) **Chopade, S. P.; Sharma, M. M.** Acetalization of ethylene glycol with formaldehyde using cation-exchange resins as catalysts: batch versus reactive distillation. *React. Funct. Polym.* **1997**, *34*, 37–45.
- (121) **Güemez, M. B.; Requies, J.; Agirre, I.; Arias, P. L.; Barrio, V. L.; Cambra, J. F.** Acetalization reaction between glycerol and n-butyraldehyde using an acidic ion exchange resin. Kinetic modelling. *Chem. Eng. J.* **2013**, *228*, 300–307.
- (122) **Mota, C. J. A.; da Silva, C. X.; Ribeiro, Paulo H. S. Goncalves, Valter L. C.** Acetalization of Glycerol over Solid Acid Catalysts. <http://www.nacatsoc.org/21nam/data/papers/Paper1742.pdf> (accessed September 18, 2017).
- (123) **Stephenson, R. M.** Mutual solubilities: water-ketones, water-ethers, and water-gasoline-alcohols. *J. Chem. Eng. Data* **1992**, *37*, 80–95.
- (124) **Dreimann, J. M.; Hoffmann, F.; Skiborowski, M.; Behr, A.; Vorholt, A. J.** **Merging** Thermomorphic Solvent Systems and Organic Solvent Nanofiltration for Hybrid Catalyst Recovery in a Hydroformylation Process. *Ind. Eng. Chem. Res.* **2017**, *56*, 1354–1359.

List of figures

- Figure 1:** Difference in melting temperature between linear alkanes and their mono-branched isomers depending on the position of the methylene group (squares: C12; circles: C14; triangles: C16; diamonds: C18; stars: C20). Data were taken from literature⁸⁻¹¹..... 7
- Figure 2:** Oiling out in binary systems..... 11
- Figure 3:** Binary LLE of n-hexane (squares), 2-methylpentane (circles), 3-methylpentane (triangles) and 2,3-dimethylbutane (diamonds) dissolved in methanol. The solid line denotes the prediction of mod. UNIFAC for all systems. 15
- Figure 4:** Binary LLE of n-hexane (squares), 2-methylpentane (circles), 3-methylpentane (triangles) and 2,3-dimethylbutane (diamonds) dissolved in methanol. The solid lines denote the prediction of COSMO-SAC (solid: n-hexane; dashed: 2-methylpentane; dotted: 3-methylpentane; dash-dotted: 2,3-dimethylbutane)..... 18
- Figure 5:** Two dimensional lattice containing a single polymer chain (black segments) and several solvent segments (white segments). Figure adapted from Flory⁸⁴ 24
- Figure 6:** Overview of the methodology for the prediction of phase equilibria of branched molecules..... 33
- Figure 7:** Procedure of defining model parameters for a ternary system containing solvent, branched isomer and linear isomer..... 34
- Figure 8:** Concept of liquid phase adsorption on porous solids 36
- Figure 9: Principal of measuring cloud-points of binary systems..... 42
- Figure 10:** DSC heating (negative heat flows) and cooling (positive heat flows) curves of pure n-hexadecane..... 44

Figure 11: Experimental procedure for measuring the SLE of the ternary system ethanol + n-hexadecane + 2,2,4,4,6,8,8-heptamethylnonane by titration.....	45
Figure 12: Principal of spinning-drop tensiometry.....	46
Figure 13: Experimental set-up for measuring adsorption isotherms.....	48
Figure 14: Definition of segments for the molecule 2,2,4,4,6,8,8-heptamethylnonane.....	54
Figure 15: LLE of the binary systems n-dodecane (squares) ¹⁰⁹ , n-tetradecane (circles) ¹⁰⁹ and n-hexadecane (diamonds) ¹⁰⁹ all with the solvent ethanol. The solid lines were calculated using the LCT in combination with CALM.....	56
Figure 16: Interaction energy between alkane molecules and ethanol as a function of the chain length of the alkanes. The values for chain lengths of 12, 14 and 16 were fitted to experimental data, the value for a chain length of 9 was determined by extrapolation.	57
Figure 17: Predicted LLE of the binary system 2,2,4,4,6,8,8-heptamethylnonane + ethanol. Experimental data were taken from literature ¹⁰⁹ , solid lines were calculated using the LCT in combination with CALM.	58
Figure 18: LLE of the binary systems n-hexane (squares) ¹¹⁰ , n-heptane (circles) ^{111,112} and n-octane (diamonds) ¹¹³ all with the solvent methanol. The solid lines were calculated using the LCT in combination with CALM.....	59
Figure 19: Interaction energy between alkane molecules and methanol as a function of the chain length of the alkanes. The values for chain lengths 6, 7 and 8 were fitted to experimental data, the value for a chain length of 5 was determined by extrapolation.	60
Figure 20: Predicted LLE of the binary systems 2,2,5-trimethylhexane + methanol (circles) ¹¹² and 2,2,4-trimethylpentane + methanol (diamonds) ¹¹³ . The solid lines were calculated using the LCT in combination with CALM.....	61
Figure 21: LLE of the binary systems methanol + n-hexane (a), methanol + 2-methylpentane (b), methanol + 3-methylpentane (c) and methanol + 2,3-dimethylbutane (d). Experimental	

cloud-points are shown as light grey circles; experimental tie lines are shown as grey diamonds. The solid line denote the fitted LLE for the system methanol + n-hexane and the predicted LLE for the three remaining systems; they were calculated using the LCT in combination with CALM. 62

Figure 22: Interfacial tension as a function of temperature for the binary systems methanol + n-hexane (squares; exp. data from literature¹¹⁴), methanol + 2-methylpentane (circles), methanol + 3-methylpentane (triangles) and methanol + 2,3-dimethylbutane (diamonds). The solid lines were calculated by a DGT approach incorporating the LCT in combination with CALM. 64

Figure 23: Predicted binary LLE of the systems methanol + 2-methylpentane (solid line) and methanol + 3-methylpentane (dashed line). The left side (a) was calculated using the LCT in combination with CALM, the right side (b) was calculated using solely the LCT. The reduced temperature T_r is related to the UCST of the system methanol + 2-methylpentane in both cases. 65

Figure 24: Interfacial concentration profile for the binary systems methanol + n-hexane (solid line), methanol + 2-methylpentane (dashed line), methanol + 3-methylpentane (dotted line) and methanol + 2,3-dimethylbutane (dash-dotted line). The lines were calculated for a temperature of 280 K by a DGT approach incorporating the LCT in combination with CALM. 66

Figure 25: Superposition of LLE (diamonds)¹⁰⁹ and SLE (triangles) of the binary system n-hexadecane + ethanol. The solid lines were calculated using the LCT in combination with CALM. 68

Figure 26: Superposition of LLE (diamonds)¹¹⁵ and SLE (triangles)¹¹⁶ of the binary system n-octadecane + ethanol. The solid lines were calculated using the LCT in combination with CALM. 69

Figure 27: LLE of the ternary system n-hexadecane + 2,2,4,4,6,8,8-heptamethylnonane + ethanol at a temperature of 298.15 K. Experimental points on the binodal curve are shown as diamonds; experimental tie lines are shown as grey stars connected by dashed lines. The

binodal curve as well as the tie lines (white stars connected by solid lines) was calculated using the LCT in combination with CALM.	70
Figure 28: Superposition of LLE (diamonds) and SLE (triangles) of the ternary system n-hexadecane + 2,2,4,4,6,8,8-heptamethylnonane + ethanol at a temperature of 283.15 K. Lines were calculated using the LCT in combination with CALM. The dashed lines denote the metastable LLE.	71
Figure 29: Superposition of LLE (diamonds) and SLE (triangles) of the ternary system n-hexadecane + 2,2,4,4,6,8,8-heptamethylnonane + ethanol at a temperature of 278.15 K. Lines were calculated using the LCT in combination with CALM. The dashed lines denote the metastable LLE.	72
Figure 30: Superposition of LLE (green) and SLE (red) of the ternary system n-hexadecane + 2,2,4,4,6,8,8-heptamethylnonane + ethanol	73
Figure 31: Molecular architecture of methyl oleate.	74
Figure 32: Superposition of LLE (diamonds) and SLE (triangles) of the binary system methyl oleate + methanol. The solid lines were calculated using the LCT in combination with ECALM. Measurements were performed by TU Berlin.	75
Figure 33: LLE of the binary system ethylene glycol + 2-pentanone. Cloud-points are shown as circles, tie lines are shown as diamonds.	77
Figure 34: Reaction mechanism of ethylene glycol and ketone adapted from Chopade and Sharma ¹¹⁹	78
Figure 35: LLE of the binary systems ethylene glycol + 2-pentanone (diamonds) and ethylene glycol + 2-hexanone (circles). The solid lines were calculated using the LCT in combination with ECALM.	79
Figure 36: Interaction energy between 2-ketone molecules and ethylene glycol as a function of the chain length of the ketone. The values for chain lengths 5 and 6 were fitted to experimental data, the value for a chain length of 4 was determined by extrapolation.	80

- Figure 37:** Predicted LLE of the binary systems ethylene glycol + 3-methyl-2-butanone (diamonds) and ethylene glycol + 4-methyl-2-pentanone (circles). The solid lines were calculated using the LCT in combination with ECALM. 81
- Figure 38:** Configuration of ethylene glycol with 2-hexanone (left side) and 4-methyl-2-pentanone (right side)..... 82
- Figure 39:** Pore size distributions of zeolite (diamonds), activated carbon (triangles) and silica gel (circles). Measurements were performed by TU Berlin. 83
- Figure 40:** Adsorption isotherms of the binary system n-octane + 2,2,4-trimethylpentane on zeolite (diamonds), activated carbon (triangles) and silica gel (circles) at a temperature of 293.15 K..... 85
- Figure 41:** Left side: Adsorption isotherms of the binary system n-octane + 2,2,4-trimethylpentane on activated carbon at temperatures of 283.15 K (diamonds; solid line), 293.15 K (triangles; dashed line) and 303.15 K (circles; dotted line). The lines were calculated by the adsorption model. Right side: Degree of swelling of activated carbon for the binary system n-octane + 2,2,4-trimethylpentane at temperatures of 283.15 K (diamonds; solid line), 293.15 K (triangles; dashed line) and 303.15 K (circles; dotted line). The mass fraction of activated carbon was 0.40 in each case. 87
- Figure 42:** Left side: Adsorption isotherms of the binary system n-octane + 2,2,4-trimethylpentane on silica gel at temperatures of 283.15 K (diamonds; solid line), 293.15 K (triangles; dashed line) and 303.15 K (circles; dotted line). The lines were calculated by the adsorption model. Right side: Degree of swelling of silica gel for the binary system n-octane + 2,2,4-trimethylpentane at temperatures of 283.15 K (diamonds; solid line), 293.15 K (triangles; dashed line) and 303.15 K (circles; dotted line). The mass fraction of silica gel was 0.55 in each case..... 88
- Figure 43:** Left side: Adsorption isotherms of the binary system n-octane + 2,2,4-trimethylpentane on zeolite at temperatures of 283.15 K (diamonds; solid line), 293.15 K (triangles; dashed line) and 303.15 K (circles; dotted line). The lines were calculated by the adsorption model. Right side: Degree of swelling of zeolite for the binary system n-octane + 2,2,4-trimethylpentane at temperatures of 283.15 K (diamonds; solid line), 293.15 K

(triangles; dashed line) and 303.15 K (circles; dotted line). The mass fraction of zeolite was 0.60 in each case..... 89

Figure 44: Left side: Adsorption isotherms of the binary system n-hexane + 2,3-dimethylbutane on activated carbon at temperatures of 283.15 K (diamonds; solid line), 293.15 K (triangles; dashed line) and 303.15 K (circles; dotted line). The lines were calculated by the adsorption model. Right side: Degree of swelling of activated carbon for the binary system n-hexane + 2,3-dimethylbutane at temperatures of 283.15 K (diamonds; solid line), 293.15 K (triangles; dashed line) and 303.15 K (circles; dotted line). The mass fraction of activated carbon was 0.42 in each case. 91

Figure 45: Left side: Adsorption isotherms of the binary system n-hexane + 2,3-dimethylbutane on silica gel at temperatures of 283.15 K (diamonds; solid line), 293.15 K (triangles; dashed line) and 303.15 K (circles; dotted line). The lines were calculated by the adsorption model. Right side: Degree of swelling of silica gel for the binary system n-hexane + 2,3-dimethylbutane at temperatures of 283.15 K (diamonds; solid line), 293.15 K (triangles; dashed line) and 303.15 K (circles; dotted line). The mass fraction of silica gel was 0.53 in each case..... 93

Figure 46: Left side: Adsorption isotherms of the binary system n-hexane + 2,3-dimethylbutane on zeolite at temperatures of 283.15 K (diamonds; solid line), 293.15 K (triangles; dashed line) and 303.15 K (circles; dotted line). The lines were calculated by the adsorption model. Right side: Degree of swelling of zeolite for the binary system n-hexane + 2,3-dimethylbutane at temperatures of 283.15 K (diamonds; solid line), 293.15 K (triangles; dashed line) and 303.15 K (circles; dotted line). The mass fraction of zeolite was 0.62 in each case..... 94

Figure 47: Adjusted interaction energies between activated carbon and linear alkane (diamonds) as well as between activated carbon and branched alkanes (circles). Left side: Binary system n-hexane + 2,3-dimethylbutane. Right side: Binary system n-octane + 2,2,4-trimethylpentane. The lines denote linear fits based on the corresponding data..... 95

Figure 48: Quasi-pure-component adsorption isotherms of the binary system n-octane (left side) + 2,2,4-trimethylpentane (right side). The adsorption on activated carbon is shown in the first row, on silica gel in the second row and on zeolite in the third row. 96

- Figure 49:** Process flowsheet for purifying linear as well as branched isomer..... 98
- Figure 50:** Superposition of ternary LLE and SLE for a temperature of 283.15 K. The shaded regions denote possible operating windows for crystallization. The marked concentration is achieved by adding ethanol to 75:25 mixture of linear and branched isomer..... 99
- Figure 51:** LLE of the ternary system n-hexane + 2-methylpentane + methanol at a temperature of 283.15 K. Experimental tie lines are shown as grey stars connected by dashed lines. The binodal curve as well as the tie lines (white stars connected by solid lines) was calculated using the LCT in combination with CALM..... 128
- Figure 52:** LLE of the ternary system n-hexane + 2,3-dimethylbutane + methanol at a temperature of 283.15 K. Experimental tie lines are shown as grey stars connected by dashed lines. The binodal curve as well as the tie lines (white stars connected by solid lines) was calculated using the LCT in combination with CALM..... 128
- Figure 53:** LLE of the binary system ethylene glycol + 2-hexanone. Cloud-points are shown as circles, tie lines are shown as diamonds. 129
- Figure 54:** LLE of the binary system ethylene glycol + 3-methyl-2-butanone. Cloud-points are shown as circles, tie lines are shown as diamonds. 129
- Figure 55:** LLE of the binary system ethylene glycol + 4-methyl-2-pentanone. Cloud-points are shown as circles, tie lines are shown as diamonds. 130

List of tables

Table 1: Melting points of ortho-xylene, meta-xylene and para-xylene ⁵	6
Table 2: Research octane number of five different hexane isomers ⁷	8
Table 3: Kinetic diameters of n-hexane, 2-methylpentane, 3-methylpentane, 2,2-dimethylbutane and 2,3-dimethylbutane ²¹	9
Table 4: Chemicals used LLE and SLE experiments.....	40
Table 5: Chemicals used for adsorption experiments.	41
Table 6: Architecture parameters defined within the LCT of all molecules investigated in chapter 5.1.1-5.1.3.....	55
Table 7: Influence parameter κ adjusted to 4 binary systems.....	64
Table 8: Architecture parameters defined within the LCT of ethylene glycol and four different ketones.....	76
Table 9: Adjusted model parameters for the binary systems ethylene glycol + 2-pentanone and ethylene glycol + 2-hexanone.....	79
Table 10: Adjusted interaction energies between n-octane (A) and adsorbent (B) ($\Delta\varepsilon_{AB}/k_B$) as well as between adsorbent (B) and 2,2,4-trimethylpentane (C) ($\Delta\varepsilon_{BC}/k_B$) for three different adsorbents at three different temperatures.....	86
Table 11: Adjusted interaction energies between n-hexane (A) and adsorbent (B) (ε_{AB}/k_B) as well as between adsorbent (B) and 2,3-dimethylbutane (C) (ε_{BC}/k_B) for three different adsorbents at three different temperatures.	91

Table 12: Initial and final water content for the binary system 2-pentanone + water for 6 tie lines at temperature $T = 313.15$ K and pressure $p = 0.1$ MPa	130
Table 13: Initial and final water content of the binary system 2-hexanone + water for 6 tie lines at temperature $T = 328.15$ K and pressure $p = 0.1$ MPa	130
Table 14: Experimental (liquid + liquid) equilibrium mass fraction w (cloud point data) for the system methanol (1) + n-hexane (2) at pressure $p = 0.1$ MPa .*	131
Table 15: Experimental (liquid + liquid) equilibrium mass fraction w (tie lines) for the system methanol (1) + n-hexane (2) at pressure $p = 0.1$ MPa .*	131
Table 16: Experimental (liquid + liquid) equilibrium mass fractions w (cloud point data) for the system methanol (1) + 2-methylpentane (2) at pressure $p = 0.1$ MPa .*	132
Table 17: Experimental (liquid + liquid) equilibrium mass fractions w (tie lines) for the system methanol (1) + 2-methylpentane (2) at pressure $p = 0.1$ MPa .*	132
Table 18: Experimental (liquid + liquid) equilibrium mass fractions w (cloud point data) for the system methanol (1) + 3-methylpentane (2) at pressure $p = 0.1$ MPa .*	133
Table 19: Experimental (liquid + liquid) equilibrium mass fractions w (tie lines) for the system methanol (1) + 3-methylpentane (2) at pressure $p = 0.1$ MPa .*	133
Table 20: Experimental (liquid + liquid) equilibrium mass fractions w (cloud point data) for the system methanol (1) + 2,3-dimethylbutane (2) at pressure $p = 0.1$ MPa .*	134
Table 21: Experimental (liquid + liquid) equilibrium mass fractions w (tie lines) for the system methanol (1) + 2,3-dimethylbutane (2) at pressure $p = 0.1$ MPa .*	134
Table 22: Experimental (liquid + liquid) equilibrium mass fractions w (cloud point data) for the system ethylene glycol (1) + 2-pentanone (2) at pressure $p = 0.1$ MPa .*	134

Table 23: Experimental (liquid + liquid) equilibrium mass fractions w (tie lines) for the system ethylene glycol (1) + 2-pentanone (2) at pressure $p = 0.1$ MPa .*	135
Table 24: Experimental (liquid + liquid) equilibrium mass fractions w (cloud point data) for the system ethylene glycol (1) + 2-hexanone (2) at pressure $p = 0.1$ MPa .*	135
Table 25: Experimental (liquid + liquid) equilibrium mass fractions w (tie lines) for the system ethylene glycol (1) + 2-hexanone (2) at pressure $p = 0.1$ MPa .*	135
Table 26: Experimental (liquid + liquid) equilibrium mass fractions w (cloud point data) for the system ethylene glycol (1) + 3-methyl-2-butanone (2) at pressure $p = 0.1$ MPa .*	136
Table 27: Experimental (liquid + liquid) equilibrium mass fractions w (tie lines) for the system ethylene glycol (1) + 3-methyl-2-butanone (2) at pressure $p = 0.1$ MPa .*	136
Table 28: Experimental (liquid + liquid) equilibrium mass fractions w (cloud point data) for the system ethylene glycol (1) + 4-methyl-2-pentanone at pressure $p = 0.1$ MPa .*	136
Table 29: Experimental (liquid + liquid) equilibrium mass fractions w (tie lines) for the system ethylene glycol (1) + 4-methyl-2-pentanone (2) at pressure $p = 0.1$ MPa .*	137
Table 30: Experimental (liquid + liquid) equilibrium mass fractions w (cloud point data) for the system methanol (1) + methyl oleate (2) at pressure $p = 0.1$ MPa . Experiments were performed by TU Berlin.	137
Table 31: Experimental (solid + liquid) equilibrium mass fractions w for the system ethanol (1) + n-hexadecane (2) at pressure $p = 0.1$ MPa .*	138
Table 32: Experimental (solid + liquid) equilibrium mass fractions w for the system methanol (1) + methyl oleate (2) at pressure $p = 0.1$ MPa . Experiments were performed by TU Berlin.	138

Table 33: Experimental (liquid + liquid) equilibrium mass fractions w (binodal curve data) for the system ethanol (1) + 2,2,4,4,6,8,8-heptamethylnonane (2) + n-hexadecane (3) at temperature $T = 298.15$ K and pressure $p = 0.1$ MPa .*	139
Table 34: Experimental (liquid + liquid) equilibrium mass fractions w (tie lines) for the system ethanol (1) + 2,2,4,4,6,8,8-heptamethylnonane (2) + n-hexadecane (3) at temperature $T = 298.15$ K and pressure $p = 0.1$ MPa .*	139
Table 35: Experimental (liquid + liquid) equilibrium mass fractions w (tie lines) for the system methanol (1) + 2-methylpentane (2) + n-hexane (3) at temperature $T = 283.15$ K and pressure $p = 0.1$ MPa .*	140
Table 36: Experimental (liquid + liquid) equilibrium mass fractions w (tie lines) for the system methanol (1) + 2,3-dimethylbutane (2) + n-hexane (3) at temperature $T = 283.15$ K and pressure $p = 0.1$ MPa .*	140
Table 37: Experimental (liquid + liquid) equilibrium mass fractions w (binodal curve data) and experimental (solid + liquid) equilibrium mass fractions w for the system ethanol (1) + 2,2,4,4,6,8,8-heptamethylnonane (2) + n-hexadecane (3) at temperature $T = 283.15$ K and pressure $p = 0.1$ MPa .*	141
Table 38: Experimental (liquid + liquid) equilibrium mass fractions w (binodal curve data) and experimental (solid + liquid) equilibrium mass fractions w for the system ethanol (1) + 2,2,4,4,6,8,8-heptamethylnonane (2) + n-hexadecane (3) at temperature $T = 278.15$ K and pressure $p = 0.1$ MPa .*	142
Table 39: Experimental density and interfacial tension for the system methanol + 2-methylpentane at pressure $p = 0.1$ MPa .*	143
Table 40: Experimental density and interfacial tension for the system methanol + 3-methylpentane at pressure $p = 0.1$ MPa .*	143

Table 41: Experimental density and interfacial tension for the system methanol + 2,3-dimethylbutane at pressure $p = 0.1 \text{ MPa}$.*	143
Table 42: Experimental adsorption isotherms of the binary system n-octane (1) + 2,2,4-trimethylpentane (2) on activated carbon at three different temperatures and pressure $p = 0.1 \text{ MPa}$.*	144
Table 43: Experimental degree of swelling of activated carbon for the adsorption of the binary system n-octane (1) + 2,2,4-trimethylpentane at three different temperatures and pressure $p = 0.1 \text{ MPa}$.*	145
Table 44: Experimental adsorption isotherms of the binary system n-octane (1) + 2,2,4-trimethylpentane (2) on silica gel at three different temperatures and pressure $p = 0.1 \text{ MPa}$.*	145
Table 45: Experimental degree of swelling of silica gel for the adsorption of the binary system n-octane (1) + 2,2,4-trimethylpentane at three different temperatures and pressure $p = 0.1 \text{ MPa}$.*	146
Table 46: Experimental adsorption isotherms of the binary system n-octane (1) + 2,2,4-trimethylpentane (2) on zeolite at three different temperatures and pressure $p = 0.1 \text{ MPa}$.*	146
Table 47: Experimental degree of swelling of zeolite for the adsorption of the binary system n-octane (1) + 2,2,4-trimethylpentane at three different temperatures and pressure $p = 0.1 \text{ MPa}$.*	147
Table 48: Experimental adsorption isotherms of the binary system n-hexane (1) + 2,3-dimethylbutane (2) on activated carbon at three different temperatures and pressure $p = 0.1 \text{ MPa}$.*	148
Table 49: Experimental degree of swelling of activated carbon for the adsorption of the binary system n-hexane (1) + 2,3-dimethylbutane at three different temperatures and pressure $p = 0.1 \text{ MPa}$.*	148

Table 50: Experimental adsorption isotherms of the binary system n-hexane (1) + 2,3-dimethylbutane (2) on silica gel at three different temperatures and pressure $p = 0.1MPa$.*	149
Table 51: Experimental degree of swelling of silica gel for the adsorption of the binary system n-hexane (1) + 2,3-dimethylbutane at three different temperatures and pressure $p = 0.1MPa$.*	149
Table 52: Experimental adsorption isotherms of the binary system n-hexane (1) + 2,3-dimethylbutane (2) on zeolite at three different temperatures and pressure $p = 0.1MPa$.*	150
Table 53: Experimental degree of swelling of zeolite for the adsorption of the binary system n-hexane (1) + 2,3-dimethylbutane (2) at three different temperatures and pressure $p = 0.1MPa$.*	151

Appendix A: Further results

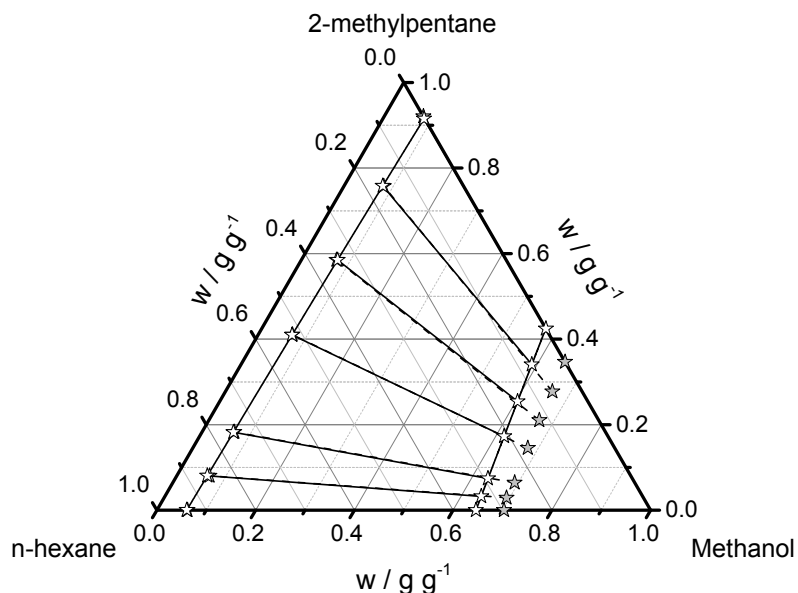


Figure 52: LLE of the ternary system n-hexane + 2-methylpentane + methanol at a temperature of 283.15 K. Experimental tie lines are shown as grey stars connected by dashed lines. The binodal curve as well as the tie lines (white stars connected by solid lines) was calculated using the LCT in combination with CALM.

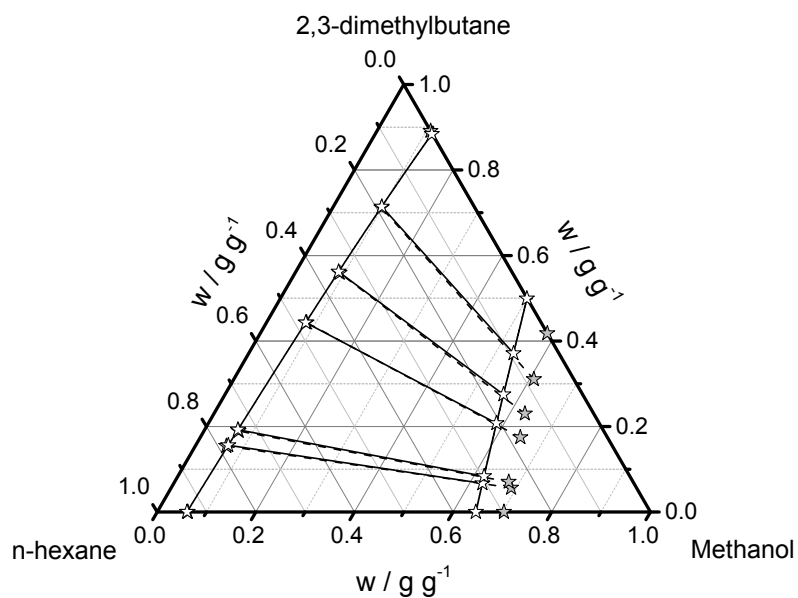


Figure 53: LLE of the ternary system n-hexane + 2,3-dimethylbutane + methanol at a temperature of 283.15 K. Experimental tie lines are shown as grey stars connected by dashed lines. The binodal curve as well as the tie lines (white stars connected by solid lines) was calculated using the LCT in combination with CALM.

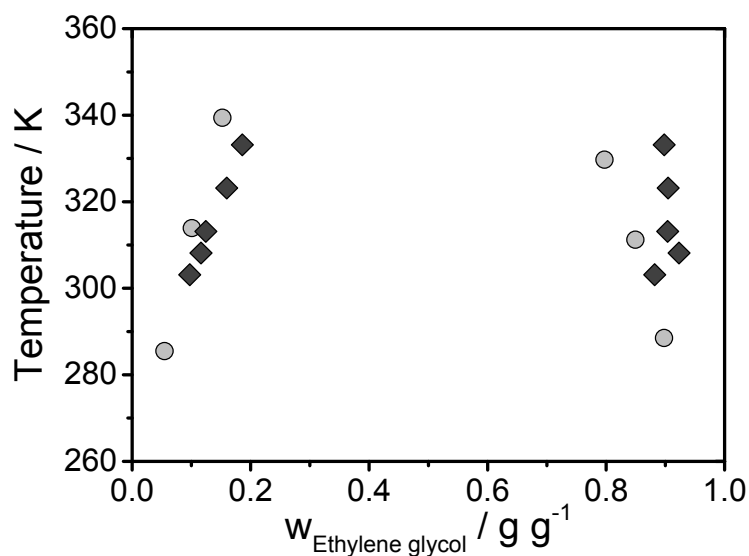


Figure 54: LLE of the binary system ethylene glycol + 2-hexanone. Cloud-points are shown as circles, tie lines are shown as diamonds.

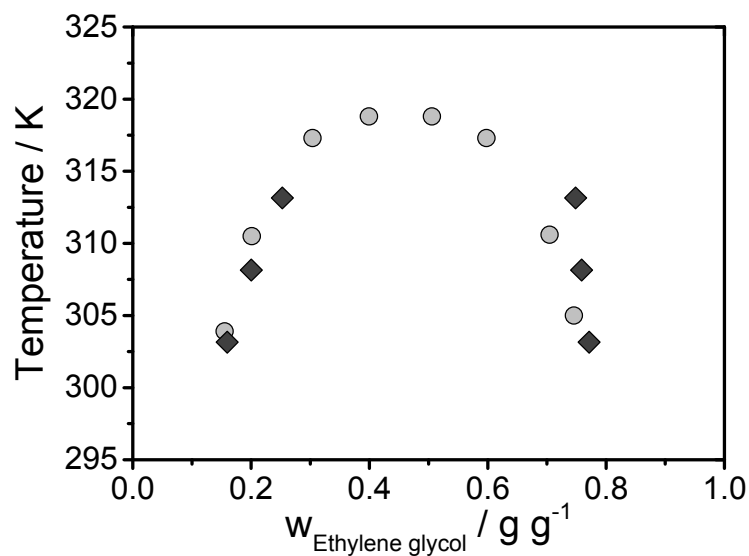


Figure 55: LLE of the binary system ethylene glycol + 3-methyl-2-butanone. Cloud-points are shown as circles, tie lines are shown as diamonds.

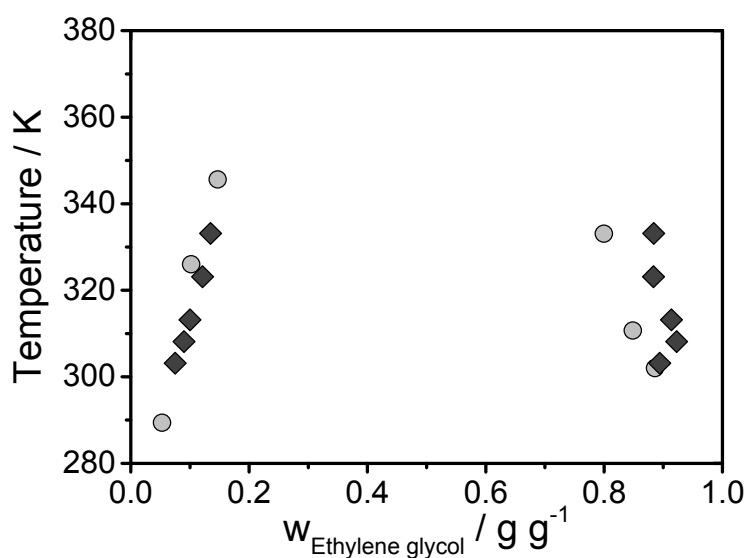


Figure 56: LLE of the binary system ethylene glycol + 4-methyl-2-pentanone. Cloud-points are shown as circles, tie lines are shown as diamonds.

Table 12: Initial and final water content for the binary system 2-pentanone + water for 6 tie lines at temperature $T = 313.15$ K and pressure $p = 0.1$ MPa.

Sample	Initial water content / g	Final water content / g
1	0.0097	0.0100
2	0.0096	0.0138
3	0.0095	0.0128
4	0.0086	0.0120
5	0.0093	0.0104
6	0.0102	0.0163

Table 13: Initial and final water content of the binary system 2-hexanone + water for 6 tie lines at temperature $T = 328.15$ K and pressure $p = 0.1$ MPa.

Sample	Initial water content / g	Final water content / g
1	0.0113	0.0562
2	0.0110	0.0357
3	0.0118	0.0486
4	0.0096	0.1503
5	0.0094	0.0721
6	0.0098	0.0335

Appendix B: Experimental data

Binary LLE

Table 14: Experimental (liquid + liquid) equilibrium mass fraction w (cloud point data) for the system methanol (1) + n-hexane (2) at pressure $p = 0.1$ MPa.*

$w_1 / -$	T / K	$w_1 / -$	T / K
0.065	288.4	0.404	307.9
0.108	299.4	0.488	305.4
0.144	306.4	0.493	305.9
0.170	307.7	0.544	302.4
0.189	308.4	0.561	301.5
0.215	308.9	0.599	297.9
0.248	309.9	0.657	290.9
0.317	308.9	0.691	283.6
0.359	308.4		

*Uncertainties are $u(w) = 0.002$ and $u(T) = 0.5$ K .

Table 15: Experimental (liquid + liquid) equilibrium mass fraction w (tie lines) for the system methanol (1) + n-hexane (2) at pressure $p = 0.1$ MPa.*

T / K	$w_{1, \text{liquid phase 1}} / -$	$w_{1, \text{liquid phase 2}} / -$
278.15	0.0368	0.7263
283.15	0.0516	0.7072
288.15	0.0528	0.6865
293.15	0.0807	0.6468
298.15	0.1068	0.6045
303.15	0.1311	0.5733
308.15	0.2178	0.4669

*Uncertainties are $u(T) = 0.1$ K and $u(w) = 0.019$.

Table 16: Experimental (liquid + liquid) equilibrium mass fractions w (cloud point data) for the system methanol (1) + 2-methylpentane (2) at pressure $p = 0.1$ MPa.*

$w_1 / -$	T / K	$w_1 / -$	T / K
0.057	278.9	0.379	301.3
0.058	279.4	0.436	299.9
0.065	282.6	0.501	296.5
0.077	290.9	0.513	296.3
0.105	295.0	0.547	294.5
0.143	299.0	0.555	294.0
0.224	301.5	0.557	294.0
0.264	302.0	0.561	293.0
0.313	301.3	0.564	293.0
0.316	303.0	0.629	285.0
0.338	301.0	0.631	283.9

*Uncertainties are $u(w) = 0.002$ and $u(T) = 0.5$ K .

Table 17: Experimental (liquid + liquid) equilibrium mass fractions w (tie lines) for the system methanol (1) + 2-methylpentane (2) at pressure $p = 0.1$ MPa.*

T / K	$w_{1, \text{liquid phase 1}} / -$	$w_{1, \text{liquid phase 2}} / -$
278.15	0.0639	0.6955
283.15	0.0767	0.6553
288.15	0.0922	0.6313
293.15	0.1297	0.5834
298.15	0.1686	0.5124

*Uncertainties are $u(T) = 0.1$ K and $u(w) = 0.009$.

Table 18: Experimental (liquid + liquid) equilibrium mass fractions w (cloud point data) for the system methanol (1) + 3-methylpentane (2) at pressure $p = 0.1$ MPa.*

$w_1 / -$	T / K	$w_1 / -$	T / K
0.062	279.3	0.302	301.0
0.075	285.5	0.328	301.0
0.105	293.5	0.346	301.0
0.122	295.0	0.369	301.3
0.140	297.5	0.408	300.4
0.159	299.0	0.433	299.5
0.184	300.6	0.479	297.5
0.217	300.6	0.484	297.5
0.233	300.8	0.545	293.0
0.248	301.0	0.586	289.8
0.264	301.5	0.603	287.5
0.278	301.0	0.609	286.5
0.297	301.0		

*Uncertainties are $u(w) = 0.002$ and $u(T) = 0.5$ K .

Table 19: Experimental (liquid + liquid) equilibrium mass fractions w (tie lines) for the system methanol (1) + 3-methylpentane (2) at pressure $p = 0.1$ MPa.*

T / K	$w_1, \text{liquid phase 1} / -$	$w_1, \text{liquid phase 2} / -$
278.15	0.0639	0.6828
283.15	0.0810	0.6536
288.15	0.0970	0.6171
293.15	0.1118	0.5755
298.15	0.1638	0.5071

*Uncertainties are $u(T) = 0.1$ K and $u(w) = 0.008$.

Table 20: Experimental (liquid + liquid) equilibrium mass fractions w (cloud point data) for the system methanol (1) + 2,3-dimethylbutane (2) at pressure $p = 0.1$ MPa.*

$w_1 / -$	T / K	$w_1 / -$	T / K
0.061	277.8	0.323	294.3
0.070	285.3	0.354	293.5
0.097	293.5	0.362	294.1
0.097	286.0	0.397	293.1
0.098	292.0	0.470	291.0
0.125	291.5	0.485	291.3
0.160	294.3	0.489	289.3
0.222	294.1	0.544	285.0
0.238	294.6	0.578	281.0
0.283	294.1	0.587	280.5
0.283	294.1	0.614	276.2

*Uncertainties are $u(w) = 0.002$ and $u(T) = 0.5$ K .**Table 21: Experimental (liquid + liquid) equilibrium mass fractions w (tie lines) for the system methanol (1) + 2,3-dimethylbutane (2) at pressure $p = 0.1$ MPa.***

T / K	$w_1, \text{liquid phase 1} / -$	$w_1, \text{liquid phase 2} / -$
278.15	0.0887	0.6230
283.15	0.1076	0.5830
288.15	0.1252	0.5456
293.15	0.2537	0.3920

*Uncertainties are $u(T) = 0.1$ K and $u(w) = 0.009$.**Table 22: Experimental (liquid + liquid) equilibrium mass fractions w (cloud point data) for the system ethylene glycol (1) + 2-pentanone (2) at pressure $p = 0.1$ MPa.***

$w_1 / -$	T / K	$w_1 / -$	T / K
0.095	289.6	0.500	314.6
0.105	291.7	0.503	315.9
0.147	303.5	0.598	313.4
0.157	305.1	0.605	313.1
0.204	308.8	0.644	311.3
0.257	312.4	0.695	307.8
0.303	312.9	0.750	299.6
0.397	314.4	0.801	290.8
0.4116	315.9		

*Uncertainties are $u(w) = 0.0003$ and $u(T) = 0.5$ K .

Table 23: Experimental (liquid + liquid) equilibrium mass fractions w (tie lines) for the system ethylene glycol (1) + 2-pentanone (2) at pressure $p = 0.1$ MPa.*

T / K	$w_{1, \text{liquid phase 1}} / -$	$w_{1, \text{liquid phase 2}} / -$
303.15	0.186	0.758
308.15	0.246	0.749
313.15	0.286	0.712

*Uncertainties are $u(T) = 0.1$ K and $u(w) = 0.022$.

Table 24: Experimental (liquid + liquid) equilibrium mass fractions w (cloud point data) for the system ethylene glycol (1) + 2-hexanone (2) at pressure $p = 0.1$ MPa.*

$w_1 / -$	T / K
0.055	285.5
0.101	313.9
0.152	339.4
0.7973	329.7
0.849	311.2
0.898	288.5

*Uncertainties are $u(w) = 0.0003$ and $u(T) = 0.5$ K.

Table 25: Experimental (liquid + liquid) equilibrium mass fractions w (tie lines) for the system ethylene glycol (1) + 2-hexanone (2) at pressure $p = 0.1$ MPa.*

T / K	$w_{1, \text{liquid phase 1}} / -$	$w_{1, \text{liquid phase 2}} / -$
303.15	0.097	0.882
308.15	0.116	0.923
313.15	0.124	0.904
323.15	0.160	0.905
333.15	0.186	0.898

*Uncertainties are $u(T) = 0.1$ K and $u(w) = 0.012$.

Table 26: Experimental (liquid + liquid) equilibrium mass fractions w (cloud point data) for the system ethylene glycol (1) + 3-methyl-2-butanone (2) at pressure $p = 0.1$ MPa.*

$w_1 / -$	T / K
0.0989	289.6
0.1555	303.9
0.2013	310.5
0.3039	317.3
0.3992	318.8
0.5055	318.8
0.5978	317.3
0.7045	310.6
0.7455	305.0

*Uncertainties are $u(w) = 0.0003$ and $u(T) = 0.5$ K .

Table 27: Experimental (liquid + liquid) equilibrium mass fractions w (tie lines) for the system ethylene glycol (1) + 3-methyl-2-butanone (2) at pressure $p = 0.1$ MPa.*

T / K	$w_{1, \text{liquid phase 1}} / -$	$w_{1, \text{liquid phase 2}} / -$
303.15	0.160	0.771
308.15	0.200	0.758
313.15	0.253	0.748

*Uncertainties are $u(T) = 0.1$ K and $u(w) = 0.011$.

Table 28: Experimental (liquid + liquid) equilibrium mass fractions w (cloud point data) for the system ethylene glycol (1) + 4-methyl-2-pentanone at pressure $p = 0.1$ MPa.*

$w_1 / -$	T / K
0.053	289.4
0.102	326.0
0.147	345.6
0.800	333.1
0.849	310.7
0.886	302.0

*Uncertainties are $u(w) = 0.0003$ and $u(T) = 0.5$ K .

Table 29: Experimental (liquid + liquid) equilibrium mass fractions w (tie lines) for the system ethylene glycol (1) + 4-methyl-2-pentanone (2) at pressure $p = 0.1$ MPa.*

T / K	$w_{1, \text{liquid phase 1}} / -$	$w_{1, \text{liquid phase 2}} / -$
303.15	0.075	0.894
308.15	0.090	0.923
313.15	0.100	0.914
323.15	0.121	0.883
333.15	0.135	0.884

*Uncertainties are $u(T) = 0.1$ K and $u(w) = 0.013$.

Table 30: Experimental (liquid + liquid) equilibrium mass fractions w (cloud point data) for the system methanol (1) + methyl oleate (2) at pressure $p = 0.1$ MPa. Experiments were performed by TU Berlin.

$w_1 / -$	T / K
0.097	259
0.099	260
0.209	279
0.305	288
0.401	291
0.510	292
0.575	292
0.610	291
0.697	289
0.801	279
0.897	258

Binary SLE**Table 31: Experimental (solid + liquid) equilibrium mass fractions w for the system ethanol (1) + n-hexadecane (2) at pressure $p = 0.1$ MPa.***

$w_1 / -$	T / K
0.0000	291.07
0.0250	290.41
0.0501	290.78
0.8301	290.52
0.8797	290.59
0.9303	285.95
0.9800	275.11

*Uncertainty of mass fraction is $u(w) = 0.0003$.**Table 32: Experimental (solid + liquid) equilibrium mass fractions w for the system methanol (1) + methyl oleate (2) at pressure $p = 0.1$ MPa. Experiments were performed by TU Berlin.**

$w_1 / -$	T / K
0.000	254.85
0.0963	252.15
0.1295	252.65
0.1503	252.65
0.2008	252.65
0.301	252.45
0.401	252.15
0.534	251.85
0.602	251.65
0.656	251.65

Ternary LLE**Table 33: Experimental (liquid + liquid) equilibrium mass fractions w (binodal curve data) for the system ethanol (1) + 2,2,4,4,6,8,8-heptamethylnonane (2) + n-hexadecane (3) at temperature $T = 298.15$ K and pressure $p = 0.1$ MPa.***

$w_1 / -$	$w_2 / -$
0.1340	0.1017
0.1407	0.3443
0.1482	0.2542
0.1551	0.1642
0.1929	0.3974
0.2454	0.4451
0.6082	0.2311
0.6658	0.1645
0.7159	0.1138
0.7556	0.0729
0.7802	0.0427
0.7874	0.0250

*Uncertainties are $u(w_1) = 0.026$, $u(w_2) = 0.006$ and $u(T) = 0.1$ K.

Table 34: Experimental (liquid + liquid) equilibrium mass fractions w (tie lines) for the system ethanol (1) + 2,2,4,4,6,8,8-heptamethylnonane (2) + n-hexadecane (3) at temperature $T = 298.15$ K and pressure $p = 0.1$ MPa.*

liquid phase 1		liquid phase 2	
$w_1 / -$	$w_2 / -$	$w_1 / -$	$w_2 / -$
0.1102	0.1516	0.7646	0.0528
0.1186	0.2851	0.7142	0.1130
0.1424	0.3899	0.6579	0.1775

*Uncertainties are $u(w_1) = 0.012$, $u(w_2) = 0.003$ and $u(T) = 0.1$ K.

Table 35: Experimental (liquid + liquid) equilibrium mass fractions w (tie lines) for the system methanol (1) + 2-methylpentane (2) + n-hexane (3) at temperature $T = 283.15$ K and pressure $p = 0.1$ MPa.*

liquid phase 1		liquid phase 2	
$w_1 / -$	$w_2 / -$	$w_1 / -$	$w_2 / -$
0.0621	0.0000	0.7030	0.0000
0.0666	0.0804	0.6937	0.0290
0.0656	0.1826	0.6925	0.0644
0.0694	0.4101	0.6786	0.1455
0.0714	0.5850	0.6694	0.2103
0.0806	0.7577	0.6623	0.2773
0.0793	0.9207	0.6532	0.3468

*Uncertainty of temperature is $u(T) = 0.1$ K . Tie lines were only measured ones.

Table 36: Experimental (liquid + liquid) equilibrium mass fractions w (tie lines) for the system methanol (1) + 2,3-dimethylbutane (2) + n-hexane (3) at temperature $T = 283.15$ K and pressure $p = 0.1$ MPa.*

liquid phase 1		liquid phase 2	
$w_1 / -$	$w_2 / -$	$w_1 / -$	$w_2 / -$
0.0636	0.0000	0.7173	0.0000
0.0645	0.1581	0.7050	0.0578
0.0724	0.1949	0.6953	0.0723
0.0815	0.4433	0.6635	0.1786
0.0915	0.5650	0.6417	0.2341
0.0999	0.7182	0.6195	0.3156
0.1091	0.8940	0.5883	0.4223

*Uncertainty of temperature is $u(T) = 0.1$ K . Tie lines were only measured ones.

Ternary SLLE

Table 37: Experimental (liquid + liquid) equilibrium mass fractions w (binodal curve data) and experimental (solid + liquid) equilibrium mass fractions w for the system ethanol (1) + 2,2,4,4,6,8,8-heptamethylnonane (2) + n-hexadecane (3) at temperature $T = 283.15$ K and pressure $p = 0.1$ MPa.*

liquid + liquid		solid + liquid	
$w_1 / -$	$w_2 / -$	$w_1 / -$	$w_2 / -$
0,1311	0,4359	0.0000	0.4414
0,1334	0,5207	0.0239	0.4388
0,1536	0,5909	0.0462	0.4200
0,1866	0,6510	0.0679	0.4035
0,5356	0,3717	0.7588	0.1440
0,6613	0,2364	0.8020	0.1121
0,7095	0,1746	0.8484	0.0749
0,7627	0,1191	0.8680	0.0390
		0.9379	0.0000

*Uncertainties are $u(w_{1,LL}) = 0.031$, $u(w_{2,LL}) = 0.014$, $u(w_{1,SL}) = 0.014$, $u(w_{2,SL}) = 0.005$ and $u(T) = 0.1$ K.

Table 38: Experimental (liquid + liquid) equilibrium mass fractions w (binodal curve data) and experimental (solid + liquid) equilibrium mass fractions w for the system ethanol (1) + 2,2,4,4,6,8,8-heptamethylnonane (2) + n-hexadecane (3) at temperature $T = 278.15$ K and pressure $p = 0.1$ MPa.*

liquid + liquid		solid + liquid	
$w_1 / -$	$w_2 / -$	$w_1 / -$	$w_2 / -$
0.1174	0.6092	0.0339	0.6148
0.1184	0.5758	0.0622	0.5886
0.1253	0.6576	0.6272	0.2675
0.1570	0.6766	0.7279	0.1782
0.1715	0.6958	0.8493	0.0914
0.1870	0.7276		
0.5158	0.4334		
0.5848	0.3487		
0.6213	0.3040		
0.6585	0.2567		
0.7039	0.2044		

*Uncertainties are $u(w_{1,LL}) = 0.034$, $u(w_{2,LL}) = 0.018$, $u(w_{1,SLE}) = 0.0004$, $u(w_{2,SLE}) = 0.0003$ and $u(T) = 0.1$ K.

Interfacial tension**Table 39: Experimental density and interfacial tension for the system methanol + 2-methylpentane at pressure $p = 0.1$ MPa.***

T / K	$\rho_{\text{light phase}} / \text{kg m}^{-3}$	$\rho_{\text{heavy phase}} / \text{kg m}^{-3}$	$\sigma / \text{mN m}^{-1}$
288.66	667	730	0.2416
292.43	664	719	0.1469
294.29	664	716	0.1088
297.62	662	709	0.0584

*Uncertainties u are $u(T) = 0.1$ K, $u(\rho) = 1$ kg m⁻³ and $u(\sigma) = 0.01$ mN m⁻¹.

Table 40: Experimental density and interfacial tension for the system methanol + 3-methylpentane at pressure $p = 0.1$ MPa.*

T / K	$\rho_{\text{light phase}} / \text{kg m}^{-3}$	$\rho_{\text{heavy phase}} / \text{kg m}^{-3}$	$\sigma / \text{mN m}^{-1}$
288.85	677	734	0.1630
291.17	675	726	0.1241
295.01	673	718	0.0716
298.09	672	714	0.0330

*Uncertainties u are $u(T) = 0.1$ K, $u(\rho) = 1$ kg m⁻³ and $u(\sigma) = 0.01$ mN m⁻¹.

Table 41: Experimental density and interfacial tension for the system methanol + 2,3-dimethylbutane at pressure $p = 0.1$ MPa.*

T / K	$\rho_{\text{light phase}} / \text{kg m}^{-3}$	$\rho_{\text{heavy phase}} / \text{kg m}^{-3}$	$\sigma / \text{mN m}^{-1}$
288.44	680	720	0.0740
289.93	679	717	0.0331
292.26	679	709	0.0226

*Uncertainties u are $u(T) = 0.1$ K, $u(\rho) = 1$ kg m⁻³ and $u(\sigma) = 0.01$ mN m⁻¹.

Adsorption isotherms**Table 42: Experimental adsorption isotherms of the binary system n-octane (1) + 2,2,4-trimethylpentane (2) on activated carbon at three different temperatures and pressure $p = 0.1$ MPa.***

T / K	$w_1^{\text{bulk phase}}$ / -	$w_1^{\text{adsorbed phase}}$ / -
283.15	0.1671	0.3635
	0.3621	0.5566
	0.4658	0.6376
	0.5727	0.7080
	0.7839	0.8625
293.15	0.1700	0.3843
	0.3724	0.5452
	0.4689	0.6649
	0.5716	0.7553
	0.7838	0.8831
303.15	0.1726	0.4650
	0.3692	0.6609
	0.4717	0.7230
	0.5748	0.7987
	0.7913	0.8700

*Uncertainties u are $u(T) = 0.1$ K, $u(w_1^{\text{bulk phase}}) = 0.004$ and $u(w_1^{\text{adsorbed phase}}) = 0.020$.

Table 43: Experimental degree of swelling of activated carbon for the adsorption of the binary system n-octane (1) + 2,2,4-trimethylpentane at three different temperatures and pressure $p = 0.1$ MPa.*

T / K	w_1^{Feed} / -	Degree of swelling / -
283.15	0.1200	1.2588
	0.2384	1.2911
	0.2970	1.2844
	0.3571	1.2985
	0.4757	1.3057
293.15	0.1198	1.2156
	0.2379	1.2317
	0.2972	1.2294
	0.3571	1.2316
	0.4758	1.2390
303.15	0.1201	1.1464
	0.2380	1.1553
	0.2977	1.1655
	0.3563	1.1638
	0.4763	1.1656

*Uncertainties u are $u(T) = 0.1$ K, $u(w_1^{\text{Feed}}) = 0.0004$ and $u(\text{Degree of swelling}) = 0.008$.

Table 44: Experimental adsorption isotherms of the binary system n-octane (1) + 2,2,4-trimethylpentane (2) on silica gel at three different temperatures and pressure $p = 0.1$ MPa.*

T / K	$w_1^{\text{bulk phase}}$ / -	$w_1^{\text{adsorbed phase}}$ / -
283.15	0.1976	0.2087
	0.4056	0.3913
	0.5091	0.4742
	0.6067	0.5740
	0.8137	0.7621
293.15	0.2058	0.2040
	0.4051	0.3842
	0.4980	0.5033
	0.6025	0.5880
	0.8060	0.7765
303.15	0.1994	0.1934
	0.4058	0.3853
	0.5058	0.4831
	0.6076	0.5716
	0.8098	0.7666

*Uncertainties u are $u(T) = 0.1$ K, $u(w_1^{\text{bulk phase}}) = 0.003$ and $u(w_1^{\text{adsorbed phase}}) = 0.008$.

Table 45: Experimental degree of swelling of silica gel for the adsorption of the binary system n-octane (1) + 2,2,4-trimethylpentane at three different temperatures and pressure $p = 0.1$ MPa.*

T / K	w_1^{Feed} / -	Degree of swelling / -
283.15	0.1099	1.2952
	0.2207	1.2952
	0.2750	1.2952
	0.3285	1.2952
	0.4399	1.2952
293.15	0.1130	1.2955
	0.2192	1.2955
	0.2750	1.2955
	0.3286	1.2955
	0.4390	1.2955
303.15	0.1086	1.2931
	0.2202	1.2930
	0.2746	1.2964
	0.3282	1.2931
	0.4386	1.2931

*Uncertainties u are $u(T) = 0.1$ K, $u(w_1^{\text{Feed}}) = 0.0007$ and $u(\text{Degree of swelling}) = 0.0003$.

Table 46: Experimental adsorption isotherms of the binary system n-octane (1) + 2,2,4-trimethylpentane (2) on zeolite at three different temperatures and pressure $p = 0.1$ MPa.*

T / K	$w_1^{\text{bulk phase}}$ / -	$w_1^{\text{adsorbed phase}}$ / -
283.15	0.0017	0.9793
	0.2000	1.0432
	0.3343	1.0365
	0.4676	1.0101
	0.7410	0.9898
293.15	0.0123	0.8438
	0.2052	1.0050
	0.3411	0.9907
	0.4722	0.9977
	0.7380	0.9905
303.15	0.0039	0.9025
	0.2111	1.0292
	0.3440	1.0058
	0.4736	1.0017
	0.7445	0.9743

*Uncertainties u are $u(T) = 0.1$ K, $u(w_1^{\text{bulk phase}}) = 0.004$ and $u(w_1^{\text{adsorbed phase}}) = 0.036$.

Table 47: Experimental degree of swelling of zeolite for the adsorption of the binary system n-octane (1) + 2,2,4-trimethylpentane at three different temperatures and pressure $p = 0.1$ MPa.*

T / K	w_1^{Feed} / -	Degree of swelling / -
283.15	0.0219	1.0443
	0.0821	1.1403
	0.1608	1.1590
	0.2039	1.1629
	0.2418	1.1645
	0.3234	1.1634
293.15	0.0808	1.1564
	0.1613	1.1645
	0.2021	1.1667
	0.2421	1.1637
	0.3221	1.1596
303.15	0.0803	1.1495
	0.1621	1.1576
	0.2029	1.1614
	0.2424	1.1618
	0.3234	1.1641

*Uncertainties u are $u(T) = 0.1$ K, $u(w_1^{Feed}) = 0.001$ and $u(\text{Degree of swelling}) = 0.006$.

Table 48: Experimental adsorption isotherms of the binary system n-hexane (1) + 2,3-dimethylbutane (2) on activated carbon at three different temperatures and pressure $p = 0.1$ MPa.*

T / K	$w_1^{\text{bulk phase}} / -$	$w_1^{\text{adsorbed phase}} / -$
283.15	0.1959	0.2268
	0.3911	0.4486
	0.4773	0.6348
	0.5785	0.7179
	0.7867	0.8818
293.15	0.1828	0.3978
	0.3829	0.5421
	0.4854	0.7106
	0.5845	0.7774
	0.7980	0.8192
303.15	0.1885	0.4810
	0.3849	0.7349
	0.4857	0.7857
	0.5867	0.7985
	0.7902	1.0257

*Uncertainties u are $u(T) = 0.1$ K, $u(w_1^{\text{bulk phase}}) = 0.002$ and $u(w_1^{\text{adsorbed phase}}) = 0.045$.

Table 49: Experimental degree of swelling of activated carbon for the adsorption of the binary system n-hexane (1) + 2,3-dimethylbutane at three different temperatures and pressure $p = 0.1$ MPa.*

T / K	$w_1^{\text{Feed}} / -$	Degree of swelling / -
283.15	0.1158	1.2013
	0.2306	1.1822
	0.2882	1.1931
	0.3467	1.2096
	0.4621	1.1927
293.15	0.1152	1.1084
	0.2309	1.1438
	0.2886	1.0910
	0.3459	1.1047
	0.4616	1.1045
303.15	0.1164	1.0614
	0.2313	1.0625
	0.2884	1.0660
	0.3467	1.0860
	0.4616	1.0501

*Uncertainties u are $u(T) = 0.1$ K, $u(w_1^{\text{Feed}}) = 0.004$ and $u(\text{Degree of swelling}) = 0.016$.

Table 50: Experimental adsorption isotherms of the binary system n-hexane (1) + 2,3-dimethylbutane (2) on silica gel at three different temperatures and pressure $p = 0.1$ MPa.*

T / K	$w_1^{\text{bulk phase}} / -$	$w_1^{\text{adsorbed phase}} / -$
283.15	0.2035	0.1881
	0.4035	0.3933
	0.5057	0.4817
	0.6023	0.5925
	0.7964	0.7893
293.15	0.2015	0.1961
	0.4032	0.3942
	0.5019	0.4933
	0.6010	0.6062
	0.7996	0.7967
303.15	0.2067	0.1820
	0.4084	0.3838
	0.5087	0.4727
	0.6081	0.5742
	0.8062	0.7762

*Uncertainties u are $u(T) = 0.1$ K, $u(w_1^{\text{bulk phase}}) = 0.005$ and $u(w_1^{\text{adsorbed phase}}) = 0.014$.

Table 51: Experimental degree of swelling of silica gel for the adsorption of the binary system n-hexane (1) + 2,3-dimethylbutane at three different temperatures and pressure $p = 0.1$ MPa.*

T / K	$w_1^{\text{Feed}} / -$	Degree of swelling / -
283.15	0.1061	1.2829
	0.2133	1.2829
	0.2662	1.2829
	0.3188	1.2829
	0.4244	1.2829
293.15	0.1067	1.2810
	0.2131	1.2810
	0.2661	1.2810
	0.3214	1.2810
	0.4261	1.2810
303.15	0.1068	1.2775
	0.2143	1.2775
	0.2654	1.2775
	0.3185	1.2775
	0.4252	1.2776

*Uncertainties u are $u(T) = 0.1$ K, $u(w_1^{\text{Feed}}) = 0.001$ and $u(\text{Degree of swelling}) = 0.000$.

Table 52: Experimental adsorption isotherms of the binary system n-hexane (1) + 2,3-dimethylbutane (2) on zeolite at three different temperatures and pressure $p = 0.1$ MPa.*

T / K	$w_1^{\text{bulk phase}}$ / -	$w_1^{\text{adsorbed phase}}$ / -
283.15	0.0010	0.9631
	0.2343	1.0668
	0.3539	1.0121
	0.4855	1.0582
	0.7313	1.0704
293.15	0.0105	0.8975
	0.2492	1.0000
	0.3671	0.9877
	0.4947	1.0108
	0.7586	0.9534
303.15	0.0047	0.9861
	0.2389	1.0332
	0.3525	1.0606
	0.4907	1.0355
	0.7402	0.9852

*Uncertainties u are $u(T) = 0.1$ K, $u(w_1^{\text{bulk phase}}) = 0.008$ and $u(w_1^{\text{adsorbed phase}}) = 0.050$.

Table 53: Experimental degree of swelling of zeolite for the adsorption of the binary system n-hexane (1) + 2,3-dimethylbutane (2) at three different temperatures and pressure $p = 0.1$ MPa.*

T / K	w_1^{Feed} / -	Degree of swelling / -
283.15	0.0187	1.0392
	0.0772	1.1300
	0.1539	1.1244
	0.1937	1.1415
	0.2311	1.1245
	0.3071	1.1239
293.15	0.0191	1.0374
	0.0767	1.1364
	0.1545	1.1267
	0.1931	1.1328
	0.2312	1.1271
	0.3213	1.1340
303.15	0.0183	1.036
	0.0775	1.1256
	0.1535	1.1260
	0.1934	1.1311
	0.2311	1.1257
	0.3083	1.1507

*Uncertainties u are $u(T) = 0.1$ K, $u(w_1^{\text{Feed}}) = 0.001$ and $u(\text{Degree of swelling}) = 0.008$.

Publications

Journal articles

1. T. Goetsch, A. Danzer, P. Zimmermann, A. Köhler, K. Kissing, S. Enders, T. Zeiner
“Liquid-Liquid Equilibrium and Interfacial Tension of Hexane Isomers-Methanol Systems” *Ind. Eng. Chem. Res.* **2017**, *56*, 9743-9752.
2. P. Zimmermann, T. Goetsch, T. Zeiner, S. Enders
“Modelling of adsorption isotherms of isomers using density functional theory“ *Mol. Phys.* **2017**, *115*, 1389-1407.
3. T. Goetsch, P. Zimmermann, R. van den Bongard, S. Enders, T. Zeiner
“Superposition of liquid-liquid and solid-liquid equilibria of linear and branched molecules: Ternary systems” *Ind. Eng. Chem. Res.* **2017**, *56*, 417-423.
4. T. Goetsch, P. Zimmermann, R. van den Bongard, S. Enders, T. Zeiner
“Superposition of liquid-liquid and solid-liquid equilibria of linear and branched molecules: Binary systems” *Ind. Eng. Chem. Res.* **2016**, *55*, 11167-11174.
5. T. Goetsch, P. Zimmermann, S. Enders, T. Zeiner
“Tuneable extraction systems based on hyperbranched polymers” *Chem. Eng. Process.* **2016**, *99*, 175-182.
6. P. Zimmermann, T. Goetsch, T. Zeiner, S. Enders
“Prediction of adsorption isotherms of n-aldehydes mixtures using density functional theory in combination with Peng-Robinson equation of state” *Fluid Phase Equilib.* **2015**, *424*, 173-181.

Presentations

1. T. Goetsch, P. Zimmermann, B. Scharzec, S. Enders, T. Zeiner
“New Model for Liquid Adsorption Isotherms of Isomeric Mixtures”
29. European Symposium on Applied Thermodynamics, **2017**, Bucharest, Rumania.
2. T. Goetsch, P. Zimmermann, R. van den Bongard, A. Köhler, S. Enders, T. Zeiner
“Vorhersage und experimentelle Überprüfung des Oiling-Out Effektes bei der Trennung von Isomeren”
Jahrestreffen der Fachgruppe Kristallisation, **2017**, Köln, Germany.

3. T. Goetsch, P. Zimmermann, R. van den Bongard, A. Köhler, S. Enders, T. Zeiner
“Prediction of liquid-liquid and solid-liquid equilibria of isomers”
American Institute of Chemical Engineers Annual Meeting, **2016**, San Francisco, USA.
4. T. Goetsch, P. Zimmermann, R. van den Bongard, S. Enders, T. Zeiner
“Überlagerung von Flüssig-Flüssig und Fest-Flüssig Phasengleichgewichten von langkettigen Isomergemischen”
Thermodynamik-Kolloquium, **2015**, Bochum, Germany.
5. T. Goetsch, P. Zimmermann, R. van den Bongard, S. Enders, T. Zeiner
“Superposition of liquid-liquid and solid-liquid equilibria of isomers”
28. European Symposium on Applied Thermodynamics, **2015**, Athens, Greece.
6. T. Goetsch, P. Zimmermann, S. Enders, T. Zeiner
“Untersuchung der Überlagerung von Flüssig-Flüssig und Fest-Flüssig Phasengleichgewichten linearer und verzweigter Moleküle”
Thermodynamik-Kolloquium, **2014**, Stuttgart, Germany.
7. T. Goetsch, P. Zimmermann, S. Enders, T. Zeiner
“Solid-Liquid-Liquid Equilibria of Aqueous Hyperbranched Polymer Solutions”
International Conference on Chemical Thermodynamics & SAICChE National Conference, **2014**, Durban, South Africa.

Posters

1. T. Goetsch, P. Zimmermann, B. Scharzec, S. Enders, T. Zeiner
“Modelling of Adsorption Isotherms Applying Two-Dimensional Peng-Robinson Equation of State”
Thermodynamik-Kolloquium, **2016**, Kaiserslautern, Germany.
2. T. Goetsch, P. Zimmermann, R. van den Bongard, S. Enders, T. Zeiner
“Vorhersage von Flüssig-Flüssig und Fest-Flüssig-Phasengleichgewichten verzweigter Moleküle”
Jahrestreffen der Fachgruppe Kristallisation, **2015**, Magdeburg, Germany.

About the author

Personal data

Name: Thomas Goetsch

Date of birth: 29.08.1987

Place of birth: Gelsenkirchen

Nationality: German

Professional career

01/2017 - 11/2017 Technische Universität Graz, Austria
Institute of Chemical Engineering and Environmental Technology

02/2014 – 01/2017 Technische Universität Dortmund, Germany
Laboratory of Fluid Separations

Education

04/2012 – 09/2013 Technische Universität Dortmund, Germany
Master of Science in Chemical Engineering

10/2008 – 03/2012 Technische Universität Dortmund, Germany
Bachelor of Science in Chemical Engineering

08/1998 – 06/2007 Städtisches Leibniz-Gymnasium Gelsenkirchen, Germany
Abitur